DISSERTATION

CORRELATION OF DNA DOUBLE STRAND BREAK REPAIR EFFICIENCY AND

SUSCEPTIBILITY TO LUNG TUMOR DEVELOPMENT

Submitted by

Donasian Ocan Ochola

Graduate Degree Program in Cell and Molecular Biology

In partial fulfillment of the requirements

For the Degree of Doctor of Philosophy

Colorado State University

Fort Collins, Colorado

Spring 2015

Doctoral Committee:

    Advisor: Michael M Weil
    Co-Advisor: Joel S Bedford

    Douglas M Thamm
    Steven W Dow
    Takamitsu A Kato

ABSTRACT

CORRELATION OF DNA DOUBLE STRAND BREAK REPAIR EFFICIENCY AND

SUSCEPTIBILITY TO LUNG TUMOR DEVELOPMENT

In this dissertation we describe the use of many CcS/Dem recombinant congenic strains (RCS) of mice to determine if there is any correlation between the DNA double strand break (DSB) repair efficiency and susceptibility to lung tumor development. A previous study involving 20 different CcS/Dem RCS of mice all derived from cross of BALB/c x STS progenitors (BALB/c is the recipient strain that is susceptible to tumor development and STS the donor is resistant) showed wide inter-strain variations in susceptibility to radiation-induced lung tumor development. As formalin fixation was used to obtain paraffin embedded tissue sections for immunofluorescence, we first evaluated different methods of euthanasia, perfusion techniques, autofluorescence reduction and antigen retrieval methods to optimize the procedures used so as to obtain reproducible results. The formation of phosphorylated histone H2AX (γ-H2AX) into discrete foci was used as the marker for DSB repair and its co-localization with 53BP1, another component of repair foci, was examined during the optimization. From the optimization phase, CO_2 asphyxiation, right ventricular perfusion, use of sodium borohydride for quenching autofluorescence and the use of sodium citrate for heat-induced epitope retrieval (antigen retrieval) gave very good quality images and were adopted for use in all subsequent experiments. To explore a possible link between heritable differences in DNA DSB repair efficiency and susceptibility to RI lung cancer in a mouse model, we quantified residual γH2AX foci in lungs of 16 different CcS/Dem RCS mice together with their founders after irradiation from a ^{137}Cs source of γ-rays at a low-dose rate of 10 cGy/hr

for 24 h. We also explored residual γH2AX foci in the peripheral blood leukocytes to compare it with foci in the lungs with the intention of using PBLs as a surrogate to assess DNA repair efficiency in the lungs for possible use in clinical applications to pre-screening patients and assess their suitability as candidates for radiotherapy, especially in fairly young. In the lungs, the results showed a high correlation between mean residual γH2AX foci number per nucleus and radiation-induced lung tumor observed in the previous study (R=0.968, p <0.0001) indicating that γH2AX can be used as a good predictor of the potential to develop RI lung tumor. Though the absolute mean values of foci in PBLs and the lungs were different, the inter-strain differences in DNA repair efficiencies correlated very closely to those in the lungs for all the six strains that were compared (Spearman rank correlation coefficient, R = 0.948), and indication that PBLs are good surrogates for DNA DSB repair efficiency in the lungs of CcS/Dem RCS mice. These results indicate that γH2AX can be used as a good predictor of the potential to develop RI lung tumor, and that, measuring γH2AX foci in PBLs can be used as a surrogate to determine DDR in the lungs of the CcS/Dem RCS mice. Since the product of the *Prkdc* gene is known to be an important player in the DDR, we tested whether the R2140C substitution has a major influence on DSB repair and a determinant in the foci counts difference in the CcS/Dem strains. We amplified the segment of the *Prkdc* gene that contains the c>t transition resulting in amino acid substitution that abolishes a *BsmBI* restriction site. The outcome of these restriction patterns suggests no direct correlation between DNA-PK and DSB repair efficiency and that another gene (or other genes) polymorphic between BALB/c and STS/A may determine the strain differences in DSB repair efficiencies.

ACKNOWLEDGEMENTS

TABLE OF CONTENTS

LIST OF TABLES

LIST OF FIGURES

xi

INTRODUCTION

1.1: The DNA Damage Response

As early as end of the 1990s and the beginning of the last decade, quite a lot has been made known about the mechanisms mammalian cells employ in attempts to overcome or reverse DNA damage. It is now well established that cells make use of a global signaling network called the DNA damage response (DDR). This response involves the use of systems that are specialized in sensing different types of damage, followed by multiple and coordinated responses that include among others, but in no particular order, the activation of transcription, cell cycle control, apoptosis, senescence, and DNA repair processes (Zhou and Elledge, 2000).This coordination is critical for cell survival, in particular to maintain the integrity of DNA replication and faithful propagation of the genome. There are three general and basic groups of molecular players that constitute the DDR mechanisms: first, cells use various molecules as "sensors" to detect DNA lesions. Second, signals are generated and amplified by "transducers" to alert other players of the presence of the lesions, and finally "effectors" are activated to achieve repair of the lesions, or where more time is required for repair in cells undergoing active division, they activate cell cycle arrest (Sherr and Roberts, 1999; Fabbro *et al*., 2004; Smith *et al*., 2010; review by Thompson, 2012). In a worse-case scenario, the apoptotic pathway is activated if the damage is too complex and repair is impossible to achieve (Watters, 1999; De Vries-Seimon *et al*., 2007; Sun *et al*., 2008; Cataldi *et al*., 2009; Reynolds *et al*., 2012). Any defects in the repair capacity of the cells that compromise the efficiency of these mechanisms can result in increased sensitivity to DNA-

damaging agents, or may allow cells with unrepaired DNA to accumulate and are expected to result in many of the DNA damage-related diseases. Although responses differ for different classes of DNA lesions, the general repair program is usually the same or similar in all living systems. Repair of damaged DNA and the general DDR signaling are events that operate collectively and share many components (Jackson and Bartek, 2009, Review by Thompson, 2012).

Many, or possibly all, cancer cells lack at least some aspects of the DDR due to selective pressures operating during tumor evolution or during development of the organism. Reduced or complete absence of DDR factors are likely to positively correlate with therapeutic outcomes where tumor cells that lack some or many of the DDR factors should be more susceptible to therapy. On the contrary, for normal cells, the inability to efficiently repair damaged DNA is expected to positively correlate with susceptibility to tumor development. This is the general hypothesis that formed the fundamental for the present dissertation study, based on the results of differences in lung tumor incidence in mice from similar genetic founders (Szymanska *et al.*, 1999).

The presence of a lesion in the DNA is recognized by various sensor proteins depending on the type of lesion and the repair pathway used. These sensors initiate signaling pathways that call into play a wide variety of cellular processes. Because there is a wide diversity of DNA-lesion types, they require multiple distinct DNA-repair mechanisms. While some lesions require simple direct reversal, most of them usually require multiple proteins operating in a sequence of catalytic events to achieve repair. For instance, during mismatch repair (MMR) which may

appear simple and straightforward, the detection of mismatches and insertion/deletion loops in the DNA sequence will trigger a single-strand incision reaction that is then acted upon by nuclease, polymerase and ligase enzymes (Villemure *et al*., 2003; Bannister *et al*., 2004, Jiricny, 2006; *Hong et al*., 2008; Martin *et al*., 2010). In base-excision repair (BER), a damaged base is often recognized by a DNA glycosylase enzyme that mediates base removal before nuclease, polymerase and ligase proteins complete the repair, just like the processes that overlap with those used in single-strand break repair (ssBR)(Martin *et al*., 2010). DNA helix-distorting base lesions are repaired by the nucleotide excision repair (NER) system that operates via two sub-pathways, one of which is a transcription-coupled NER for lesions that cause block of transcription, and another is a global-genome NER used in non-transcribed regions (Hoeijmakers, 2001). During NER the damaged portion of the DNA is excised as a 22-30 base oligonucleotide producing single-stranded DNA (ssDNA) that is acted upon by DNA polymerases and associated factors before the final ligation (Hoeijmakers, 2001). From these examples, it can be appreciated that DNA damage repair is no simple business. Occasionally, some DNA lesions are not repaired at all but are just bypassed during DNA replication by polymerases with less stringent requirements than polymerases that carry out high fidelity replication (Loeb and Monnat, 2008).

Undoubtedly, the most complex type of DNA damage, with respect to the input required for repair, is DNA double strand break (DSB). As will be elaborated in more details later, DSBs have a high degree of complexity and as a result cells have evolved equally more complex mechanisms to match the needs for fairly efficient repair (Mladenov and Iliakis, 2011; Schipler and Iliakis, 2013). The principal mechanisms or pathways used to repair DSB are non-homologous end-joining (NHEJ) (Lieber, 2008; Mahaney *et al*., 2009; Lieber, 2010; Lieber *et*

al., 2010) and homologous recombination (HR) (San Filippo *et al.,* 2008). The cells employ what is their equivalent of the national security agency to carry out a constant surveillance of the integrity of DNA within their confines and when a DSB occurs, the sensors detect the resultant changes. Different sensors are reported to be used in NHEJ and HRR (reviewed by Thompson, 2012, and Wang and Lees-Miller, 2013).

1.1.1: Non-homologous end joining

Of the two pathways used in DNA DSB repair, NHEJ is active throughout the cell cycle since it is involved in rejoining free DNA ends without the need for sequence homology. This repair mechanism is therefore very prone to errors and could be a likely source of novel mutations. In contrast, HR involves the use of a homologous DNA sequence as a template for resynthesis and is most active in S and G2 phases of the cell cycle. According to Wang and Lees-Miller (2013), NHEJ can be conveniently divided into (**a**) end-detection and tethering, (**b**) processing, and (**c**) ligation.

Following DSB, a number of proteins get involved in a complex and coordinated network of events that ultimately result in the repair of the DNA break. Intact DNA in the resting cells usually exists in a supercoiled conformation and any break will result in transient relaxation that causes local topological alteration in the DNA double helical structure. The conformational changes are immediately sensed by the mechanisms the cell uses to detect abnormal physical arrangement of the DNA. These will trigger a number of chemical changes within the cell among which is the activation of kinases through post-translation modifications that play very significant roles in DNA damage response. While activation of kinases in response to DNA

damage are through phosphorylation, other types of post-translation modification of proteins involved in DNA damage response are also known to occur (review by Thompson, 2012).

The key players in the phosphorylation events ultimately leading to amplification of DNA damage response (DDR) are a group of phosphatidylinositol 3-kinase (PI3K)-like kinases (PIKK), such as ataxia telangiectasia mutated (ATM), ataxia telangiectasia mutated and Rad3 related kinase (ATR) and DNA-dependent protein kinase catalytic subunit (DNA-PKcs) (Falck *et al.* 2005; An *et al.*, 2010). These PIKKs are recruited to DNA lesions by DNA damage sensors and it is now fairly well established which sensors work in conjunction with which kinases (An et al., 2010; reviewed by Kouranti and Peyroche, 2012). The MRN complex (Mre11, Rad50, and Nbs1) helps to recruit ATM (Di Virgilio *et al.,* 2009). ATRIP recruits ATR, (Yang and Zou 2006; Mohni et al., 2010; Ohashi et al., 2014); and Ku70/80 complex helps to recruit DNA-PKcs (Calsou et al 2003; Hammel *et al.*, 2010). In the review, it is clear that there are numerous additional mediator or adaptor proteins including BRCA1, MDC1, 53BP1 and Claspin that function as scaffolds providing docking platforms to bring together PIKKs and their substrates to achieve faithful repair.

In most cases, DDR pathways drive the assembly of macromolecular complexes on damaged chromatin and the accumulation of these proteins can be readily detected by fluorescence imaging as nuclear foci because of their high local concentrations at damaged sites Lisby and Rothstein, 2004). Based on appropriate antibodies generated against them, many of the DDR factors that are components of the foci can easily be detected and because these proteins usually surround DNA lesions, they are often used as DNA damage site markers. These foci are not static though. According to available data, they are highly dynamic structures which are

recruited, retained, and eventually disassembled in a coordinated manner after the repair is completed (Kouranti and Peyroche, 2012).

It is now known that cells employ different mechanisms and molecules (may be in hundreds) to achieve the repair function and it would require volumes of reviews to highlight the roles and possible mechanisms of actions of all the factors known to date. The MRN complex, for instance, has been reported to act as a sensor that detects damage in the DNA (Lee and Paull, 2005; Di Virgillo *et al.*, 2009), and is also thought to be involved in the recruitment of ATM to the DSB where the recruited dimeric ATM undergoes dissociation into its monomers that are auto-phosphorylated on multiple residues to become active kinases (Bakkenist and Kastan, 2003).

The serine threonine protein kinase DNA-PKcs that is a member of the phosphatidyl inositol 3-kinase-like protein kinase (PIKK) family is very important in DSB repair (Calsou et al 2003; Uematsu *et al.*, 2007; Hammel *et al*., 2010). Recently, the involvement of DNA-PK in processes that occur during NHEJ was described in greater detail (Wang and Lees-Miller, (2013). In the first stage of the process there is recognition of free DSB ends and binding by the Ku70/Ku80 heterodimer with high affinity, forming a ring-like structure around the DNA ends to help protect the DSB termini from diffusing apart, which would subject the ends to degradation by nucleases (Walker *et al*., 2001; Shao *et al*., 2012). The Ku proteins have been known for a long time to play important surveillance and sensing roles in DSBs as their presence at the ends of the DSB also acts as signals for the recruitment of DNA-PKcs (Mimori and Hardin, 1986; Mimori *et al*., 1986). Once recruited, the DNA-PKcs and Ku combination tether the DNA ends in a synaptic

complex (Cary *et al.,* 1997; DeFazio *et al*., 2002). The interaction with DSB-bound Ku augments the protein kinase activity of DNA-PKcs (Gottlieb and Jackson, 1993) an essential requirement for the role of DNA-PKcs during NHEJ (Kurimasa *et al*., 1999a, 1999b; Zhao *et al*., 2006). Whether DNA-PK is the major player in the NHEJ mode of DNA repair is still an unresolved matter since other accounts indicate ATM as the key initiator. The second major step in NHEJ involves enzymatic processing of DNA ends. It has been reported that IR frequently produces DNA termini containing non-ligatable 3′-phosphate groups, e.g. 3′-phosphoglycolates, or 5′-hydroxyl groups that must be converted to 3′-hydroxyls and 5′-phosphates before ligation can occur (Povirk *et al*, 2007; Zhou *et al*., 2009; Mohapatra *et al.,* 2013; Menon and Povirk, 2014).

Other similar kinases are involved in the appropriate pathways of the DDR depending on the type of damage. In mammalian cells, the major target of the kinases at the site of DNA damage is the variant histone H2AX that becomes phosphorylated on Ser-139 by ATM, ATR or DNA-PK (Rogakou *et al*., 1998). Several downstream substrates of the ATM and ATR kinases act as mediators that recruit additional substrates and add to the scaffolds upon which complexes are assembled in order to help amplify and relay the generated signals for successful DSB repair (Yano *et al.,* 2009). Some proteins that play the role of mediators include MRN, MDC1, 53BP1, and BRCA1 among others. Upon H2AX phosphorylation, the γH2AX formed then helps to recruit more MDC1 in a cycle that amplifies H2AX phosphorylation. How that is achieved is not exactly known, but it is possibly by tethering ATM or preventing γH2AX de-phosphorylation (Stucki and Jackson, 2006). In this way, MDC1 and H2AX allow the recruitment of many additional factors to sites of damage leading to the generation of IR-induced foci (IRIF) that contain multiple proteins.

Further downstream of γ-H2AX formation, the presence of the γ-H2AX and MDC1 provide additional signals for recruitment of 53BP1 and the E3 ubiquitin ligase RNF8 to the site, therefore augmenting the amplification of the IRIF. According to many authors, the recruited RNF8 then mediates ubiquitination of H2AX and possibly other proteins, leading to recruitment of 53BP1 to the site assisted by other participants like RAP80 (Kolas *et al*., 2007; Mailand *et al*., 2007; Wang and Elledge, 2007; Wang *et al.,* 2007; Sakasi and Tibbetts, 2008; Poulsen *et al.,* 2010).

As already mentioned, some of the DNA ends produced during the IR-induced DSB are reported to contain non-ligatable groups like 3'phosphoglycosylates and 5' hydroxyl-containing moieties that can complicate DSB repair and have to be removed before repair can be achieved (Povirk *et al.*, 2007). Their removal may involve several types of proteins and phosphatases that have been explored by many researchers. Their removal may be effected by many types of kinase and phosphatase enzymes (Weinfeld *et al*., 2011), phosphodiesterase enzymes (Bahmed *et al*., 2010; Huang *et al.,* 2011), or nucleases such as exonuclease 1 (Exo1), Mre11 and Artemis enzymes (Rass *et al.,* 2009; Weterings *et al*., 2009; Xie *et al*., 2009; Bahmed *et al*., 2010), all of which are reported to be involved in processing damaged DNA termini to remove the otherwise non-ligatable DSB ends that would make the DSB very difficult or impossible to repair. Other repair factors such as the Werner syndrome helicase/exonuclease (WRN) help to facilitate repair of regions of damaged DNA through the use of nearby sequence microhomology in a less-well-characterized Ku-independent NHEJ pathway known as microhomology-mediated end-joining (MMEJ) (Kusumoto *et al.,* 2008; Truong, *et al*., 2013; Sharma *et al*., 2015) as well as the alternative end-joining (AEJ) sub-pathway (McVey and Lee, 2008; Frit *et al.*, 2014). In the final stage of NHEJ, DNA ligase IV (LIG4), which exists in complex with x-ray repair cross-

complementing 4 (XRCC4) protein and XRCC4-like factor (XLF), helps to ligate the processed DNA ends (Mahaney *et al*., 2009; Lieber, 2010; Wang and Lees-Miller, 2013). Even though both NHEJ and MMEJ are error-prone, they can operate in any phase of the cell cycle.

From the foregoing accounts, one can appreciate the complexity of DDR and the fact that NHEJ pathways do not proceed in a linear, stepwise fashion from initial binding of Ku and ultimate ligation by LIG4. Even to the 'initiated' and from what little is so far known, there is considerable uncertainty regarding the timing and order of the intervening steps during NHEJ, and indeed the entire DDR. The process takes place within a dynamic, multi-component protein-DNA complex. Moreover, after DSB detection by Ku, subsequent recruitment of specific end-processing factors may be determined by the nature of the lesion to be repaired, cell cycle stage and/or the type of tissue. It is so far a matter of speculation and occasionally contradicting opinions regarding the roles of some of the participants in the DDR signaling mechanism. For instance, some reports state that DNA-PKcs may only be required for a subset of the more slowly repaired and complex lesions (Reynolds *et al*., 2010), whereas ATM and Artemis are required for repair of DSBs in heterochromatic regions (Riballo *et al*., 2004; Vakoc *et al.*, 2006; Kwon *et al.,* 2008; Lieber, 2008; Kwon *et al*., 2010). As pointed by Nagasawa *et al*. (2010), there are some unsolved problems and unresolved issues in radiation cytogenetics in which they reviewed data on the roles of homologous recombination and non-homologous end joining. This is not surprising considering that some of the players such as the complex protein DNA-PKcs is such a large molecule and can undergo modifications at various sites, about 40 of which are phosphorylation sites (Davis *et al*., 2014).

Phosphoproteomic studies by different groups have identified hundreds of new DNA damage-

induced phosphorylation events in cells (Stokes *et al*., 2007; Bennetzen *et al*., 2010), and many of these are attributed to the activity of ATM in DNA damage (Matsuoka *et al*., 2007; Bensimon *et al*., 2010). However, there are likely to be functional redundancies between the kinases that modulate DNA damage-induced phosphorylation events as ATM phosphorylates the targets of DNA-PK and/or ATR and conversely, DNA-PK also phosphorylates several ATM target proteins in ATM-defective cells (Stiff *et al*., 2004; Calle'n *et al*., 2009).

A recent and surprising observation was reported regarding the activation of cellular DNA damage response (DDR) in a natural host cells (RPTE) that were infected with the BK polyomavirus (BKPyV) (Jiang *et al.,* 2012). A triple knockdown of the above three players, ATM/ATR/DNA-PKcs, did not abolish the activation of γ-H2AX during BKPyV infection. The result indicated the possibility that there may be some as yet unidentified kinases that can cause γH2AX formation in addition to these well characterized established players. Alternatively this may be a process that is unique to the BKPyV-infected cells.

Table 1.1. A summary of DDR mechanisms and components showing a few of the myriad of proteins involved.

DDR mechanism	Major lesion acted upon	Key protein components involved
Non –homologous end joining (NHEJ)	Radiation- or chemically-induced DSBs plus V(D)J and CSR intermediates	Ku and DNA-PKcs, XRCC4, XLF/Cernunnos, ligase IV. MRE11-RAD50-NBS1 complex, Artemis PNK, Aprataxin and poly μ and,λ,53BP1
Homologous recombination	DSBs, stalled replication forks, inter-strand DNA cross-links and sites of meiotic recombination and abortive Topo II action	RAD51, XRCC2, XRCC3, RAD51B, RAD51C, RAD51D, DMC1, RAD52, RAD54, BRCA2, RPA, FEN1, DNA pol and associated factors, MRN, CtIP, BRCA1, RPA and ATM signaling pathway
ATM-mediated DDR signaling	DSB	ATM, MRN and CHK2. Promoted by mediator proteins such asMDC1, 53BP1 MCPH1/BRIT1, and by ubiquitin ligases RNF8,RNF168/RIDDLIN and BRCA1
ATR-mediated DDR signaling	ssDNA resected DSB	ATR, ATRIP and RPA plus the RAD9-RAD1-HUS1 (911) complex, RAD17 (RFC1-like) and CHK1,.MRN, CtIP and mediator proteins such as TOPBP1, Claspin, MCPH1/BRIT1 and BRCA1

1.1.2: Homologous recombination repair

In contrast to NHEJ, HR is generally restricted to S and G2 phases of the cell cycle due to its dependence on and use of sister-chromatid sequences as the template to mediate faithful repair (Li and Hayer, 2008; Hayer *et al.*, 2010). Unlike in mammalian cells where HR only uses the sister chromatid restricting it to the intra- or post-replication cell cycle phases, in yeast the homologous chromosome is used allowing yeast to perform HR throughout the cell cycle. The presence of several HR sub-pathways has also been reported (Leob and Monnat, 2008), but irrespective of which pathway is followed, HR is initiated by the binding of the Mre11-Rad50-Nbs1 (MRN) complex to the free DSB ends. Subsequent resection results in 3′-overhangs that are mainly ssDNA extending over several hundred bases. These ssDNA overhangs are stabilized by the replication protein A (RPA), and subsequently replaced by the recombinase RAD51. Homology searching usually results into invasion of the homologous sister chromatid followed by DNA synthesis by DNA-polymerase δ and η using the free 3′-OH as a primer. Upon synthesis the resulting fragments undergo ligation by DNA-Ligase I and finally substrate resolution occurs with the help of the BLM helicase in complex with TopIIIα/RMI1 (Cheok *et al.*, 2005; Chu and Hickson, 2009).

Both NHEJ and HR may rely on proteins from other pathways in order to increase their efficiency and accuracy. There is accumulating evidence to show that some of the proteins that modulate mismatch repair (MMR) also participate in both HR and NHEJ (Hong *et al.*, 2008; see review by Martin *et al.*, 2010). For instance, it has been demonstrated that human MSH2-deficient tumor cell lines lose their ability to repair DSB by HR pathway as compared to hMLH1-defifcnet cell lines or MMR competent cells line (Villemure *et al.*, 2003). Another good example was shown during integration of a thymidine kinase-neomycin(*tk*-neo) fusion gene

11

construct with an *I SceI* restriction site introduced to disrupt the *neo* sequence and used to transfect either wild type isogenic or MLH-1-null mouse embryonic fibroblasts followed by selection with G418 (Bannister *et al.,* 2004). Eventually there was much lower number of stably transfected wild type MEF cells containing the constructs than the MLH-1 null cells. This may only occur because the spell-checking function of MMR modulated the NHEJ repair during integration of the fusion construct that only allowed a few of the constructs being integrated into wild type cells. Possibly because such stringent spell-checking may have been lacking in the MLH-1 null cells, a large number of the fusion constructs were able to be integrated into the genomic DNA of the host cell, with all attendant errors. This may indicate that HR and NHEJ pathways of DNA damage may rely on or work hand-in-hand with the other pathways to achieve DDR and efficient DSB repair.

1.2: Low-Dose-Rate Irradiation Protocol: Rationale for Its Preferential Use

In the past, lower dose-rate irradiation was not widely used for two important reasons: first a number of such early radiation studies were either limited by available tools to deliver such a low dose, or they were poorly designed such that reduced dose-rates delivered to the same total dose as acute dose rates were less effective in producing tumor regression. Secondly and more importantly, there was lack of any good understanding of the mechanisms by which lower dose rates induce cell death as well as other relevant endpoints (Gridley *et al.,* 2005).

As time went by and beginning as early as the 1960s, more studies highlighted important observations of the sparing effect of low-dose-rate (LDR) radiation exposures, among which were reports of studies involving HeLa cells that were also shown to accumulate in the G2 phase

of the cell cycle during LDR exposure (Bedford and Hall, 1963; Hall and Bedford, 1964; Bedford and Mitchell, 1973; Mitchell and Bedford, 1977). In one such study, it was noted that as the dose rates were lowered and the exposure times extended, the adverse biological effects were reduced, giving the cells more opportunity to repair any damage to the DNA (Bedford and Hall, 1963). Following these intriguing observations, which both perplexed and excited other researchers from radiation oncology point of view, three interesting points were brought to the fore as was elaborated and summarized in a review (Williams *et al*., 1998). First, it was observed that low-dose/low-dose-rate irradiation could be more effective in killing tumor cells than high dose-rate irradiation under certain conditions. Secondly, it was noted that lower dose irradiation delivered over an extended period of time may preferentially sensitize neoplastic cells to a subsequent high-dose-rate exposure, and finally, it was reported that low-dose/low-dose-rate radiation could induce radioresistance in some normal cells (Azzam *et al*., 1996) At lower dose-rates, cell proliferation is reported to continue during the irradiation with the ultimate outcome being a complex functional interplay of cellular radisensitivity, dose/cell cycle and tissue adaptability (Hall, 1971). These observations were attributed to a number of dose-rate dependent effects on biological processes that are critically relevant to cell survival, which processes include induction of altered gene expression, sub-lethal damage repair, potentially-lethal damage repair, induction of perturbation in cell cycle redistribution and susceptibility to apoptosis, among others, all of which tend to favor normal cell survival and neoplastic cell demise.

It was also demonstrated using mammalian cells that significant reduction in radiosensitivity of normal cells could be achieved by continuous LDR exposure than for acute exposure (Stackhouse and Bedford, 1993a, 1993b). A previous study had observed that there is a limit to

the effective dose rate that achieved the reduction in radiosensitization of normal mammalian cells (Wells and Bedford, 1983). For instance, a study on the protective effects of low-dose/low-dose-rate fractionated exposures demonstrated a reduction in the risk of cancer formation in *Trp53* normal or cancer-prone *Trp53* heterozygous female C57BL/6 mice that were exposed 5 days/week to single daily doses (0.33 mGy, 0.7 mGy/h) totaling 48, 97 or 146 mGy over 30, 60 or 90 weeks (Mitchell *et al.,* 2008). One clear outcome from the study was that the induction of protective response can only be beneficial within a defined dose range. It showed that there are upper dose thresholds above which protective adaptive responses do not occur and adverse effects may outweigh the benefits and that there are similar lower dose thresholds that must be exceeded to induce protective effects *in vivo.*

Many studies in patients receiving various TBI regimens as a component of bone marrow or stem cell transplantation protocols have generally supported use of LDR or increased fractionation as a means to minimize normal tissue toxicities, increase the total dose of radiation that can be safely delivered, and improve tumor control (Evans, 1983; Regnier, 1992; Corvo *et al*., 1999; Gopal *et al*., 2001; Song *et al*., 2003).

It was proposed in one early study that radiation-induced lung toxicity may be ameliorated by the use of continuous protracted or fractionated radiation, since repair of sub-lethal damage is greater for the lung and GI tract than for hematopoietic tissue (Dutreix *et al*., 1981). A continuous increase in normal tissue tolerance was observed for early radiation-induced pneumonitis with decreasing dose rate, but a less pronounced sparing effect was noted for late complications.

It is however important to note that responses to low dose rate irradiation differ in cultured cells

and under *in vivo* conditions. For instance, when similar measurements were performed in cells isolated from patients undergoing computed tomography (CT) examinations where the practically undergo *in vivo* irradiation and repair, the few induced DSBs were efficiently repaired and levels returned to the basal level within 24 h (Löbrich *et al.,* 2005). The outcome was different for cultured normal human cells where induction of extremely low levels of DSBs by IR doses in the mGy range such as those used in CT scanning showed that DSBs remained unrepaired for many days after the exposure, which was attributable to a probable lack of efficient DNA damage recognition and repair under *in vitro* condition (Rothkamm and Löbrich, 2003, Grudzenski *et al.,* 2010).

These observations and similar others are of significant clinical implications regarding the role of tissue microenvironment in response to IR. Such inconsistencies between *in vitro* and *in vivo* data highlight the importance of *in vivo* studies, and call for rational considerations when using the results of such experiments for application in human radiological risk assessments and/or estimates. As stated by Gridley *et al*., (2005). Important observations that have emerged from several reports point to the same universal outlook, namely, that simplistic extrapolation from data obtained *in vitro* is not sufficient to predict the outcome *in vivo* and that comprehensive evaluation of new treatment options in animal models is essential before contemplating translation to the clinic (Gridley *et al.,* 2010).

That is not to discount the use of *in vitro* assay results since these could provide very useful data that will lay good foundations upon which study protocols could be designed to obtain reliable *in vivo* results. For instance, a study using continuous LDR exposure was able to distinguish

between normal *Atm+/+* and heterozygous *Atm+/-* individuals that could not be apparent when acute exposure was used, showing the obvious advantage LDR exposure has over acute exposure (Blocher *et al*., 1991). Similar outcomes were reported from an *in vitro* assay where the use of a 1-Gy single acute (high-dose-rate) γ-ray dose delivered to non-cycling contact-inhibited monolayer cells had clear differences between normal individuals (*ATM+/+*) and probands (*ATM-/-),* but no clear distinctions were seen between *ATM+/+* and *ATM+/-* (Kato *et al.,* 2006). When 24 h of continuous LDR irradiation was used at a dose rate of 10 cGy/h, appreciable differences were observed for individuals of known ATM genotypes, i.e. *ATM+/+* compared with *ATM+/-*individuals.

It must be noted too that these responses and beneficial or detrimental effects of LDR exposures were not universal as demonstrated in the C57BL/6 *TP53* study mentioned above where adverse effects were not seen for other tumor types (Mitchel *et al*., 2008, 2013). Similarly protective effects were reported to be lost when the exposure is extended beyond some period, pointing to that fact that every situation must be assessed on a case by case basis. These variations in the outcomes or endpoints have lately been reviewed by Mitchel (2015), pointing out the dose limitations and procedures used for radiation protection in the nuclear industry and regulatory assumptions upon which they are founded. It provides useful information on cellular and animal studies showing the influence of radiation-induced protective effects on diverse diseases, and that the radiation dose range for effective IR outcome is tissue type-dependent even in the same animal and, in the case of active disease the time of intervention also matters (Mitchel *et al*., 2013; Mathias *et al*., 2015).

A number of pre-clinical reports involving different types of tumors indicate that LDR total body irradiation (TBI) can significantly delay tumor growth (Anderson *et al*., 1982). In one study there was decrease in the incidence of lung metastases (Hosoi and Sakamoto 1993) and in another a decrease in the incidence of spontaneous lymphoma was observed (Ishii et al, 1996b). The use of 0.15-0.20 Gy total body irradiation (TBI) also suppressed lung metastasis and induced long-term remissions in chronic lymphocytic leukaemia (CLL) and non-Hodgkin's lymphoma (NHL) (Hosoi, (2006). To date however, there is still no unified agreement as to the precise and exact mechanism by which radiation dose rates influence some of these processes, while for some tumor types, the whole process leading to the disease outcome remains unknown (Mitchell, 2015).

From the results of various studies and observations, low dose rate radiation exposure followed by immediate quantification of repair foci in exposed cells provides a much more sensitive assay for DNA DSB repair efficiency than time-delayed measurements after acute high dose rate exposures, which have been the cornerstone of radiation experiments. Based on these observations from the various studies, the present study has been rationally designed to use the continuous low dose rate protocol to assess the differences in the response of a set of strains of mice known as CcS/Dem recombinant congenic strains (RCS) developed by the Demant group (Demant and Hart, 1986) and will be described in details later in section 1.7 of this chapter.

1.3: Biological Consequences of Ionizing radiation: Repair of Complex DNA lesions

About 80% of DNA lesions induced by sparsely ionizing radiation are reported to be complex clusters of bi-stranded (on opposing strands) and tandem (on same strand) non-DSB lesions

(Magnander *et al.,* (2010; Georgakilas *et al*., 2013). Earlier researchers and medical workers found out soon after the discovery of ionizing radiation and its use in medicine that it could also have detrimental effects on tissues and organs. This became a concern in radiotherapy or in situations where accidental exposure may occur, as various reports showed (West and Bonner, 1980; Mannironi *et al*., 1989; deLara *et al*.. 1995). Thus, radiation is a double-edged sword that can both treat and cause disease. An unqualified statement can be made that the most severe damage to cells by ionizing radiation is through the direct and indirect damage to the DNA helix by the high-energy particles or the photons that shatter the chemical bonds of the DNA backbone. The size and extent of the resulting lesions differ widely depending on the dose and quality of the radiation. If not repaired properly the damage can result in genomic instability and consequently tumor formation.

DNA damage can occur through direct interaction with radiation in which a base or bases are extracted creating apurinic/apyrimidinic (AP) sites in the DNA rungs. Alternatively lesions resulting from DNA-protein or DNA-DNA covalent bindings result in rigid crosslinks that can render the DNA molecule non-functional. Fortunately, cells have endogenous free radical scavengers to mitigate the extent of the damage as well as some intrinsic states of chromatin structures that act as inbuilt determinants of the cell's scavenging capacity (Magnander and Elmorth, 2012).

The mechanism and effects of ionizing radiation in causing DNA damage usually vary depending on radiation quality and ionization density. Damage is usually caused due to effect of the linear energy transfer (LET) capacity of the ionizing radiation resulting in direct hit on the

DNA, as opposed to the indirect oxidative stress-induced DNA damage usually caused by free radicals formed during metabolic reactions. The radicals act by ionizing water molecules and solvents in the immediate vicinity/environment of the DNA. The major outcome of direct hits that cause radiation-induced DNA damage is usually complex DNA lesions, like double-strand breaks (DSB) and clustered damage in which two or more lesions are formed within two helical turns. The damage to DNA may be non-DSB clustered lesions or single DSBs. High LET radiation damage is mainly clustered lesions where two or more DSBs are present in close proximity or in combination with other lesions (Magnander and Elmroth, 2012).

The integrity of the entire DNA is usually dependent on the intact complete turn of the helix made of the 10 base pairs in the turn. The main mechanism of by which DSBs arise can be explained in energy terms (van Der Schans, 1987). Since the energy of the hydrogen bonds between the bases is what helps to hold the DNA strands together, these will not be able to withstand the distortions that result when the phosphodiester bonds between the sugar backbones are broken on both strands within a distance of 10-20 base pairs and this discontinuity of the sugar-phosphate backbone gives rise to a DSB. This results in relaxation of the chromatin structure and changes in topological organizations which affects the integrity of the entire DNA and chromosome.

A study by Rothkamm and Löbrich (2003) established that DSB are induced linearly in direct correspondence with dose. Different methodologies so far used to measure the relationship between DSB and radiation dose give similar yields for DSB induced in cells for sparsely ionizing radiation, results of which show that for different cell types, the typical number of DSB

induced per Gy is usually in the range of 20-35. Their findings were similar to those observed by other investigators (see review by Prise *et al*., 1998; Magnander *et al*., 2010; Claesson *et al*., 2011).

Earlier reports had indicated the important roles of scavenging molecules within the cells on the number and extent of DSBs (Oleinick and Chiu, 1994; deLara *et al*., 1995). Subsequently it was shown that the important role played by scavengers goes hand-in-hand with contribution by the structure of the chromatin itself in determining the number of DSBs (Magnander *et al*., 2010; Magnander and Elmroth, 2012). According to these observations or findings, the greater the concentration of scavengers, the fewer the radicals formed in or close to the DNA and conversely, the lower the scavenging capacity of the cell and the more open and relaxed the chromatin, the higher the number of DSBs induced.

The response and the distribution of the DSBs is also very highly dependent on the quality of the ionizing radiation, which in turn determines the LET delivered as well as the amount of energy deposited in the cells or tissues. Sparsely ionizing radiations such as photons or electrons usually induce breaks that are randomly distributed within the nucleus, with random sized DNA fragments in mammalian cells. However, when the ionization density is increased by using alpha particles and heavy ions, the size distribution of DNA fragments after irradiation are no longer random within the nuclei. Rather, there is excess of short DNA fragments with corresponding breaks that are concentrated along the particle tracks. High-LET radiation is now known to induce up to 3.5 times more DSB per Gy compared with photons when shorter fragments are included in the assay (Mannironi *et al*., 1989; Prise *et al*., 1998; Claesson *et al*., 2011). The

radio-response and formation of DSB is also cell cycle dependent and differs between proliferating and non-cycling cells for both low- and high-LET radiation (Claesson *et al.*, 2011). Therefore when reporting the response to ionizing radiation, all these factors need to be taken into consideration and stated clearly for a more accurate analysis and interpretation of the results.

1.4: The Role of Histone H2AX in DNA Damage Response

The structure of chromatin has a major impact on DDR and is itself greatly modified in response to DNA damage (Rogakou *et al.*, 1998; 1999). The best characterized example of changes in chromatin structure is the ATM/ATR/DNA-PK-mediated phosphorylation of serine-139 of the histone H2A variant, H2AX, on chromatin flanking DSB sites. The direct results of histone H2AX phosphorylation (to form γ-H2AX) are thought to include ubiquitin-adduct formation in the affected and modified regions, as well as the recruitment of other DDR factors that have chromatin-modifying abilities (Fernandez-Capetillo *et al.*, 2004). All these chromatin changes together are thought to contribute towards amplifying DSB signaling (Thiriet and Hayes, 2005) and to promoting efficient DSB repair (Bonner *et al.*, 2008). The major role of γ-H2AX appears to help in relaxing chromatin and in maintaining its de-condensed state (Kruhlak *et al.*, 2006). This should allow other players in the DSB repair process to occupy their rightful functional domains to achieve a successful repair. There is some evidence that ATM activation leads to chromatin relaxation at sites of DSBs (Kuhne *et al.*, 2004) and H2AX tyrosine-142 phosphorylation was recently shown to function in DDR (Xiao *et al.*, 2008). From all the emerging research it is apparent that the major players in the DDR are multifunctional and it therefore seems likely that further DDR-induced chromatin modifications await discovery. Overall, different types of post-translational modifications of different proteins are the major

driving forces governing chromatin remodeling (Strahl and Allis, 2000). These modifications are essential for the processes that lead to DDR and DSB repair. In the present study described in this dissertation, detection of γ-H2AX^{Ser139} is the core procedure used to accomplish the work.

1.4.1: Historical Perspective

Previously, researchers noted that the bulk of mammalian H2A histones that are usually visible when run on an SDS gel of total cell extracts belong to the H2A1 subfamily. However, two other subfamilies H2AX and H2AZ each of which constitute about 10% of the total H2A were detected (West and Bonner, 1980). The H2AX and H2AZ homologues have been present throughout eukaryotic evolution but little attention was paid to them earlier on. It is now well-known that budding yeast also contains three H2A species; the two most plentiful being members of the H2AX subfamily, while the other is a member of the H2AZ subfamily (West and Bonner, 1980).

From these observations, Bonner and group surmised that these complexities of the H2A protein family suggested that histones may perform novel and unforeseen roles in chromatin. Using the human H2AX cDNA sequence, they found out that the human C-terminal protein sequence KATQAS^{139}QEY was similar to the C-terminal sequence KATKAS^{129}QEL reported for budding yeast H2A1. The finding demonstrated that higher eukaryotes contain H2A species with a C-terminus very different from that of their major H2A species but at the same time there is striking homology with that of major yeast H2A as later on seen by Mannironi *et al.*, (1989). However, the formation of ionizing radiation-induced foci (IRIF) at damage sites (see reviews: Bekker-Jensen and Mailand, 2010; Belyaev, 2010) first came to light after human cells were

subjected to immunofluorescence staining with antibodies specific for RAD51 (Haaf *et. al.,* 1995) or components of the MRN complex (Maser *et. al.*, 1997).

Based on that knowledge, the Bonner group started their quest to determine the exact location of γ-H2AX molecules within the cells induced to undergo DSBs, and, equipped with the generated antibody specific to the C-terminus of human γ-H2AX (which they termed anti-γ), they demonstrated that mammalian H2AX was extensively phosphorylated in cells within minutes after ionizing radiation-induced DNA DSBs. The group coined the name γ-H2AX for this phosphorylated mammalian H2AX species which they noted had its phosphorylation site localized to Ser^{139}, and that hundreds to several thousand H2AX molecules became phosphorylated over large chromatin domains surrounding the DSBs up to about 2Mb pairs of DNA on either side of the break point (Rogakou *et al.*, 1998; Wang *et al.*, 2005; Rodriguez *et al.,* 2006). Moreover, it was soon noticed that although histone H2A.X is expressed throughout the cell cycle and deposited all over the chromosomes, its phosphorylation occurred preferentially at sites that flank double-stranded breaks (Rogakou *et al.*, 1999).

1.4.2: Practical and Clinical Implications

Since many researchers now use the appearance of γH2AX as small punctate foci within the nuclei of cells exposed to ionizing radiation to demonstrate the presence of DSBs, there is a need to understand many other aspects of this important molecule in order to guide practical applications for research and clinical purposes. Based on the use of kinetic experiments, it became known that γH2AX foci appear within a few minutes of irradiation and some foci grow for about 30 minutes to diameters of up to 0.5 µm. The foci appear to be unchanged in number

during the first 60 minutes after irradiation but they undergo progressive decrease in numbers thereafter (Rogakou *et al*., 1999).

However, these observations may not or do not always apply in every situation since the kinetics of DSB repair are now known to be cell type-dependent. Following those initial observations, techniques were improved and numerous other proteins are now known to be localized in the nuclear foci at the sites of DSBs (Bhogal, *et al.,* 2009; review by Jeggo and Lavin, 2009; review by Thompson, 2012).

The activation and successful accomplishment of DNA damage signaling and repair mechanisms that occurs in response to ionizing radiation involve a large number of proteins and repair factors. So far, three major kinases are known to mediate the formation of γH2AX, namely: ATM, ATR and DNA-PK that are members of the phosphoinositide 3-kinase-related kinase (PIKK) family. The major drivers of DDR following DSB appear to be ATM and DNA-PK which seem to function redundantly to activate and modulate IR-induced γH2AX formation (Stiff *et al*, 2004; Wang *et al*, 2005). ATR on the other hand appears to function in γH2AX formation mainly at sites of replication-associated breaks (Furuta *et al*., 2003) and is probably responsible for the presence of γ-H2AX foci in non-irradiated control samples. The formation and loss of γH2AX foci has been measured following exposure to radiation doses as low as 1mGy, and foci yields have been shown to increase linearly with dose (Rothkamm and Lobrich, 2003).

It is therefore clear that any factor/factors that interfere with or compromise the function of any

of the many DSB repair proteins can lead to defective DSB rejoining causing retardation in the rate of γ-H2AX foci loss (Rogakou *et al*., 1999; Rothkamm and Lobrich, 2003; Rothkamm *et al*., 2003; Li *et al*., 2003; Kuhne *et al*., 2004). These results suggest a close one-to-one relationship between the initial and residual radiation-induced DSBs and γH2AX foci and this is what forms the core of the approach used to evaluate the correlation between the reported lung tumor incidence (Szymanska *et al*., 1999), and the radiation-induced γ-H2AX foci numbers presented in this dissertation. This is because the more inefficient the repair as indicated by persistent γ-H2AX foci, the more likely transforming mutations that will lead to carcinogenesis.

It has also been reported that H2AX accounts for about 2% of the total H2A family (in lymphocytes and HeLa cells) (Takahashi and Ohnishi, 2005) to as much as 20% in human cells (Celeste *et al.,* 2002), but its expression level seems to be a very critical factor in DNA damage response as it was noted that the loss of just one H2AX allele in p53$^{-/-}$ mice caused a dramatic increase in the onset of tumor, both the time it takes for the tumor to appear and the increase in incidence (Celeste *et al*., 2002; Bassing *et al*., 2003). Cells derived from H2AX knock-out mice were observed to be radiosensitive and show reduced capacity to repair DSBs. In this context therefore, any interpretation of reduced γH2AX foci number should be made with care, as it may not necessarily be due to malfunction or deficiency of the many kinases and other factors involved in DDR, but may be due to deficiency of H2AX itself. The many functions that have been suggested to be performed by H2AX are all related to DNA damage response. The H2AX$^{Ser-139P}$ is thought to act as a chromatin anchor helping to prevent the dissociation of break ends and enhance the fidelity of DSB repair (Bassing and Alt, 2004; Fernandez-Capetillo *et al*., 2004; Soutoglou *et al*., 2007). It may perform this function in conjunction with Ku proteins to

prevent the broken DNA ends from flaying apart. It is also suggested to participate in chromatin remodeling to assist DSB processing (van Attikum and Gasser, 2005), and in concentrating DNA damage signaling and repair proteins at DSBs, in which case γ-H2AX can be envisaged to act as a scaffold where other repair factors dock (Kinner *et al*.,2008). Other functions of H2AX were suggested to include helping with signal amplification and transduction to enhance the sensitivity of the DNA damage-induced cell cycle checkpoint for cells that sustain DNA damage during G2 phase (Fernandez-Capetillo *et al*., 2002). For DSBs that undergo repair through an Artemis-dependent pathway, H2AX is reported to participate in the molecular activities required for the processing of such radiation-induced DSBs (Riballo *et al.*, 2004). Additionally, H2AX is reported to help in recruitment of cohesin during DSB HR repair (Lowndes and Toh, 2005). Clearly, just as the kinases and other repair factors play fundamental roles in DDR, H2AX is not the odd one out as far as apparent multi-functionality is concerned.

1.4.3: Measurement of DNA DSB

The quest for methods to measure DSB originated from results of research begun in the 1980s that suggested direct correlation between DSB and cell death and it became generally accepted that because of its complexity and its cytotoxic effects, DSB is the most biologically important form of DNA damage. Methods started with the use of electrophoretic techniques and, with its improvement, it became possible to separate DNA fragments and the amount of extracted DNA corresponding to the number of breaks induced could then be easily quantified. In a recently reported case (Magnander and Elmorth 2012), further development of this method has also made it possible to analyze the size distribution of the resulting DNA fragments, important for a more correct determination of DSB induced by densely ionizing radiation, outlined in previous reports

(van Der Schans, 1987; Rydberg 1996).The use of phosphorylated histone H2A variant X, (known as γ-H2AX) for investigating the formation of and DSB repair process is now a well-established method. This is done either by direct microscopic detection of repair foci in individual cells or by indirect assessment using flow cytometry. It was demonstrated in studies in the last two decades that histone H2AX is rapidly phosphorylated at Serine 139 in response to DSB (Rogakou *et al*., 1999; Burma *et al*., 2001),). The methods developed by Horn *et al*., (2011) have been adopted by major international laboratories as a standard for determining radiation exposure. By using labeled antibodies against γ-H2AX, many investigators use immunofluorescence techniques routinely to detect foci in irradiated cells to confirm the presence of DSB formation and repair in progress at specific time-points. Through calibrated measurements and from the size of the histone relative to the length of linear DNA, it is now known that the phosphorylation process occurs on histones thousands to millions of base pairs (~2Mbp) flanking the site of the actual lesion as was first reported by the Bonner group (Rogakou *et al.,* 1998, 1999).

An important caveat is worth pointing out though. It has been demonstrated that phosphorylation of H2AX can occur in response to other processes such as V(D)J (variable, diversity, joining) recombination (Chen *et al.,* 2000) and replication stress (Ward *et al.,* 2001). Since the foci represent a signal rather than actual DNA fragmentation, and because processes other than DSB repair that can lead to foci formation, interpreting data from measurement of γ-H2AX foci has to be done with a lot of caution. Accordingly, the method is often combined with detection of other proteins activated at sites of DSB, e.g. 53BP1, and analysis of co-localization between several participating proteins are called for to give more reliable data. Because of this consideration,

preliminary experiments were performed as described in this dissertation to ensure reliable results.

1.5: The roles of other molecular players in DNA damage response

As stated above, there are many molecular players in the DDR and DNA repair. Ataxia telangiectasia mutated (ATM) as well as the related kinase ATM and Rad3-related (ATR), both activated by DNA damage, are among the many components of DNA damage signaling in mammalian cells. The former is regulated by the MRN complex that senses double strand breaks (DSBs). Single strand DNA (ssDNA) that is generated by processing of DSBs, as well as ssDNA present at stalled replication forks is reported to be sensed by ATR in collaboration with its interacting partner, the ATR-interacting protein (ATRIP) (Cortez *et al.*, 2001; Zou and Elledge, 2003). The topological distortions caused by DSBs and replication protein A (RPA)-coated ssDNA are the major signals that trigger the recruitment of the two kinases (Ball *et al.,* 2005; Falck *et al.,* 2005). Both kinases phosphorylate proteins to initiate a signaling cascade involving many common substrates among which are the checkpoint kinases Chk1 and Chk2, which latter are reported to initiate a secondary wave of phosphorylation events to amplify and extend signaling. In a review by Shiloh (2003), as many as 25 ATM and ATR substrates have been identified, the majority of which are candidates based on known roles in damage signaling.

Previously, it was very difficult to tease apart the network of substrates and components of the DDR, but newer methods based on peptide IP with phosphotyrosine antibodies and mass spectrometry (MS) helped to unravel the mysteries and created the first steps towards identifying the substrates of these tyrosine kinases (Ziv *et al*., 2006). Based on such techniques, ATM and

ATR are now known to share some degree of substrate specificity, as they both recognize Ser-

Gln (SQ) and Thr-Gln (TQ) motifs (Matsuoka *et al.,* 2007), and antibodies to phospho-SQ or

phospho-TQ sites have enabled identification of a few ATM substrates by protein IP (Matsuoka

et al., 2007; Stokes *et al.,* 2007).
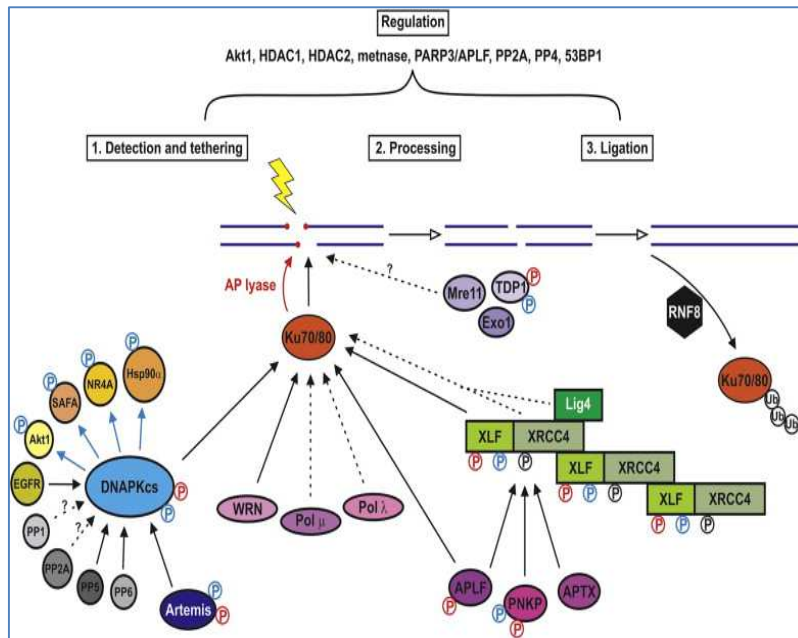
Figure 1.1. A simplified representation of the NHEJ pathways conveniently divided into i) end detection and tethering, ii) processing and iii) ligation, together with the multiple proteins thought to be involved in making the process successful. (Adapted from Wang and Lees-Miller 2013).

1.6: The Lung: Anatomical Perspective and Cell Types of Interest in Lung Cancer.

The adult lung is a structure with complex anatomy and a large number of cell types present at

varying frequencies according to the anatomical region of the respiratory system (Bertoncello

and McQualter, 2010). The trachea and mainstem bronchi that constitute the cartilaginous

airways have luminal epithelium consisting of two main columnar cell types: ciliated cells and

Clara-like cells. Ciliated cells are terminally differentiated and do not have self-renewal capacity,

while the Clara-type cells that produce different types of secretoglobins, the most abundant of

which is Scgb1a1, or CC10([Rawlins *et al*., 2007 ; Rawlins and Hogan, 2008). The epithelium of the more distal airways that consist of small bronchi and bronchioles, contain mainly columnar cells. Here, Clara cells predominate over ciliated cells and there are more neuroendocrine cells than in the trachea. The most distal region of the lung is organized into a complex system of alveoli consisting of alveolar type I cells (AEC I or AT1), the respiratory epithelial cells that provide thin-walled gas exchange surface, and cuboidal alveolar type II cells (AEC II or AT2) with surfactant-filled secretory vesicles that contain surfactant protein C (SP-C). The transitional region between the conducting epithelium in the terminal bronchioles and respiratory epithelium in the alveoli is known as the bronchio-alveolar duct junction (BADJ) (Rawlins and Hogan, 2006; Kim *et al*., 2005). These different regions of the lung are likely to use different progenitor cells for maintenance and repair. Studies that have examined the turnover of the linings of tissues and organs such as the intestine or the skin have shown that the adult lung has a slow rate of turnover compared to these other tissues. There is evidence that the basal cells of the lungs also possess regenerative potential in the proximal airways that give rise to basal cells, Clara cells and ciliated cells (Hong *et al.,* 2004). Being continuous with the external environment, the lungs are not any less constantly exposed to potential toxic agents and pathogens present in the environment than the skin or the intestines. It must therefore be able to respond quickly and effectively to cellular damage or loss, and the latter requirements suggest there must be some lung stem/progenitor cells to help regenerate damaged epithelial cells.

Lung cancer is among the leading causes of cancer deaths worldwide with the five-year survival being only about 15 per cent (Howlader *et al.*, 2008; Jamal *et al.*, 2011; ACS, 2012; NCHS, 2013, ACS, 2014). Lung cancer is reputed to be responsible for more deaths than prostate, colon,

pancreas and breast cancers combined. The latest estimate figures for the USA help to show this grim picture (Table 1.2).

Table 1.2: Estimated new cancer cases and deaths by the lapse of the current year 2014: top 10 cancer types and the top 10 causes of cancer-related deaths in the US.

Rank	Cancer Type	Estimated Cases (%)	Rank	Cancer Type	Estimated Mortality (%)
1	Prostate	14.0	1	Lung	27.2
2	Breast	14.0	2	Colorectal	8.6
3	Lung	13.5	3	Breast	6.8
4	Colorectal	8.2	4	Pancreas	6.8
5	Melanoma	4.6	5	Prostate	5.0
6	Urinary Bladder	4.5	6	Leukemia	4.1
7	Non-Hodgkin Lymphoma	4.3	7	Liver	3.9
8	Kidney	3.8	8	Non-Hodgkin Lymphoma	3.2
9	Uterine	3.2	9	Urinary Bladder	2.7
10	Leukemia	3.1	10	Esophagus	2.6

Adapted from: Cancer Facts & Figures 2014, American Cancer Society

Efforts towards the improvement of clinical outcomes therefore require a better understanding of the normal lung and the biology and mechanisms of lung tumor formation. As a result of concerted research, there is now better knowledge of the histopathology of different tumor types which have formed the standard for similar classifications. On that basis, lung cancers in humans are now divided into distinct but broad histopathological classes: small cell lung cancer (SCLC) which constitutes up to 20% of all lung cancers, and non-small cell lung cancer (NSCLC) making up about 80% of all lung cancers. The latter have been further subdivided into adenocarcinomas, squamous cell carcinomas, bronchio-alveolar carcinomas and large cell carcinomas (Bhattacharjee *et al*., 2001; Travis *et al*., 2002; Hayes *et al*., 2006; Sun *et al*.,2007). Small cell lung cancers are predominantly located in the bronchioles.

Squamous cell carcinomas are thought to originate from the proximal airways, while the

progenitors of adenocarcinomas, the most common type of lung cancer, are more frequently detected in the distal bronchioles that contain the conducting epithelial cells, and in the terminal alveoli that are lined with respiratory epithelial cells. It is also a matter of speculation that these different subclasses arise from distinct cells of origin localized within defined regional compartments (Giangreco *et al.*, 2007; review by Asselin-Labat and Filby, 2012; Farago *et al.*, 2012). Improved attempts to isolate and properly characterize stem/progenitor cells in the different compartments of the lung will enable further evaluation of their respective roles in tumor initiation so as to form a consensus appropriate for tailor-made solutions.

Just as our understanding of lung stem cell biology is limited, the identity of the cell of origin in lung tumorigenesis is not known with any certainty. Most adenocarcinomas display Clara or Alveolar Type II (AT2) cell markers and are generally peripheral or are found within the luminal portions of the bronchus. Previously, AT2 cells were implicated to be the target cells in rodent and human lung adenocarcinomas and a consequent study did show that adenocarcinomas were found to be positive for the AT2 cell-specific marker, pro-surfactant apoprotein-C (SP-C) (Jackson *et al.,* 2001). Other murine models and human specimen had also led to implication of Clara cells as the origin of adenocarcinomas. In the study by Jackson *et al.* (2001), cells which the authors referred to as double positive cells (DPCs), as they expressed both SP-C and the Clara CCA (also known as CC10 or CCSP), were found in adenomas, particularly in lesions continuous with bronchiolar hyperplasia. The counterparts of these DPCs or cells that showed very similar properties as the DPCs are reported to exist in normal lung at the BADJ where they function in lung homeostasis and possess characteristics of regional stem cells.

Available data suggest that there are bronchio-alveolar stem cells (BASCs) that play a role in both bronchiolar and alveolar cell injury repair and homeostasis (Kim *et al.,* 2005). These authors used the Sca-1^{pos} CD34^{pos}CCA^{pos} cells as the markers for BASCs to demonstrate that these cells were located exclusively at BADJ, showing that a regional stem cell population is likely present in the distal lung of mice. There were already evidence from different earlier studies that support the presence of BASCs at the BADJ and these were based on the use of BrdU^{pos}CCA^{pos} cells during early airway renewal (Reynolds *et al.,* 2000a; Reynolds *et al.,* 2000b; Hong *et al.,* 2001; Giangreco *et al.,* 2002). The locations of these makers were precisely where the BASC were later identified by Kim *et al.* (2005). Many other studies too have provided evidence for BASCs as bona fide stem cells that share characteristics with previously defined adult stem cell populations (Chiasson *et. al.,* 1999; Doetsch *et.al.,* 1999; Johansson *et. al.,* 1999; Tropepe *et al.,* 2000; Kruger *et al.,* 2002; Morris *et al.,* 2004; Blanpain *et al.,* 2004). It became part of our interest to see how the different cell types respond to ionizing radiation and consequently they were all analyzed based on their known location and not necessarily using any specific makers. The different cell types based on known locations are presented in Fig 1.2.
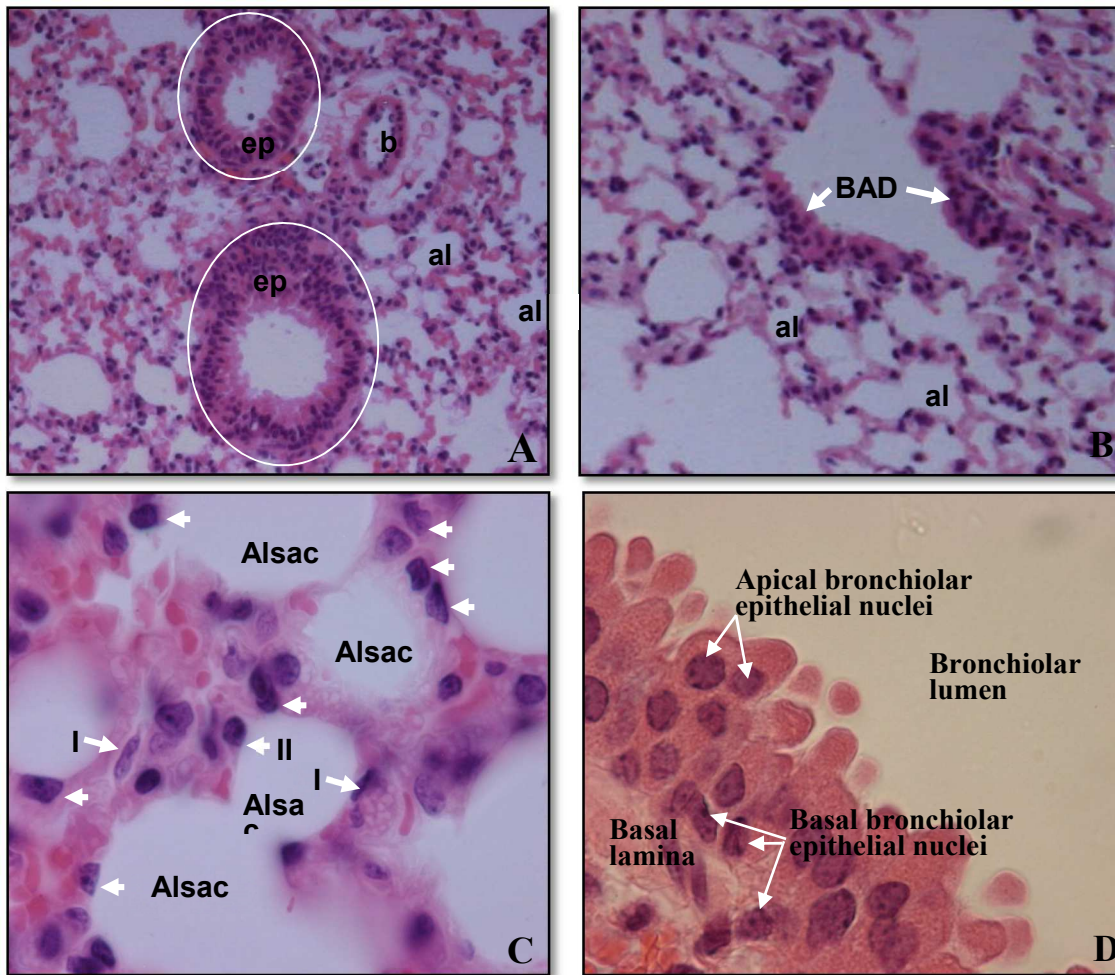
Figure 1.2: Major anatomical features of the lung relevent to the dissertation study: **(A)** a cross section of the lung showing the bronchiolar epithelia, **ep** (rings) with surrounding alveolar sac structures (**al)** and blood vessel (**b)**; **(B)** terminal bronchiole with bronchio-alveolar duct juction (BADJ) and surrounding alveolar sac structures; **(C)**, alveolar sacs (**Alsac**) with surrounding alveloar cells showing type I (arrows) and type II (arrow heads) pneumocyte (alveolar cell) nuclei; **(D)**, bronchiolar epithelium with the major components of interest indicated.

1.7: Recombinant Inbred (RI) and Recombinant Congenic Strains (RCS) of Mice: Useful Tools to Dissect Phenotypic Correlations and Explore Responses to Ionizing Radiation

The laboratory mouse has proven to be an excellent tool for dissecting complex genetic pathways

that control lung tumorigenesis, as well as other types of tumors that are common to both mice

and humans. In an extensive review Demant (2003) described how the use of segregating crosses

between susceptible and resistant mouse inbred strains or recombinant congenic (RC) strains has led to the mapping of over 40 lung cancer susceptibility loci in mice. The tumors developed as a result of induction using the highly potent mutagens N-ethyl-N-nitrosourea (ENU) and urethane.

In previous years, considerable progress was achieved in mapping genes that control disorders in humans, which eventually led to successful positional cloning of the responsible gene (Collins, 1992). These successes were largely restricted to single gene mutations, which are often relatively rare. It soon became apparent that the genetic control of susceptibility to many common diseases, including cancer, is multigenic and hence very difficult to analyze in that way (Risch, 1992). The need for a different approach led to the "candidate gene" approach being developed to map the genes relevant for the studied trait first in the mouse, and subsequently use the information about homology of chromosomal regions between mouse and human to study the relevant region in humans (Nadeau, 1990, Kwon and Goate, 2000). This approach relied on prior knowledge of the biology, physiology or functional characteristic of the condition being explored and where the risk is small. Currently the genome wide association and quantitative trait loci approaches have superseded it.

By then, the Demant group had already started to develop a novel genetic tool for the mapping and studying genes controlling such multigenic quantitative traits in the mouse, with subsequent development of the recombinant congenic strain (RCS) series consisting of different sets (CcS/Dem, OcB/Dem and HcB/Dem). Each set is made up of approximately 20 different strains, and because of the breeding technique used, every individual strain has about 12.5% genes from a common "donor" inbred strain, and the remaining 87.5% genes from a common "background"

inbred strain (Demant and Hart, 1986). Their reasoning that formed the basis for this type of breeding is that, consequently, the non-linked genes of the "donor" strain involved in multigenic control of complex traits are likely to be distributed into different RCS, where they can be mapped and studied separately or their phenotypes become distinct. In this way, the multigenic difference between the donor strain and background strain becomes transformed into a set of single gene differences between the background strains on the one hand, and individual RCS on the other (Groot *et al.,* 1992).

There are other ways to generate congenic strains too as illustred by the approach to select for desired traits. This can be achieved through a prototypic strategy where a single mouse was used to sire each generation using criteria designed to select against the transmission of chromosomes, other than the one containing the replacement genomic region (Weil *et al.,* 1997). This chromosome elimination strategy can result in up to over 16 chromosomes free of donor DNA in mice of the third backcross (N3) generation.

To date a number of RCS series have been developed, not only by the Demant group, but in a number of laboratories including the Jackson laboratories (Reifsnyder and Leiter, 2001), Charles River Laboratories, L'Arbresle, France (Burgio *et al.,* 2007), and McGill University (Fortin *et al.,* 2001), among others. However, whatever the source of background and donor founder parents, each of the RCS series was developed to explore specific phenotypic traits but all were developed and work on the same principle. The founder strains are always on the opposite ends of the spectrum with reference to the phenotype being investigated. The donor strain is usually resistant and the recipient (background) is usually the susceptible phenotype.

Three series of RCS were produced by the Demant group using the following background and donor strain pairs: BALB/cHeA and STS/A (the CcS/Dem series), C3H/DiSnA and C57BL/1OScSnA (the HcB/Dem series), and O20/A and B10.O20/Dem (the OcB/Dem series) (Stassen *et al.* 1996). These strains were generated primarily to study genes controlling tumorigenesis, and collectively they allow analysis of genetic control of virtually all major tumor types in the mouse (Demant *at al.,* 1989; Demant, 1992). All the CcS/Dem and HcB/Dem RCS contain the X chromosome of the background strain, and therefore no markers need to be tested for this chromosome. From experimental results, the actual frequencies of donor strain alleles were found to be about 11.1%, for CcS/Dem series, 11.0% in the OcB/Dem series, and 12.3% in the HcB/Dem series. This was in agreement with the theoretically expected 12.5% (Demant and Hart 1986; Demant *et al.,* 1989; Demant 1992), and from the available genetic characterization of the CcS/Dem and OcB/Dem RCS series it is possible to fully exploit the RCS system for genetic and biological study of multigenic traits. The distribution of DNA of donor strain origin in the RCS mice also have been reported to differ in the mice of CcS/Dem and OcB/Dem series as seen in the number of fragments of donor origin in the different chromosomes of each CcS or OcB series strains (Stassen *et al.,* 1996). More than 90 % of the genetic material from the ''donor'' strain in a RC strain is concentrated in 9 to 13 discrete contiguous chromosomal regions with intermediate length (5–25 cM), that are usually located on 7 to 11 different chromosomes (Demant, 2003). Although some of the markers had/have not been typed, the authors safely made the assumption that many of them have become homozygous and thus fixed during the more than 10 generations of inbreeding that followed the development of the RCS series strains. Moreover, the heterozygous loci appear to be "clustered", with each cluster considered as a single heterozygous locus, because in many instances several closely linked

markers were tested in the heterozygous segments. Additionally, because the donor DNA is distributed on the different chromosomes of the recipients as noted above, the RCS system has the advantage of a fairly reduced genetic complexity, making selection of interesting combinations of strains differing in specific chromosomal regions a rather semi-straightforward undertaking (Stassen *et al.,* 1996).

It should also be pointed out that each RCS donor-recipient pair cannot be a universal tool to dissect all traits, rather, a particular pair will have a different phenotype with respect to another trait. For instance, the CcS/Dem series was developed to study genes controlling the development of lung tumors because the background (recipient) BALB/cHeA strain is susceptible and the donor STS/A strain is highly resistant to lung tumors. The order of donor and background (recipient) may need to be reversed for studying colon adenomas/adenocarcinomas since BALB/cHeA is resistant while STS/A is highly susceptible to development of colon adenomas/adenocarcinomas. Separation of several major genes determining the number of 1,2-dimethylhydrazine (DMH)-induced tumors occurred in the CcS strains, and that these genes are different from another set of genes which determine the size of the colon adenomas as well as from the genes controlling development of tumors in other organs following DMH treatment (Moen *et al*., 1991). In a subsequent study, one of the colon tumor susceptibility genes *(Scc-1, susceptibility to colon cancer-I)* was mapped, as well as four other *Scc* genes that appeared to be novel genetic factors (Moen *et al.,* 1992), as none of them was identical with or linked to any of the genes such as *RAS, TP53, APC, MCC* or *DCC* that are frequently mutated in familial and sporadic colon cancers in humans (Fearon and Vogelstein, 1990). These results show that the RCS are effective tools for the genetic dissection of multigenic traits and have been used for

infectious disease investigations (Banus *et al.,* 2005).

The RCS mice were developed for analysis of multigenic traits (Demant and Hart 1986; Demant *et al.* 1989; Demant 1992) and the RCS series used in the present study comprises approximately 20 inbred strains produced by backcrossing and subsequent inbreeding from two parental founder inbred strains: a background strain (BALB/cHeA) and a donor strain (STS/A). Together, the 20 CcS/Dem RCS set contains approximately 95% of the genes of the donor strain. The essential feature of the RCS system (which discriminates it from the recombinant inbred strains) is that unlinked genes of a multigenic trait are separated into individual RC strains, thereby creating a number of single gene traits. Thus, each gene can be mapped and studied independently from the other genes. However, it should be noted that in case of many genes controlling the same trait, more than one gene can be "captured" in one RC strain. Unlike recombinant inbred strains in which the strain distribution pattern provides evidence for linkage (Bailey, 1981), an F2 cross or backcross of a particular RC strain is necessary to obtain linkage (Demant and Hart 1986). Apart from its main feature, the RCS system has another valuable characteristic. Owing to many generations of inbreeding, all individuals of each strain are genetically virtually identical, which makes the study of quantitative traits possible. Furthermore, the extensive genetic characterization of the RCS, which improves continuously, makes detailed mapping experiments feasible. Most of the mappings to determine positions of the markers are performed according to the genetic and physical maps of the Whitehead Genome Center (http://www.wi.mit.edu). They therefore have the nomenclature Dxx*Mit*ss where <u>*D*</u> stands for DNA fragment used, <u>xx</u> for the chromosome number, <u>*Mit*</u> the lab code and <u>*ss*</u> the sequential number of the individual loci on the fragment.

Studies in the last decade that are all based on the use of recombinant congenic strain of mice have led to the characterization of tumors on histological level (Quan *et al*., 2009), where tumors were seen to lie outside the bronchial basement membrane and tend to reach a larger size than the tumors at other locations in the lung.

Through approaches based on the use of RCS mice, a number of chromosomal loci that influence qualitative aspects of mouse lung tumors have been mapped, including loci controlling 3-dimensional shape of tumors, the presence of nuclear cytoplasmic inclusions, and the presence of infiltrating lymphocytes, demonstrating the feasibility of genetic analysis of qualitative characteristics of lung tumors (Tripodis and Demant, 2001; Tripodis and Demant, 2003; Kakarlapudi *et al.,* 2008). Lung tumors in these mice also differ in many other aspects, including tumor locations within the bronchial tree and this has been used to characterize lung tumors in mice (Horlings and Demant, 2005). Just like in the CcS/Dem series, the OcB/Dem strains which are constructed based on the same principle, have highly significant strain differences in the regional location of chemically induced lung tumors (Demant and Hart, 1986). Again, like in the CcS strains, the susceptible O20 mice developed significantly larger lung tumors than the resistant OcB-9 mice. In O20 mice, a large proportion (42%) of lung tumors is located around or along the bronchiolar structures (peribronchial tumors) than in OcB-9 mice (2%) (Horlings and Demant, 2005). The observations formed the rationale for concentrating on the bronchiolar epithelium in the current study, since these structures are the ones most prone to developing tumors.

1.8: The issues studied in this dissertation

In this dissertation many CcS/Dem recombinant congenic strains (RCS) of mice were used to determine if there is any correlation between the DNA double strand break (DSB) repair efficiency and susceptibility to lung tumor development.

A potential adverse consequence of cancer radiation therapy is the induction of secondary tumor(s) that may arise in the penumbra of the primary radiation field and it is possible that some cancer patients are more susceptible than others to radiation-induced (RI) second malignancies, and this may result partly from inefficient repair of DNA double strand break (DSB) generated in the surrounding normal tissues during treatment. The overall study explored a possible link between heritable differences in DNA DSB repair efficiency, which is influenced by many factors, and susceptibility to RI lung cancer in a mouse model.

The success of an experimental investigation depends on the reliability of protocol/procedures used, so we intended to optimize the methods of euthanasia and processing of lung tissues for *in vivo* detection of γH2AX foci formation. The effect of different techniques used for euthanasia, perfusion and background reduction as well as improving antigen binding as formalin fixation that significantly affects the outcome had to be explored. It was also part of our interest to see how the different cell types within the same tissue respond to ionizing radiation.

After optimizing the assay techniques, the main study explored a possible link between heritable differences in DNA DSB repair efficiency, which is influenced by many factors, and susceptibility to RI lung cancer, based on a previous study involving 20 different strains of CcS/Dem RCS mice derived from BALB/c x STS progenitors and had showing wide inter-strain

41

variations in susceptibility to RI lung tumor development.

Another part of the study was aimed at using peripheral blood lymphocytes as a surrogate to assess DNA repair efficiency in the lungs. The aim was that, if the lymphocyte results are found to correlate with those of the lung study, it would allow the use of lymphocytes which, unlike lung tissues, are readily available for use to predict the susceptibility to radiogenic lung cancer.

Lastly, since the product of the *Prkdc* gene (the kinase DNA-PK) is known to be one of the important players in DDR, it was decided to determine whether the R2140C substitution in DNA-PK has a major influence on DSB repair and therefore a determinant in the foci count differences in the CcS/Dem strains where it occurs and the strains with no such substitution.

REPAIR OF RADIATION-INDUCED DNA DAMAGE IN THE LUNGS OF MICE: ASSESSING DIFFERENT EUTHANASIA METHODS AND RADIATION DOSE-RATES ON IRRADIATION OUTCOME

Summary

The success of an experimental investigation depends on the reliability of protocol/procedures used, so here we intended to optimize the methods of euthanasia and processing of lung tissues *in vivo* (for the detection γH2AX foci formation). To achieve this, procedures were developed using mice irradiated acutely or at low dose rate with ^{137}Cs gamma rays. For convenience, acute exposures were used to develop the methodology for euthanasia and tissue preparation. The suitability and reliability of low dose rate irradiation as an effective technique for *in vivo* lung studies was also evaluated. Euthanasia by CO_2 asphyxiation, pentobarbital injection, and direct cervical dislocation were evaluated. Intra-tracheal, left ventricular whole body or right ventricular direct pulmonary perfusion techniques were also evaluated, all using normal saline and neutral buffered formalin (NBF) as the perfusion media. Slides of 5µm tissue sections were stained with hematoxylin and eosin (H&E) and light microscopy was used to identify changes in the lung architecture, and to evaluate the extent of vascular congestion. Immunofluorescence staining was performed to test methods that improve antibody binding and reduce background autofluorescence. Fluorescent microscopy was used to obtain images that were assessed for foci characteristics for each of the parameters evaluated. Intra-tracheal perfusion resulted in severe vascular congestion with very high background autofluorescence. There was no advantage of

pentobarbital use over CO_2 asphyxiation on foci formation and quality, and right ventricular perfusion gave the best quality pictures for analysis of foci. CO_2 asphyxiation and right ventricular perfusion methods were therefore adopted for use in all subsequent experiments. The use of sodium borohydride for quenching autofluorescence and sodium citrate for antigen retrieval gave very good quality images and were used throughout the main study that followed. Low dose/low-dose-rate irradiation allowed more accurate quantification of DNA DSB foci than acute dose rate irradiation, confirming the previous observations from other workers.

Background

The overall goal of this study was to correlate radiation-induced DNA double strand break (DSB) repair efficiency with radiogenic lung cancer susceptibility of recombinant congenic (RC) strains of mice (Demant and Hart, 1986). At the time we initiated the research few *in vivo* studies on DNA DSB repair using γH2AX had been published (Rube et al, 2008a; Rube et al, 2008b; Rube *et al.,* 2009; and recently Davies *et al.*, 2014). There was little information or report that emphasized how the outcome of the response can be affected by the different agents used for euthanasia, since most of the known DNA damage repair mechanisms have been determined in cultured cells. We wanted to determine if sample preparations could be part of confounding variables and their effects therefore needed to be determined. For that reason, we decided to optimize the *in vivo* assay. We were particularly concerned about minimizing the time between the completion of the dose delivery and tissue fixation with the intent to stop the repair process immediately after irradiation, while at the same time prevent any further resolution of the repair foci through de-phosphorylation. The foci are known to undergo rapid disappearance shortly following the termination of dose delivery, particularly at DSB sites where the repair process is complete.

For the purpose of this study, the major intent was to refine the protocol in this mouse model by testing if different methods of euthanasia will affect the desired endpoint, namely the formation of γH2AX that can be visualized by immunofluorescence microscopy as discrete nuclear foci at sites of DSB (Rogakou *et al*., 1998; Rothkamm *et al.,* 2003) so as to obtain reliable and unbiased results. The limited spectrum of strains of mice compared in most studies makes it difficult to apply the results to the wide variations in the human populations. The intent of our study was to extend the assessment of repair capacities of individuals within a genetically complex population.

The result of this project has the potential to provide more clinically relevant data that will mirror the extent of radio-sensitivity in such a genetically complex general population and be used as a foundation for future decisions on radiation use in diagnosis, treatment or practices where individuals encounter radiation exposure. Together with other improved models, the study can serve in solving one of the recurrent and emerging problems that the advances in technology has directly or inadvertently caused, namely causing or aggravating cancer through use of the very means used to diagnose and/or treat it. It may seem trivial to say diagnostic techniques like computed tomography (CT) or routine thoracic radiographs can be a source of danger to some individuals, but a study in which normal individuals were able to repair DSBs to background levels after a CT scan, a patient who had previously shown severe side effects after radiotherapy displayed levels of γ-H2AX foci at various sampling times post-irradiation that were several times higher than those of normal individuals and this patient had a substantial DSB repair defect after CT (Löbrich *et al*., 2005) or X-rays (Rothkamm *et al.,* 2003). These data show that the *in vivo* induction and repair of DSBs can be assessed in individuals exposed to low radiation doses, adding a further dimension to DSB repair studies and providing the opportunity to identify

repair-compromised individuals after diagnostic irradiation procedures.

The mice used in the actual study were the CcS/Dem RCS, a collection of 20 inbred strains derived from common founder parental strains by mating BALB/cHeA mice which are susceptible to radiation-induced lung tumor development, and STS/A mice that are resistant. Moreover, the genes that control the development of the different tumor types are randomly segregated in the 20 RC strains (Demant and Hart, 1986; Groot *et al*., 1992; Stassen *et al*., 1995; Quan *et al.,* 2011). The response of each strain can therefore be correlated with their known susceptibility to lung tumor development (Szymanska *et al*., 1999).

However, to obtain results that will contribute to a better understanding of the effects of radiation in a tissue context for any organ or tissue, an investigator's first task is to choose a method that does not interfere with the intended endpoint. There was therefore a need to evaluate the most suitable procedures before their eventual application in the study. This is especially true as the euthanized animal's lung tissue is the subject of analysis to ensure that the euthanasia method will not significantly alter the tissue microenvironment composed of a mix of cells in different stages of the cell cycles. Even seemingly inoffensive chemical methods, such as carbon dioxide or nitrogen inhalation, may confound pulmonary studies as both agents can alter the cellular architecture of lung tissue, let alone the biological reactions that occur. Clearly, investigators need familiarity with the detailed effects of various euthanasia methods on the outcome of their science before making intelligent choices.

Three methods of euthanasia were therefore evaluated in this preliminary study with the intent to select the method with the least effect on the DNA double strand break (DSB) repair response,

which is also convenient to undertake without compromising the quality of the data used for analysis in the main study. Although it requires prolonged exposure for some of the agents to cause cellular damage in the lungs (see review by Asselin-Labat and Filby, 2012) the short term effect on normal tissue may not be negligible.

The DNA DSB response of cells in the lungs of irradiated mice was measured using two DSB markers, phosphorylated histone variant H2AX (known as γ-H2AX) (Rothkamm *et al.*, 2003) and p53 binding protein 1 (53BP1) (Huyen *et al.,* 2004) which form discrete foci in the cells at the sites of DSBs. However, the visualization of these foci can be affected by a number of factors introduced during sample preparation, which required evaluating.

Among the procedures that were evaluated are the known methods used for autofluorescence remediation and antigen retrieval methods used to improve antigen binding. There has been ample evidence to show that successful visualization of fluorescent markers in formalin-fixed paraffin-embedded (FFPE) tissues is usually hampered by intrinsic autofluorescence of the many types of molecules and compounds that are components of the tissues (Banerjee *et al*., 1999; Baschong *et al*., 2001; Billinton and Knight, 2001; Collins, 2006; Monici, 2005; Viegas *et al*., 2007). The use of FFPE-solid tissues for immunofluorescence complicates visualization by causing background staining that arise from the secondary antibody being used as well as autofluorescence due to endogenous proteins in the tissues (Pino, 1985; Wieczorek *et al.,* 1997; Boenisch, 2001). Endogenous peroxidases are usually completely destroyed by diluted solution of (0.003-3%) H_2O_2 but different tissues may require different concentrations of H_2O_2 solution (Albrechtsen *et al.,* 1980), and since H_2O_2 works best in methanol it has its limitations for

immunofluorescence studies (Boenisch, 2001). Agents that help to quench autofluorescence operate by causing a shift in the excitation and emission spectrum of the fluorescent material in the tissue such that the intensity of the emitted wavelength is away from the part of the spectrum that is of interest.

During formalin fixation and post-euthanasia treatment of tissues, protein-protein interactions are usually interrupted leading to modification of the tertiary structure of the proteins and loss of their innate antigenicity. The tissues therefore have to undergo various types of treatments to restore their antigenic capacity, processes known as antigen retrieval (AR) (Ramos-Vera and Beissenherz, 2000; review by Ramos-Vera, 2005). A method of AR introduced by Shi *et al* (1991) is based on the principle that chemical changes between proteins and formalin can be reversed, at least partially, by use of temperature, a process known as heat-induced epitope reversal (HIER). Though the mechanism is not known with absolute certainty, it is achieved mainly through hydrolysis of methylene cross-links or bridges that are formed between proteins which are the main cause of the conformational changes that follow formalin fixation. However, since it is now known that different antigen seem to have optimal buffers implying that there is no universal AR solution for all types of tissues (Imam *et al*., 1995; Hayat, 2002), there is need to evaluate those reported by other users to obtain reliable results. For instance, some class of antigens are unmasked better in Tris buffer (pH =10) (Shi *et al* 1993, 1995), while the use of 0.01 M citrate buffer (pH = 6.0) first introduced by Cattoretti *et al.,* (1992) is suitable for unmasking many antigens types and has since become the gold standard in immunohistochemistry, with many techniques for HIER having been tried including microwaving (Gown *et al*., 1993), autoclaving (Bankfalvi *et al*., 1994), high temperature water

bath and pressure cooking (Norton *et al*., 1994), and steam heating (Taylor *et al*., 1996).

The result of a comparative study indicates that the different AR methods can yield similar intensities following immunostaining if the heating times are adjusted appropriately (Taylor *et al*., 1996). Some antibodies also perform best under defined conditions and may not bind well for some type of samples prepared by a known technique. Additionally results are not uniform for all types of tissues and should be interpreted with a lot of caution. Such a situation was noted in staining for p53 over-expressed in benign and malignant tissue samples from oral mucosa (Dowell and Ogden, 1996). This therefore calls for individualized determination of the most appropriate condition for a laboratory setting, sometimes through trial and error. In the present work, microwave-based HIER was used for all experiments involving FFPE samples.

This part of the study was therefore based on the hypothesis that the outcome of the staining for radiation-induced DNA DSB foci determination is dependent on the procedures used during post-irradiation processing of the lung samples.

Materials and Methods

Animals: The animals used in the optimization study were BALB/cHeA strains of mice which are susceptible to radiation induced tumor development, and C3H mice that are known to be resistant. The animals were housed at the Laboratory Animal Resources (LAR) facility at Colorado State University (CSU). Feeding and watering were provided around the clock. All animal protocols were approved by the CSU Institutional Animal Care and Use Committee (IACUC).

Irradiations: Two mice of each strain were transported to the MRB building that houses the cesium irradiators. They were placed in 8 cm x 5 cm x 5 cm Plexiglass containers at the time of irradiation and the desired irradiation dose was delivered to the whole-body using γ-rays from either a J.L Shepherd Model 81-14 6000Ci ^{37}Cs Sealed Source-059 irradiator, Serial No.641 in room MRB 004, at an acute dose of 1.2 Gy/min for 2 min, or from a J.L. Shepherd Model 81-14 600Ci ^{37}Cs Sealed Source-070 irradiator Serial No. 7014 in room MRB 006, at a low dose rate of 10 cGy/h for 24h. For both irradiation dose rates, the cumulative dose was 2.4 Gy. The irradiators are pre-calibrated to deliver the desired dose at a fixed distance from the lead window of the source housing. Sham-irradiated mice that served as controls were treated under similar conditions but without the source being exposed. For low dose rate irradiation which required maintaining the animals in the room for 24 h, temperature and humidity were maintained at ~23ºC and ~55% respectively.

Methods of euthanasia: Three methods of euthanasia were evaluated, namely CO_2 asphyxiation, pentobarbital injection, and cervical dislocation. For each of the three euthanasia methods, two mice were used. The procedures for use of CO_2 as well as other methods were approved by the Institutional Animal Care and Use Committee of Colorado State University.

Perfusion: Immediately after euthanasia, the thoraco-abdominal wall was opened and a solution of 2% heparin in normal saline was used to perfuse the lung cavities through different routes. One route was through the trachea, and the second was by perfusion through the right ventricle to inject the saline directly into the lungs via the pulmonary artery, with the left atrium nicked to prevent blood returning into the heart. The third route was through the left ventricle via the aorta

and the blood that would otherwise return to the heart flowed out freely by nicking the right atrium. Neutral buffered formalin (NBF) was then used to perfuse and fix the tissues through the same routes as the saline, before the whole lung was harvested and stored in NBF for 24h and later transferred to 70% ethanol until ready for further tissue processing. Carcasses were placed in closed, opaque containers or bags for transportation and disposal at the LAR.

Tissue processing: The lungs were trimmed, transferred to fresh room temperature 70% ethanol and transported to the Diagnostic Medical Center of the Veterinary Teaching Hospital of Colorado State University. The tissues were dehydrated and embedded in paraffin wax to form blocks from which thin sections about 5 μm thick were cut and floated on distilled water in a water bath preheated to a maximum temperature of 45°C. The tissue sections were then mounted on the silane-coated glass area of Histobond® plus microscope slides (StatLab, McKinney, TX) flat and wrinkle-free, and the slides were left to dry completely at room temperature by draining them vertically before heating them in an oven for 20-60 min at 56-60°C.

Histochemistry and Immunofluorescence staining: For each method of euthanasia, sections on the slides were de-waxed and stained with Hematoxylin and Eosin (H&E) for use to identify any changes in the tissue architecture and the extent of vascular congestion using a light microscope. For immunofluorescence staining, the slides were washed in xylene 3 times for 3 min each, followed by rehydration in graded alcohol solutions, starting with 100% ethanol for 5 min, then 90% twice for 5 min each, and finally 50% twice for 5 min each. Sections were either subjected to antigen retrieval or not, with or without autofluorescence reduction treatments (details in Results section). After blocking non-specific binding sites using a solution of 10% normal goat

serum, immunodetection of γ-H2AX and 53BP1 were performed by incubating the slides at 4 ºC overnight or for 1 h at 37 ºC using monoclonal mouse anti-γ-H2AX antibodies (Millipore, clone JBW 301) diluted 1:500, and polyclonal rabbit anti-53BP1 antibodies (Bethyl, Montgomery, TX) diluted 1:300 to measure the response of the lung tissue/cells to irradiation and their ability to form foci in the process of attempting to repair DNA DSB. These antibodies were then detected with fluorophore-conjugated goat secondary antibodies specific to each of the primary antibodies (AlexaFluor-488 conjugated goat anti-mouse for anti-γ-H2AX and Rhodamine Red conjugated goat anti-rabbit for anti-53BP1) followed by imaging using a fluorescent microscope (Nikon Eclipse E600) to identify the location of the foci and determine where the DNA DSB repair occurs. The CoolSNAP-$ES^®$CCD camera-equipped fluorescent microscope is controlled by programmed OptiScan^{TM} motorized stage systems (Prior Scientific & Photometrics, Tucson, AZ) and coupled to a computer equipped with MetaMorph software Version 7.3 (Molecular Devices, Sunnyvale, CA). The entire setup is capable of capturing images in an alternating order to discriminate 4′,6-diamidino-2-phenylindole (DAPI) (blue), AlexaFluor-488 (green), and Rhodamine Red (red) channels by excitation using a Mercury arc lamp. From the captured images, both 2D and 3D images can be generated to allow better foci localization and quantification. Image processing and color combining can allow counting the number of foci per nucleus for quantitative estimation. Tissues from mouse strains that are efficient in DSB repair are expected to have fewer foci than those less efficient in repair immediately following protracted low dose rate irradiation or in the case of acute exposures allowing 45 min to 60 min for repair before the tissues are isolated and fixed.

Data analysis: The results obtained were compared for the three methods of euthanasia after irradiation using non-irradiated mice as controls. The histology of the lungs and the number of DSB repair foci present at the time tissues were fixed with NBF were scored for each euthanasia and perfusion method used. The data generated from MetaMorph was logged directly into a MS Excel spreadsheet and used for statistics and to generate graphs. The MS Excel spreadsheet was also used as data source for SigmaPlot for Windows version 11.0 (Systat Software Inc, San Jose, CA) for statistical analysis. One way repeated measures analysis of variance (ANOVA) was performed to determine any variations in the triplicate experimental repeats when the foci were being counted for each individual mouse and to determine any significant differences in foci numbers between mouse strains used in the optimization. One way ANOVA was also used to compare foci count differences among and between strains of mice.

Results and Discussion

Bronchial and bronchiolar epithelium was selected for quantification of repair foci because these cells are thought to be the target cells for radiation-induced lung cancers in mice. However, other cell types were analyzed either for qualitative characteristics of DSB rejoining in other regions of the lung including the alveoli, the endothelium and other stromal compartments. Analysis for quantitative reporting was also confined to the first six bronchiolar epithelial nuclei in each image frame to avoid creating a bias that would result in exclusion of image frames where fewer foci may be seen in any image field. Some nuclei contained so many foci that it was not possible to clearly distinguish the boundary of one focus from the other leading to those nuclei being excluded from analysis.

Comparing the methods used for euthanasia and perfusion

During the evaluation stage, the time taken to euthanize the mouse and isolate the tissues varied with the technique used. The time required to harvest the lungs post irradiation was on dependent on how long it took the mouse to show no muscle reflexes. However, the heart was still pumping after the thoraco-abdominal wall was opened. It took about 7-9 min post-irradiation from cervical dislocation to harvesting the lungs from the mouse, which was the shortest time required, to about 11-14 min for pentobarbital overdose. Euthanasia by CO_2 asphyxiation was intermediate. Of the three methods of perfusion tested, intra-tracheal perfusion had the worst outcome with severe vascular congestion in the lungs (Fig 2.1A). Although whole body perfusion through the left ventricle gave acceptable results (Fig 2.1B), there was still a relatively high number of red blood cells (RBCs) that dampened the signals enough to interfere with confident quantification of the foci (Fig 2.2B).
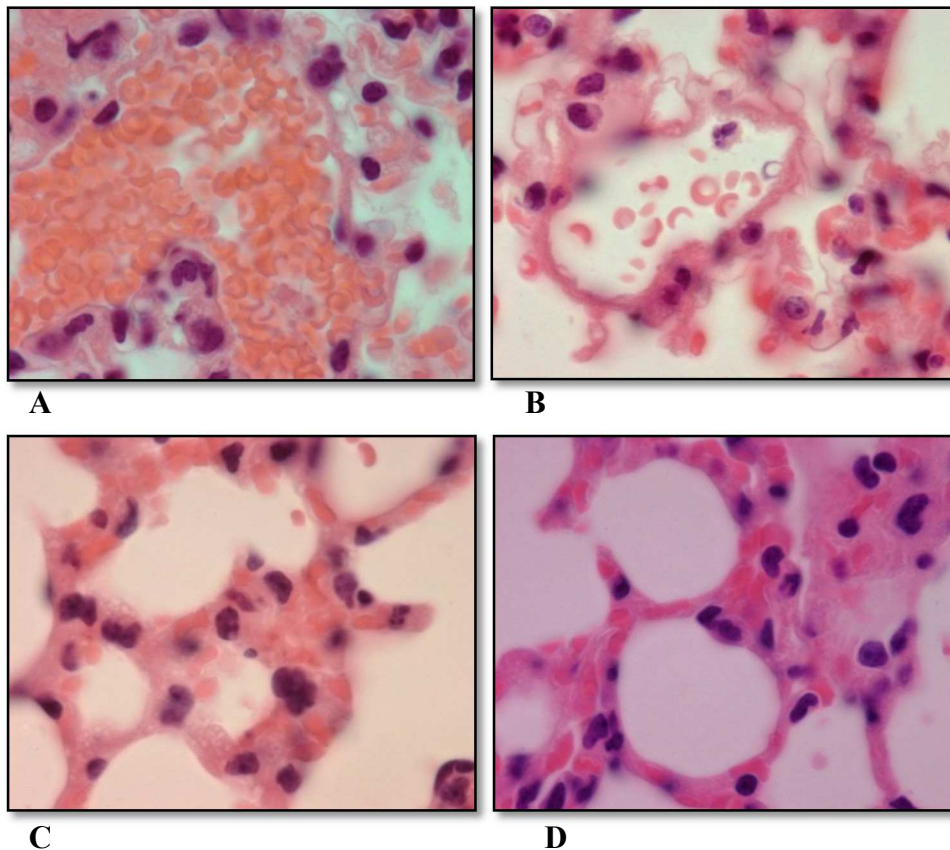
Figure 2.1: Comparing perfusion techniques: A, intra-tracheal perfusion led to congestion of blood in the lungs with very high fluorescent background in subsequent immunofluorescence staining. B, whole body perfusion through the left ventricle had fewer RBCs and less autofluorescence but the residual RBCs still interfered with foci determination in the alveolar compartments. C and D, right ventricular perfusion produced the best results. In D the post perfusion insufflation with neutral buffered formalin led to well distended alveolar space that enabled easy identification of both type I and type II alveolar cells.

When subjected to immunofluorescent staining there was very high fluorescent background that interfered with identification and quantification of the foci (Fig 2.4). On the basis of these results, right ventricular perfusion followed by intra-tracheal insufflation was adopted as the method of choice for lung tissue preparation for the rest of the study since it not only produced the least background autofluorescence during imaging (see following section) but it also gave the best outline of the structures being used to assess the outcome of irradiation in the lungs of mice.

Effects of sodium borohydride and sodium citrate treatments on autofluoresescence and antibody binding

Antigen-antibody interactions and subsequent detection using fluorescent markers are affected by many factors in formalin-fixed paraffin-embedded (FFPE) tissues (see review by Ramos-Vera, 2005). Since autofluorescence is known to be among the factors that can adversely affect successful visualization of immunodetection markers in FFPE during immunohistochemistry IHC), we tested several methods that have been shown to reduce autofluoresence in other systems (Neumann and Gabel, 2002). In addition, we tested antigen retrieval techniques to reverse protein crosslinking and improve antigen binding. We therefore undertook a comparison of 3% H_2O_2 solution (Ranieri *et al.,* 2007) and sodium borohydride ($NaBH_4$) (Cancy and Cauller, 1998; Baschong *et al*., 2001) freshly prepared as a 1 mg/mL solution in PBS to give an effervescent solution, for background and autofluorescence reduction. Sodium borohydride was assessed based on its frequent use to treat FFPE tissues during immunohistochemistry with good outcome (Ngwenya *et al*., 2005; Sun *et al.,* 2010). The slides were washed three times for 10 min each in the effervescent solution and rinsed in water, all the washings being carried out at room temperature. This treatment resulted in significant reduction of background autofluorescence (compared to H_2O_2 or just washing the slides with PBS containing a 0.05% Tween-20 or plain PBS) giving much improved visualization (Fig. 2.2C). On the other hand, boiling the tissues in a solution of 0.1 mM sodium citrate in PBS, 0.05% Tween 20 (pH 6.5) at about 95 °C for 10 min followed by cooling for 30 min at room temp and washing in PBS gave even better visualization than without such treatment (Fig.2.2C compared to 2.2A and 2.2B).

Although use of $NaBH_4$ can help to reduce even the severe autofluorescence caused by RBCs (Fig 2.4A) it alone could not improve visualization of the fluorescent markers. Similarly, while

antigen retrieval helps improve antibody binding to its target, it only moderately increased the apparent visual intensity, probably due to masking by the strong background autofluorescence that gives a fuzz rather than a distinct spot of the fluorophore being imaged and overall image quality (Fig.2.2B). It therefore required the combination of both to give the best outcome (Fig 2.2C), compared to each treatment individually. Another observation that was made as the images were being analyzed was the intensity of the foci when Alexa-488 (green) was used as the fluorophore compared to Alexa-594 or Rhodamine (red). There was a better contrast between the blue (DAPI) nuclear background and the red foci/spots than between the blue DAPI staining and the green foci/spots. Counting the foci was easier with the red foci than with the green foci even when there is some background autofluorescence.
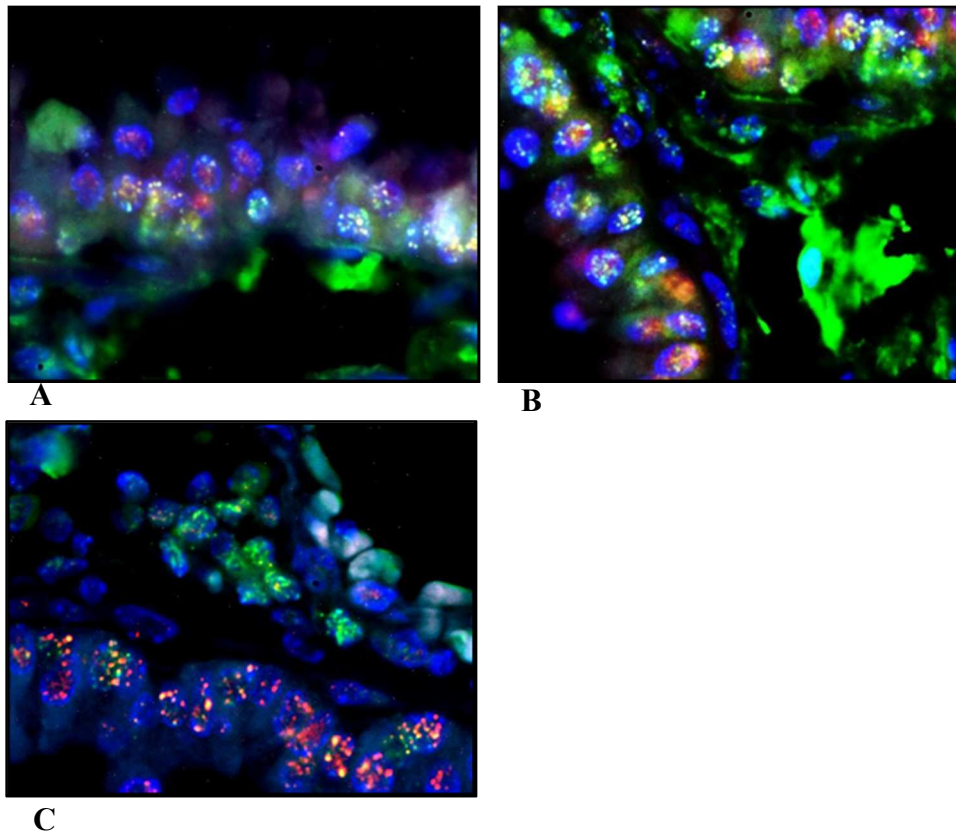
Figure 2.2: Comparing sample treatment during staining for immunofluorescence. In panel A, there was no sodium citrate treatment and washing was performed using PBS containing 0.5% Tween-20 without sodium borohydride treatment. A, the slide was washed with sodium borohydride to reduce autofluorescence and treated with sodium citrate for antigen retrieval while in In C, the section was treated with sodium citrate for antigen retrieval but without sodium borohydride treatment for autofluorescence reduction.

Auto-fluorescence dependence on the wavelength

To evaluate the effect of autofluorescence on image quality, two commonly used fluorophores as conjugates to the secondary antibody were tested during immunofluorescence as described above. The secondary antibody to the anti-53BP1 was conjugated to Rhodamine while the secondary to anti-γH2AX was conjugated to AlexaFluor-488. Additionally, quenching was compared with the red fluorphore and the green as can be seen in Fig. 2.3. Combined with

sodium borohydride treatment which appeared to help reduce the background, there was apparently more autofluoresecence in the red than from the green part of the spectrum as can be seen from the results presented in Fig 2.3. A closer inspection of Fig.2.3 shows clearly that background autofluoresecence is more intense when the green wavelength is used than with the red or the blue region of the spectrum. To ensure there was no confounding interference from ineffective antigen binding due to improper antigen retrieveal and general autofluorescence, the section was treated with sodium citrate for antigen retrieval and sodium borohydride for general background autofluorescence.
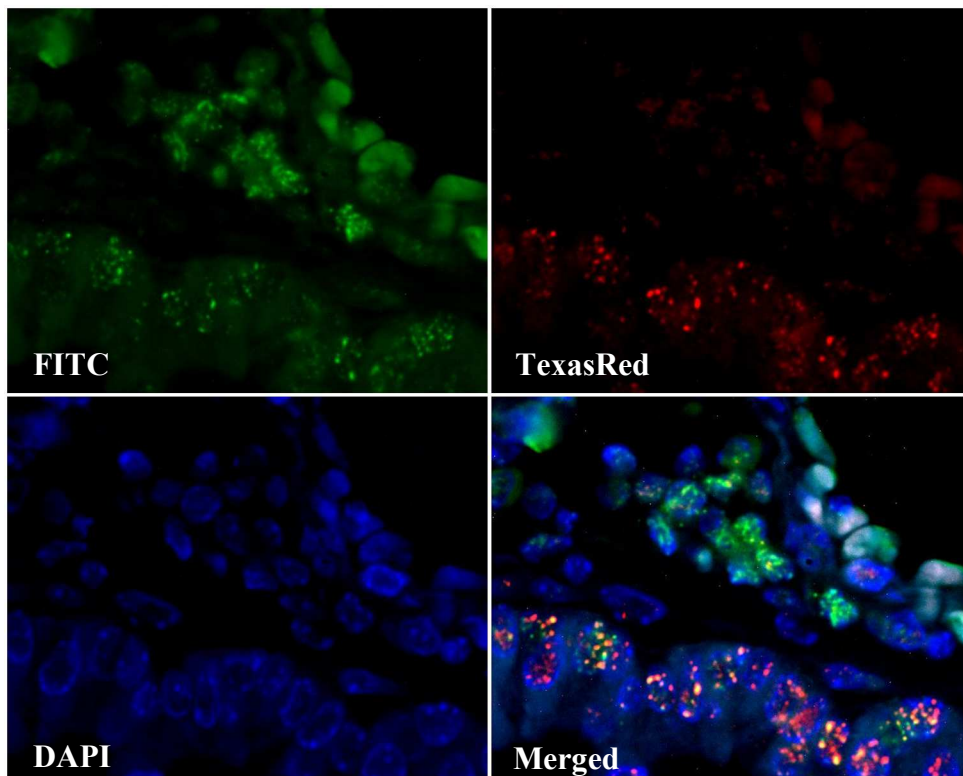
Figure 2.3: The effect of autofluorescence on image quality. Background autofluoresecence is more intense when the green excitation wavelength is used (FITC for γH2AX) than with the red (TexasRed for 53BP1) or the blue region (DAPI) of the spectrum. The section was treated with sodium citrate for antigen retrieval and sodium borohydride. Note: The merged image is the same one as in Fig 2.2A above. Comparison of the green and red images provide a clear advantage of using the red fluoresecence for foci quantification.

This comparison of the green and red images on a blue background cleary shows better image quality when the red fluorophore is conjugated to the secodary antibody for foci quantification. A quick look at the images in Fig 2.4 further shows the advantage of using red fluorophore. Here the images were obtained from lung sections from non-irraidated mice, and stined with AlexaFluor-594 conjugated goat anti-rabbit as the secomndary antibody. Nothwithstanding the intense autofluorescence, the γH2AX fcoi are clearly visible against a blue background.
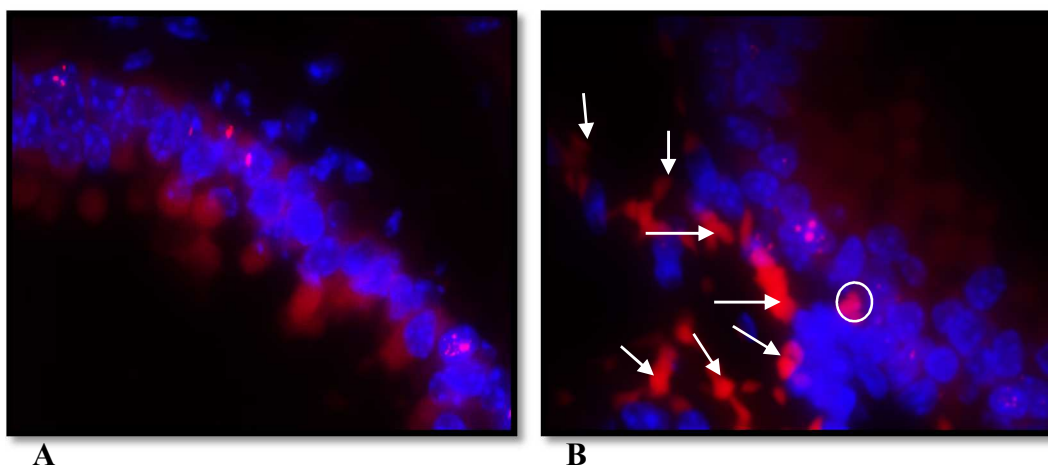
Figure 2.4: BALB/c, non-irradiated. A) No Sodium borohydride used. Note the prominent γH2AX staining in some of the cells. This was a common occurrence in BALB/c strain. The other stains had some staining in the non-irradiated state but the foci sizes were smaller. B) Increased RBCs autofluorescence (arrows and ring), a result of incomplete perfusion. Here Alexa-594 was used as the fluorophore to illustrate the sharp contrast between the red and the blue colors that facilitates quantification.

Co-localization of γ-H2AX and 53BP1

After optimizing sample processing and immunofluorescence staining and before performing the actual quantification of γH2AX foci as a measure of the DSB repair capacity of the stains, confirmatory co-localization analysis of γH2AX and 53BP1 to the sites of DSB repair was undertaken. For foci generated by both acute and low dose rate exposures, the images taken

using the green, red, and blue channels as 10 stacks of 0.5 µm thickness each, were converted to a single plane 2D images using maximum image projection (MIP) algorithm and color-combined in order to display the foci within nuclear boundaries. In most cases these two repair factors co-localized to give a yellow spot when the images from the red and green channels are merged as shown (Fig. 2.5). However there are instances where the spots in two channels do not co-localize. This reproduction of what others have already seen allowed us to proceed to the next stage of the investigation.
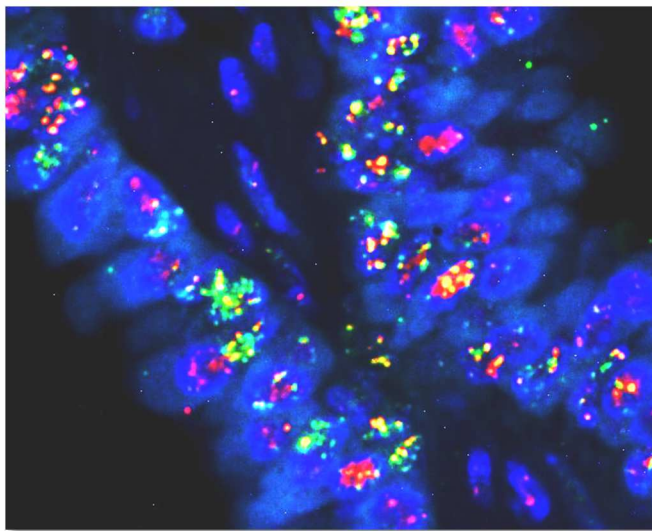
Figure 2.5: Confirming the co-localization of the known DSB repair promoting factors, 53BP1 (red) and γH2AX (green) repair. The images were taken using the green red and blue channels of a Nikon fluorescent microscope as 10 stacks of 0.5µm thickness each. The stacks for each image channel were converted to a single plane using maximum image projection (MIP) and color-combined. The two repair factors co-localize (yellow) when the channels are merged.

Comparing foci distribution following exposures at different dose rates

A baseline optimization assay was then performed to determine the ease of measuring the number of residual foci per nucleus after irradiation following an acute dose of 2.4 Gy/min as compared to a low dose rate exposure of 10 cGy/h over 24 h. Manual or automatic quantification of γ-H2AX foci *in vivo* was difficult after the acute exposure, regardless of

whether the lungs were harvested 30 or 45 min post-irradiation (Fig. 2.6A) because the foci were too numerous and appeared or tended to coalesce, or it was difficult to define the boundaries between neighboring foci. Low dose rate irradiation was therefore used and gave more manageable quantification by manual counting of the foci (Fig 2.6B). The results confirmed that C3H strain repaired DNA damage more efficiently than the BALB/c strain as expected (a *t*-test performed to compare residual foci numbers in C3H and BALB/c showed a significant difference between the two strain, $p < 0.001$, see details in paragraph below).

A   **B**
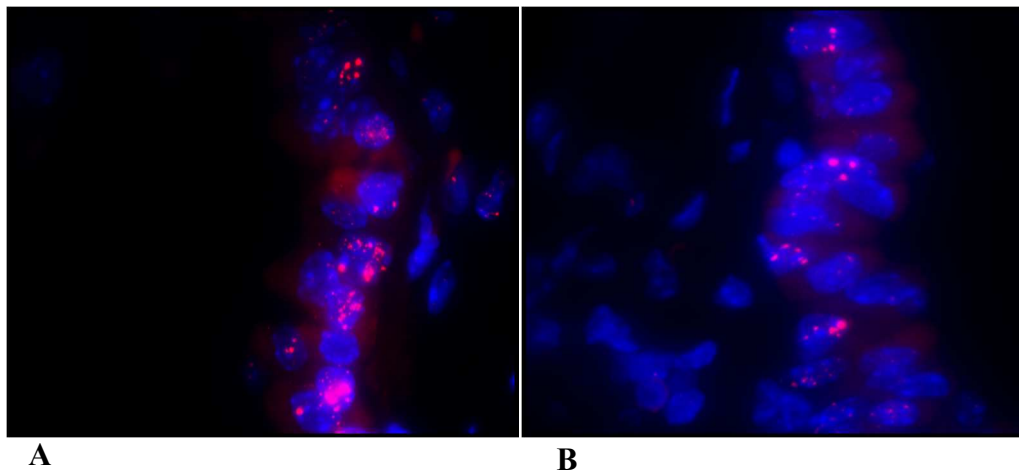
Figure 2.6: Comparing foci distribution in C3H mice exposed to different dose rates of γ-ray irradiation. In A, the mouse was irradiated with 2.4 Gy of γ-rays delivered over 2 min and euthanized 30 minutes post-irradiation and in B, the mouse was irradiated at a low dose rate of 10 cGy/h for 24 h and sacrificed immediately post-irradiation. Objective and unbiased quantitative determination of foci numbers could only be performed in B.

The non-irradiated normal lung tissues were almost completely negative for γH2AX foci, save for a few epithelial cells in the basal layer where distinct nuclear γH2AX foci were present. Although there was no assessment of repair kinetics determined by counting foci with various time point post-irradiation, the number of γH2AX foci was clearly different for the different irradiation dose rates.

The DSB repair efficiencies of C3H and BALB/c undergoing low dose rate irradiation were compared by counting the residual foci immediately after exposure. Fig. 2.7 gives plots of foci distribution for the two strains. The histogram for C3H is skewed to the left of the combined plot compared to that of BALB/c, a clear indication that C3H has much better repair capacity. Based on a comparison of the average foci using Student's *t*-Test, there were significant differences between the two strains, with the foci numbers in the BALB/c strains almost twice that in C3H strain (p<0.001). The repair of DSB was therefore confirmed to be more efficient in C3H strain than in BALB/c strain as expected.
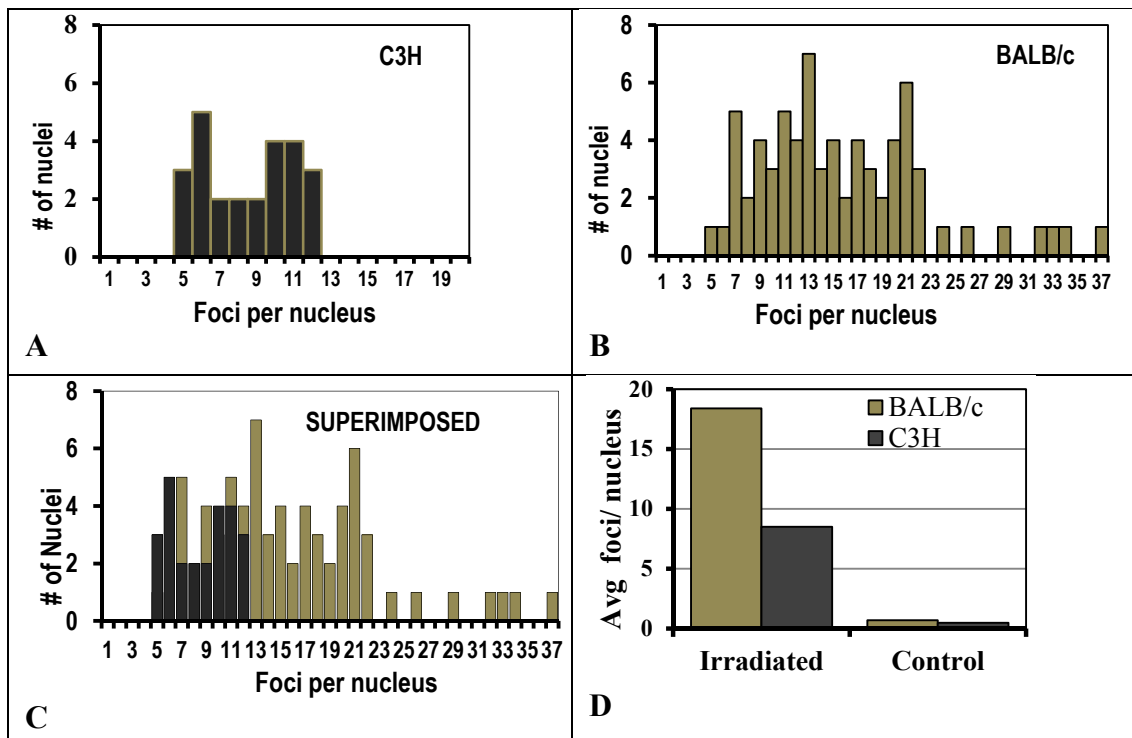
Figure 2.7: A baseline optimization assay performed in known repair-efficient and repair-inefficient strains of mice by measuring the number of residual foci per nucleus in C3H mice and BALB/c irradiated using γ-rays at a low dose rate of 10 cGy/h of for 24 h. The distribution of foci per nucleus for C3H strain (A) and for BALB/c (B) are shown, as well as the two histograms superimposed for comparison (C). The average number of foci per nucleus is greater in irradiated BALB/c mice than C3H mice while the non-irradiated controls are not different (D). This demonstrates less efficient DNA DSB repair in BALB/c strain.

Conclusion

Based on the results of the optimization experiments, right ventricular perfusion followed by intra-tracheal infusion was adopted as the method of choice for lung tissue preparation for the main study. Similarly, since a combination of sodium borohydride for autofluorescence quenching and sodium citrate for antigen retrieval had the least background and gave the best definition of the structures/foci used to assess the outcome of irradiation in the lungs of mice, this combination was used for the rest of the study. As for the ease of quantification, a sharp contrast was obtained when Alexa-594 was used as the fluorophore as compared to Alexa-488 and the former was therefore adopted for use in the main study.

Chapter 3 :

QUANTITATIVE ASSESSMENT OF γ-H2AX FOCI IN THE LUNGS OF CcS/Dem RECOMBINANT CONGENIC STRAINS OF MICE

Summary

The adult lung has a complex anatomy with a large number of cell types at its different anatomical regions. However, the identity of the cells that give rise to the different types of lung cancer is still limited or is not known with certainty. Improved attempts to isolate and properly characterize the progenitor cells in the different compartments of the lung will enable further evaluation of their respective roles in radiation-induced tumor initiation. In this study, twenty sets of CcS/Dem recombinant congenic strains of mice were used to dissect the location of cells in the lungs that are most sensitive to ionizing radiation (IR). The mice were irradiated with 2.4Gy delivered using γ-rays from a ^{137}Cs source at a low dose rate of 10cGy/h for 24h and euthanized immediately post-IR by CO_2 asphyxiation. Thin sections were prepared for immunofluorescence and rabbit anti-γ-H2AX primary antibody and AlexaFluor594-conjugated goat anti-rabbit secondary antibody were used to detect γ-H2AX as a marker for radiation-induced DNA DSB. Images were acquired by fluorescent microscopy and analyzed for characteristics of γ-H2AX foci within the nuclei in different compartments and cell types within the lung. The results show that more γ-H2AX foci are formed in the epithelial cells of the conducting airways than in the respiratory airways (the alveoli) and those of the stromal cell nuclei in the parenchyma of the lung. The foci are also larger in size than in the other

compartments of the lungs. Within the conducting airways comprising the bronchi and bronchioles, more foci are formed in the basal calls of epithelium than in the nuclei of the apical cells of the epithelium. With respect to the location of the foci within the nucleus, about 85-90% of the foci are present within the euchromatin or only peripheral to the heterochromatin of the nuclei. Only about 10-15 % of the foci are located within the heterochromatin. Among the largest foci seen, some are up to 2 μm in diameter. All these observations are irrespective of the CcS/Dem strains. In general, it appears that the epithelial cells are more sensitive to ionizing radiation than the other cell types in the lung.

Background

The adult lung is one of the structures with complex anatomy with a large number of cell types present at different frequencies according to the anatomical region of the respiratory system (Bertoncello and McQualter 2010) (See Fig.3.1A and B). The trachea and main bronchi in adults are the cartilaginous airways with two major types of luminal columnar epithelial cells: ciliated cells and Clara-like cells. Ciliated cells do not undergo self-renewal and are terminally differentiated while the Clara-type cells have secretory capacity and produce secretoglobins as the major secretory product. The more distal airways consist of small bronchi and bronchioles that contain predominantly Clara cells, compared to the mainly columnar type ciliated cells of epithelium. The bronchi and bronchioles contain more neuroendocrine cells than in the trachea, with the letter composed mainly of apparently a single layered epithelium. The most distal region of the lung that constitutes the respiratory epithelium is organized into the alveoli that consist of two major alveolar cell types: alveolar type I cells (AEC I or AT1) that are the respiratory epithelial cells with thin-walled gas exchange surface, and cuboidal alveolar type II cells (AEC II or AT2) with secretory functions and therefore have plenty of secretory vesicles containing the

surfactant protein C (SP-C). As one moves from the conducting epithelium in the terminal bronchioles to the respiratory epithelium in the alveoli, there is a transition region that has been termed the bronchio-alveolar duct junction (BADJ) (Rawlins *et al*., 2007). These different regions of the lung are likely to use different progenitor cells to maintain their kind and for repair. Although the lungs are similarly constantly exposed to potential toxic agents and pathogens present in the environment like other tissues and organs in the body, studies that have examined the turnover of the linings of tissues and organs such as the intestine or the skin have shown that the adult lung has a slow rate of turnover compared to these other tissues. It must therefore be able to respond quickly and effectively to cellular damage and the latter requirement suggests there must be some lung stem/progenitor cells with high proliferative potential to help regenerate damaged epithelial cells.

Like many other organs and tissues in the body, the lung is one of the most commonly exposed to environmental radiation, whether for therapeutic or diagnostic purposes. As a result the lung cells are subject to DNA damage, the most complex type of which is the DNA double strand break (DSB). Luckily, because of their complex and continued evolutionary abilities, cells always employ more complex mechanisms for DSB repair as a result of constant and continued evolution, enabling them to overcome such environmental insults. The two principal mechanisms cells use for DNA DSB are non-homologous end-joining (NHEJ) and homologous recombination (HR) (Lieber, 2008; Mahaney *et al*., 2009; Lieber, 2010; Lieber *et al*., 2010; reviews by Khanna and Jackson, 2001; Thompson, and Schild, 2001; van Gent *et al*., 2001; Jeggo *et al*., 2011;). There is a constant surveillance of the integrity of DNA within the cells and when DSB occurs sensors detect these changes and signal for activation of the repair process.

Even so, not all cell types benefit from both these mechanisms of DNA damage repair at all times. The repair through the NHEJ for example involves factors like Ku proteins that are reported to be playing the main sensing role in recognizing DSBs. Once detected Ku protein then binds and activates the protein kinase DNA protein kinase catalytic subunit (DNA-PKcs) leading to recruitment and activation of end-processing enzymes, polymerases and DNA ligase IV. Likewise, a less-well-characterized Ku-independent NHEJ pathway, called microhomology-mediated end-joining (MMEJ) or alternative end-joining (AEJ), is also reported to exist and available evidence suggest that MMEJ always results in sequence deletions (McVey and Lee, 2008; Sharma *et al.*, 2013; Truong *et al.,* 2015). It could therefore be a major source of mutation if it were widely used in DSB repair. While both NHEJ and MMEJ are error-prone, they can operate in any phase of the cell cycle, but HR by contrast is generally restricted to S and G2 because it uses sister-chromatid sequences as the template to mediate faithful repair. As a result, cells that are more highly differentiated and rarely undergo proliferation do not benefit from this pathway. Although there are several HR sub-pathways (Leob and Monnat, 2008; Shrivastav *et al.,* 2008), HR is always initiated by ssDNA generation, which is promoted by various proteins including the MRE11-RAD50-NBS1 (MRN) complex. In events catalyzed by RAD51 and the breast cancer susceptibility proteins BRCA1 and BRCA2, the ssDNA then invades the undamaged template and, following the actions of polymerases, nucleases, helicases and other repair components, DNA ligation and substrate resolution occur. Reports also suggest that in very rare circumstances, HR can be used to restart stalled replication forks and to repair inter-strand DNA crosslinks, a repair process that is reported to occur in Fanconi Anaemia (FA) and involves the FA protein complex (Bogliolo, *et al.,* 2007).

Available epidemiological data suggest that lung cancer is among the leading causes of cancer deaths worldwide with the five-year lung cancer survival being only 15% (Jemal *et al.,* 2011; ACS, 2014). It is reputed to be responsible for more deaths than prostate, colon, pancreas and breast cancers combined (NCHS, 2013). A better understanding of the normal lung and the biology and mechanisms of tumor formation as well as the differences among individuals to reverse or minimize it will go a long way towards the improvements of clinical outcomes.

In humans, there are distinct types of lung cancer that can be divided into defined classes based on their histopathological appearance. The major types of lung cancer are small cell lung cancer (SCLC) and non-small cell lung cancer (NSCLC), with the latter accounting for up to 80% of all lung cancers. Based on their histology, the NSCLC can be further subdivided into adenocarcinomas, squamous cell carcinomas, bronchio-alveolar carcinomas and large cell carcinomas (Bhattacharjee *et al*., 2001; Nicholson, *et al*., 2002; Hayes *et al.,* 2006; Sun *et al*., 2007), and based on their location, SCLC are predominantly found in the bronchioles while squamous cell carcinomas are thought to originate from the proximal airways (Travis, 2008; Farago *et al.,* 2012). Based on clinical findings, adenocarcinomas are the most common type of lung cancer and are more frequently detected in the distal part of the lung where the bronchioles with conducting epithelial cells terminate into the alveoli that are lined with respiratory epithelium (Fig 3.1).

These different subclasses are thought to arise from distinct cells of origin which are usually localized within distinct compartments of the lung (Giangreco *et al.,* 2007; Farago *et al.,* 2012). Improved attempts to isolate and properly characterize the progenitor cells in the different

compartments of the lung will enable further evaluation of their respective roles in tumor

initiation when combined with or even in the absence of the causal factors like ionizing radiation.
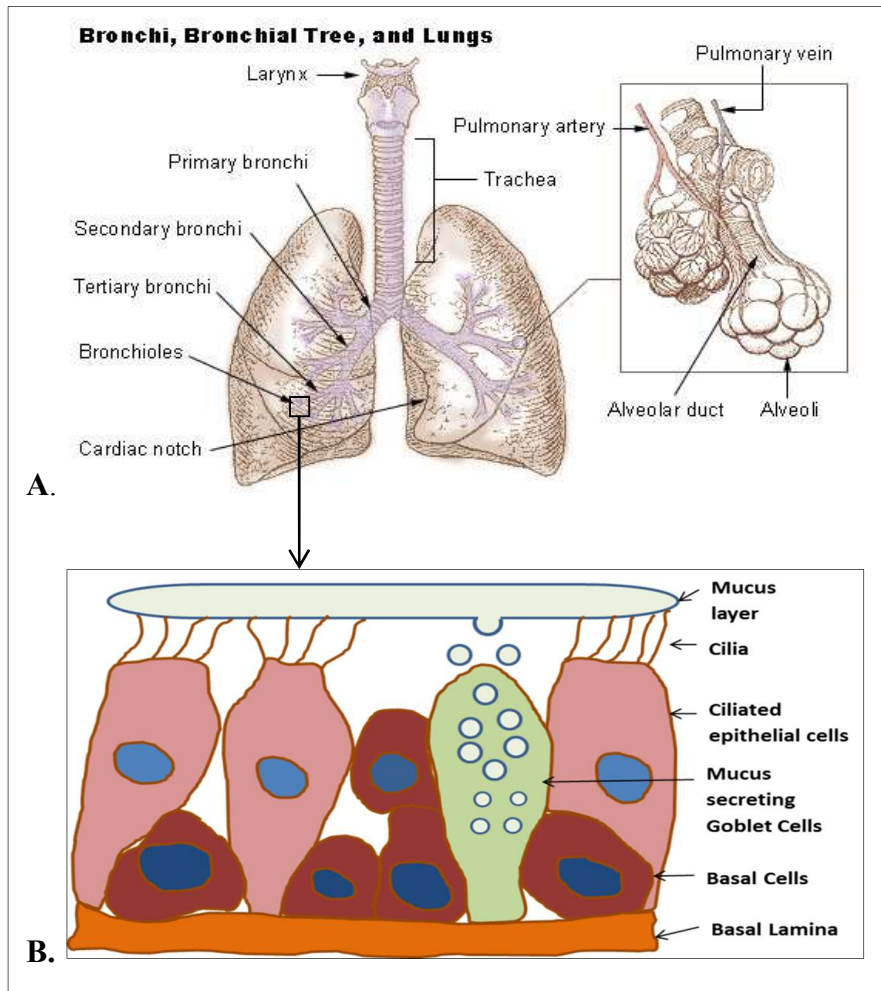
Figure 3.1: Schematic representation of the structures of lung's conducting passage way at the macroscopic (https://www.google.com/#q=bronchi+bronchial+tree+and+lungs) (A), and cellular levels (B). Different epithelial cell types and populations each residing in distinct anatomical locations, line the conducting airways. Basal, secretory, and ciliated cells line the trachea and the bronchial conducting airways. In addition to the above cell types, non-ciliated columnar Clara cells comprise the majority of the proximal bronchiolar and terminal bronchiolar epithelium in mice and alveolar type I (AT1) and type II (AT2) cells constitute the alveolar epithelium.

For a long time, there has been limited understanding of lung stem or progenitor cell biology,

making it difficult to identify the cells of origin in lung tumorigenesis with any certainty. For

instance, there is some incongruent information regarding adenocarcinomas. A report by Rosai and Sobin, (1995) stated that most adenocarcinomas were shown to display either Clara or Alveolar Type II (AT2) cell markers and are generally peripheral to or are found within the luminal portion of the bronchus.

A different study reported that adenocarcinomas are positive for the AT2 cell-specific marker pro-surfactant apoprotein-C (SP-C) and implicated Alveolar Type II cells as the target cells in rodent and human lung adenocarcinomas (Rehm *et al* 1988a, 1988b, 1989; Jackson *et al.,* 2001). In other studies involving murine models and human specimen, Clara cells were implicated as the cell of origin in adenocarcinomas (Gunning *et al.,* 1991; Mason *et al*., 2000; Mori *et al.,* 2001). In yet another study, cells which the authors referred to as double positive cells (DPCs) as they express both SP-C and the Clara cell-specific marker CCA (also known as CCSP) were found in adenomas, particularly in lesions continuous with bronchiolar hyperplasia that were later observed to be located at the bronchio-alveolar duct junction (BADJ) in normal lung (Kim *et al.,* 2005). According to these authors, these DPCs were observed to possess characteristics of regional stem cells in normal adult lungs, and the available set of data suggest that they play a role in both bronchiolar and alveolar cell injury repair and homeostasis. The Sca-1^{pos} CD34^{pos}CCA^{pos} cells were used as the markers for BASCs to demonstrate that these cells were located exclusively at BADJ, showing that a regional stem cell population is present in the distal airways of the lung of mice

It was also previously shown that there are pollutant-resistant cells with the characteristics of stem cells at the BADJ that appear to maintain cell populations following injury to the terminal

bronchioles (Giangreco *et al.,* 2002). Figure 3.2 shows the location of the terminal bronchiole where the BADJ cells can be found

Other authors too, provide additional evidence of the presence of BASCs at the BADJ where dual labeling resulted in BrdU^{pos}CCA^{pos} cells characteristic of stem-like or progenitor cells identified during early airway renewal after injury and these were located mainly at the BADJ (Hong *et al.,* 2001). Meanwhile, cells associated with neuro-epithelial bodies, that express lower levels of Clara cell secretory protein (CCSP), and are deficient in a phase I xenobiotic enzyme, were reported to serve as multi-potential progenitor cells that participate in the renewal of airway epithelium after injury (Reynolds *et al.,* 2000a; 2000b). The various studies generally point to the location of these cells where the BASC were described. Studies that are all based on the use of recombinant congenic strain of mice have led to the characterization of tumors at the histological level revealing the adenomas-adenocarcinomas of either alveolar or papillary type tumors being of peribronchial and non-peribronchial origin. Other similar studies had suggested Clara cells or alveolar type II cells as being the origin of mouse lung adenomas, or their common precursors (Jackson *et al.,* 2001; Rosai and Sobin, 1995). Further probes using the Clara cell-specific marker CC10 and alveolar type II cell-specific marker pro-surfactant apoprotein-C (SP-C) in the peribronchial and non-peribronchial tumors yielded mixed results as peribronchial tumors stained positively for SP-C but negatively for CC10 [Kim et al 2005) similar to observations from previously analyzed mouse lung adenomas (Rehm *et al*., 1988a, 1998b, 1989).
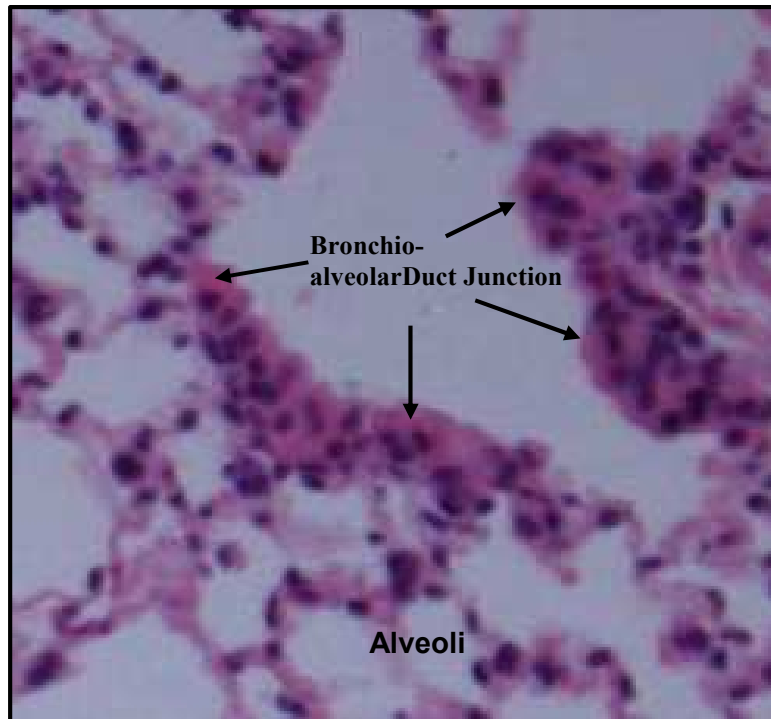
Figure 3.2: H&E section showing the bronchio-alveolar duct junction between the terminal bronchiole where the conducting airway merges with, and terminates into the respiratory exchange compartment of the lung. The former are lined by bronchiolar epithelial cells while the latter are lined by Alveolar type I and type II cells.

Notwithstanding these discordant results, the results overall provided some evidence to suggest that peribronchial tumors originated from cells of alveolar type II lineage outside, but close to the bronchus.

Through similar approaches based on the use of RCS mice, a number of chromosomal loci that influence qualitative aspects of mouse lung tumors have been mapped, including loci controlling 3-dimensional shape of tumors, the presence of nuclear cytoplasmic inclusions, and the presence of infiltrating lymphocytes, demonstrating the feasibility of genetic analysis of qualitative characteristics of lung tumors. A good example of such a study was reported by Horlings and Demant, 2005) regarding the location of tumors in relation to the bronchial tree as a robust

descriptor of lung tumors in mice. Just like in the CcS/Dem series, highly significant strain differences in the regional location of chemically induced lung tumors were observed in the OcB/Dem strains which are constructed based on the same principle as the CcS/Dem strains (Demant, 2003). Again, like in the case of the CcS strains, the susceptible O20 mice develop significantly larger lung tumors than the resistant OcB-9 mice. Lung tumors in these mice also differ in many other aspects, including locations within the lung with regard to the bronchus. In O20 mice, larger proportions (42%) of lung tumors are located around or along the bronchiolar structures than in OcB-9 mice (2%) (Fijneman *et al.*, 1996).

Based on these observed outcomes of differences in extent of tumor development in these strains, our working hypothesis was that the efficiencies of radiation-induced DNA DSB repair in lungs of these CcS/Dem RCS mice inversely correlate with susceptibilities to lung tumor development.

Any attempt to characterize the lung compartments with respect to their sensitivity to radiation-induced DNA damage using γ-H2AX formation as the yardstick is therefore worth the effort. Although it will still require further work to make a definitive prediction based on a study like this, its contribution towards solving this complex puzzle cannot be underestimated. Indeed previous studies have pointed to the role of BASCs as a source of new tumors in the adult lungs.

Materials and Methods

Animals: The animals used in the study were 20 sets of CcS/Dem recombinant congenic strains (named CcS-1 to CcS-20) between 11 to15 weeks of age and were derived from a cross between

two founder parental strains, the recipient founder being BALB/cHeA that are susceptible to developing radiation induced lung tumors, and the donor founder being STS/A strain that are resistant. The animals were shipped by airfreight from the Rosewell Park Cancer Institute, Buffalo, NY, and on arrival were housed at the Laboratory Animal Resources (LAR) facility of Colorado State University where food and water were provided ad libitum. All animal protocols were approved by CSU's Institutional Animal Care and Use Committee (IACUC). From the time the animals arrived, they were allowed to acclimate for at least 7-10 days before any manipulation.

Irradiations: On the day of irradiation, four mice of each strain were transported to the site of irradiation under stress-free conditions and were placed in plexiglass containers of dimensions 5 cm x 5 cm x 8 cm at the time of irradiation. The desired irradiation dose was delivered to the whole-body using a γ-rays from a J.L Shepherd Model 81-14 600Ci ^{137}Cs Sealed Source-070 irradiator, Serial No. 7014 in room MRB 006, at a low dose rate of 10 cGy/h for 24 h. The correct dosimetry was established by measuring the distance from source to the rack at time of set up and maintained by regular calibration. Two sham-irradiated mice from each group served as controls where they were treated under similar conditions but without the source being exposed. In both cases the temperature and humidity were maintained at the recommended standards (~22ºC and ~ 55%).

Euthanasia and tissue isolation: Within about 3 min after removal from the irradiator, the mice were euthanasia using CO_2 asphyxiation, their thoraco-abdominal walls were opened and right ventricular perfusion with 10 mL of 2% solution of heparin in normal saline was performed by

injecting the saline directly into the lungs via the pulmonary artery after a nick in the left atrium to prevent blood returning into the heart. The same volume of 10% neutral buffered formalin (NBF) was then used to perfuse and fix the lung through the same routes as the saline, before the whole lung was harvested and stored in 10% NBF for 24 h. The whole lung was transferred into 70% ethanol until ready for tissue processing. The lung lobes were then trimmed and transferred to fresh room-temperature 70% ethanol and taken to the Diagnostic Medicine Center of the Veterinary Teaching Hospital, Colorado State University, for processing. The tissues were dehydrated, and embedded in paraffin wax to form blocks from which thin sections about 5μmthickness were cut and floated on water at 50-60ºC wrinkle-free and later mounted on silane-coated HistoBond® slides (StatLab, McKinney, TX) for histochemistry and immunofluorescence.

Immunofluorescence staining: The slides were de-waxed using Xylene (Sigma) three times for 3 min each and then rehydrated by washing in graded concentrations of ethanol (Pharamaco, Shelbyvile, KY) starting with 100% once for 5 min, followed by 95% ethanol twice for 5 min each, and finally 50% ethanol twice for 5 min each. The slides were rinsed in dH_2O once for 5 min. All the washes were performed on a rocking platform oscillating a low speed. For antigen retrieval, tissue slides were boiled in 0.1 mM sodium citrate (pH 6.5) containing 0.05% Tween 20 for 15 min in a microwave oven at power setting 3 to maintain a temperature of ~95-100ºC and prevent overflow of the buffer solution with consequent tissue dry-out. After allowing the slides to cool at room temperature for 30-35 min, the slides were washed in dH_2O three times for 5 min each and then in PBS once for 5 min. Autofluorescence quenching was performed by washing the slides in 1 mg/mL solution of sodium borohydride in PBS (freshly prepared) three

times for 10 min each, followed by rinsing in dH$_2$O. The slides were then incubated in 10% normal goat serum for 30-35 min at room temperature to block non-specific binding sites in the tissue sections. Immunofluorescence staining was performed using monoclonal rabbit anti-γ-H2AX antibodies (clone EP854(2)Y, Millipore) diluted 1:500 in 10% normal goat serum as the primary antibody and incubation was at either 37ºC for 1 h, room temp for 2 h, or 4ºC overnight. The slides were then rinsed twice in PBS and then washed with PBS three times for 5 min each. AlexaFluor 594-conjugated goat-anti rabbit IgG as the secondary antibody, diluted 1:500 in normal goat serum, was added to the tissue slides and incubation was performed at 37ºC for 1 h. The tissue slides were then rinsed once in PBS followed by three washes in PBS for 5 min each. The slides were drained of any liquid and DAPI-containing antifade (VECTASHIELD®, CA) was added to the slides and cover-slipped. The slides were store in the dark until ready for imaging using a fluorescent microscope.

Image acquisition and processing: Imaging was performed using a fluorescent microscope (Nikon E600) equipped with CoolSNAP® CCD camera controlled by a (Prior Photometrics, Tucson AZ) coupled to a computer equipped with MetaMorph software version 7.3 (Molecular Devices, Sunnyvale, CA) that is capable of capturing images in an alternating order to discriminate 4′,6-diamidino-2-phenylindole (DAPI) (blue channel) and AlexaFluor-594 (red channel) by excitation using a Mercury arc lamp (Chui Technical Corp, NY). From the captured images both 2D and 3D images were generated to allow better localization and quantification of foci. The acquired images were processed by maximum image projection (MIP) algorithm to give a 2D image from each channel. The MIP images were then color-combined to allow for qualitative or quantitative assessment of the foci with respect to position within the nucleus,

relative sizes and distribution in the different cell types within the lungs based on the known anatomy of the lung. Tissues from mouse strains that are efficient in DSB repair are expected to have fewer foci than those less efficient in repair immediately following protracted low dose rate irradiation.

Data analysis: The results obtained were compared for the different cell types within the lung with respect to repair of radiation induced DSB, with non-irradiated mice as controls. The data generated from MetaMorph version 7.3 was logged directly into a MS Excel spreadsheet and used for statistical analysis and to generate graphs. The MS Excel spreadsheet was also used as data source for SigmaPlot for Windows (version 11.0) (Systat Software Inc., San Jose, CA) for statistical analysis. Different tests of variations using the SigmaPlot platform were performed, including one way repeated measures analysis of variance (ANOVA) performed for the different groups of mice to test for normality of distribution in the foci and for intra-group variation to test for variations in experimental outcomes (sample processing and foci counting). The all pairwise multiple comparison procedures (Tukey Test) was performed to compare the means of foci per nucleus between the different strains. In addition the Spearman rank correlation test was used to compare mean foci counts and the previous data from the mean % lung tumor incidence from Szymanska *et al*, 1999, after computing the fractions of the means for the mean foci counts and the mean % lung tumor incidence.

Results and Discussion

The major focus of the quantification was the areas within the region of the lung which are most likely to give rise to the major type of lung cancer. Though different regions of the lung may

give rise to lung tumors, the most common type of tumors are the ones that arise from the epithelial linings. (Bhattacharjee *et al*., 2001; Nicholson, 2002; Travis *et al*., 2002; Hayes *et al*., 2006; Sun *et al*., 2007). Bronchial and bronchiolar epithelial linings were the main ones selected for quantification of repair foci because these cells are thought to be the target cells for radiation-induced lung cancers in mice. Analysis for quantitative reporting was also confined to the first six bronchiolar epithelial nuclei in each image frame to avoid creating a bias that would result in exclusion of image frames where fewer foci may be seen in any image field. Those nuclei containing so many foci that were impossible to clearly distinguish the boundary of one focus from the other were excluded from analysis as the optimization stage. Small cell lung cancers are predominantly located in the bronchioles, while squamous cell carcinomas are thought to originate from the proximal airways. On the other hand, adenocarcinomas, the most common type of lung cancer, are more frequently detected in the distal bronchioles that contain the conducting epithelial cells.

Basal layer cells of the bronchiolar epithelium are most sensitive to ionizing radiation

To be able to select the areas or section of the lung to use for the comparative analysis of the foci formed in the different CcS/Dem strains, the formation of foci in the lungs after radiation with low dose rate of 10 cGy/h for 24 h followed by processing by immunofluorescence staining to visualize the foci was assessed to determine the distribution of the foci in the different cell types and in the different anatomical locations within the lungs. The anatomical locations of the different cell types was confirmed after examination and assessment of H&E stained sections of the lung, especially the bronchi, bronchiole and alveoli, as based on the known anatomy of the lung (Fig. 3.3A). Non-irradiated sections were also subjected to similar treatment. As can be seen in Fig. 3.3B, some foci did form in the cells near the basal/germinal layer of bronchiole in the

non-irradiated cells. No such foci were observed in the more differentiated apical nuclei towards the lumen of the bronchioles. These foci are expected to be formed in proliferating basal epithelial nuclei which are likely due to replicative break points formed in the lagging strands of the DNA (Okazaki fragments) during the S-phase of the cell cycle. It is important to note that foci are not formed exclusively where DSBs occur. Even the free DNA ends of Okazaki fragments formed during normal replication, or any factor that can lead to stalling of the replication fork may result in the formation of foci (Han *et al*., 2006; Ewald *et al.,* 2007).

Cells in all the different sections of irradiated lung almost invariably had foci. However, there are many more foci formed in the basal epithelial cells than in the nuclei of the apical cells. There are also fewer foci formed in the stromal cell nuclei in the parenchyma of the lung where most of the cells are expected to be highly differentiated (Fig.3.3C and 3.3D).

These characteristic features of the foci sizes may be related to the kind of damage incurred by the different cell types. It is possible that the more differentiated cells sustain less IR-induced DSB. The more actively proliferating cells represented by the basal cells of the bronchiolar and bronchial epithelial linings have their DNA in a more open conformation that is less compacted by chromatin. On the other hand it is expected that in the cells that are mainly withdrawn from the active cell cycle, represented by the apical cells of the bronchi and bronchioles, there is a higher amount of chromatin network that offer those DNA a higher degree of sheltering compared to the more actively proliferating cells.
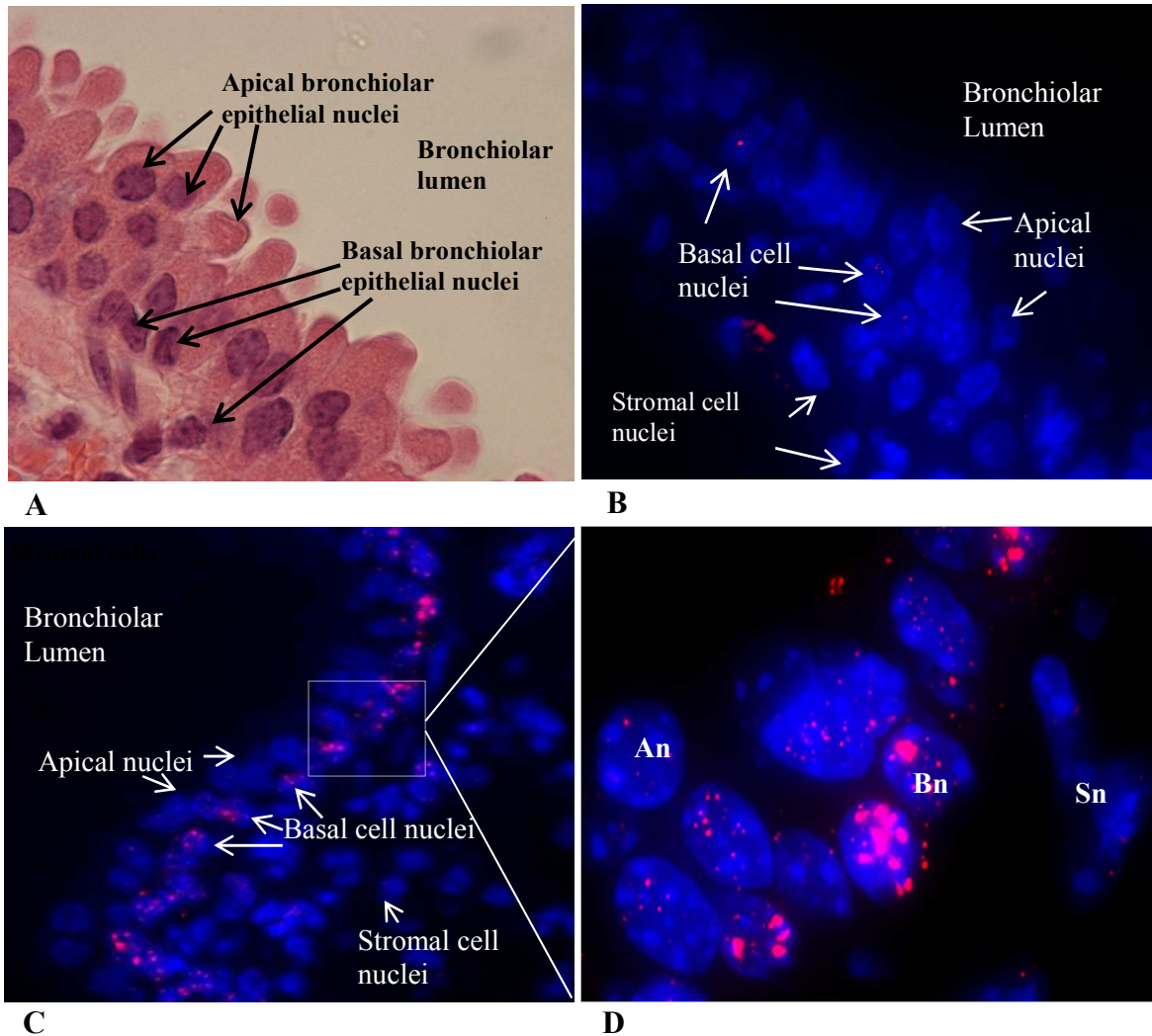
Figure 3.3: Formation of radiation-induced foci varies with the different cell positions/types in the bronchiole of the lung. A) H&E stained section of the bronchiole to show the location of the different cells. B) Non-irradiated section showing some foci formed in the cells near the basal/germinal layer of bronchiole in proliferating basal epithelial nuclei which are likely due to replicative breaks (Okazaki fragments formation) in the DNA during the S-phase of the cell cycle. No such foci were observed in the more differentiated apical nuclei towards the lumen of the bronchiole. C) Section of irradiated lung showing many radiation-induced foci formed in the basal epithelial cells compared to the apical cells. Even less foci are formed in the stromal cell nuclei in the parenchyma of the lung. D) Higher magnification of the inset in C to illustrate the foci characteristics in the different epithelial compartments. (**An**, apical nucleus; **Bn**, basal nucleus; **Sn**, stromal cell nuclei).

Regarding the foci number in basal epithelial compared to those in the stroma or apical epithelial cells, it is not surprising that the bronchiolar epithelial cells that are highly proliferative have the

most foci. Not all of these foci may have resulted from direct hit by the LET radiation generating IR induced DSB. Some of these may have been produced as a byproduct of base damage in S- or G2-phase cells whereby the process of DNA replication encountered an unrepaired base damage or single strand lesion while the other strand opposite the lesion is undamaged. This kind of collision can cause further replication problems on that undamaged strand leading to DSB over and above those in non-replicating cells, resulting in more γH2AX foci appearing in the more actively proliferating cells. On the contrary, cells that are terminally differentiated like those in the apical layer of the bronchiolar epithelium, and in the alveoli and stromal compartments of the lungs, fewer foci were observed compared to cells at the basal layer of the bronchiolar epithelium. The only logical explanation attributable to this observation is as stated above, i.e. the amplification of DSB from simple base damage or ssDNA damage that conflict with the replication machinery leading to exaggerated number of IRIF. It is unlikely that the cells with more foci received any more radiation dose than their counterparts, since they are all within the same tissue environment.

Although the checkpoint mechanism usually leads to arrest of any cell cycle progression till the damage is repaired, there is evidence to suggest that this may not always be the case. Nagasawa *et al*. (2010) noted that even cells in the G1/G0 when irradiated will go on to form chromatid-type or chromosome-type aberrations, involving both inter- and intra-strand exchanges. In this respect therefore cells can carry on with the cycle regardless of the integrity of the genome leading to eventual induction of tumor formation.

The other factor that is not usually considered when measuring IRIF numbers is the transcriptional status of the individual cells or group of cells. A cell in active state of

transcription is like a pugilist who is caught with the arms well away from his most vulnerable spots. The actively transcribing DNA is wide open to most brutal blows from radiation and can easily sustain a DSB compared to inactive ones. It is also possible that the basal cells in state of proliferation are also more transcriptionally active and therefore are more prone to damage by ionizing radiation from γ-rays.

Foci sizes are cell type-dependent within the lungs but not strain dependent

A cursory look at the foci formed within the lung reveals obvious differences in the sizes of IRIF among the different cell types. Cell of the conducting epithelium of the bronchi and bronchioles tend to form larger foci than cells in both the alveolar epithelium and the stromal compartments of the lung parenchyma (Fig. 3.4). In general the foci formed in the stromal cell nuclei and the nuclei of the respiratory epithelial cells of the alveoli were smaller than those seen in the conducting epithelial cells of the bronchioles (Fig. 3.4) and this observation is a common occurrence in all the CcS/Dem strains and their STS and BALB/c founders.

Using calibrated images generated after color combination of the two channels, the diameters of the largest foci were measured and compared in the different strains of mice. To rule out the obvious possibility that the observed foci were the result of overlap of adjacent foci in different places of the stack that appeared as a single focus after MIP, a montage of the image stack from each individual channel was generated and then color-combined (Fig 3.5).

Alveolar Region   **Bronchiolar Epithelium**
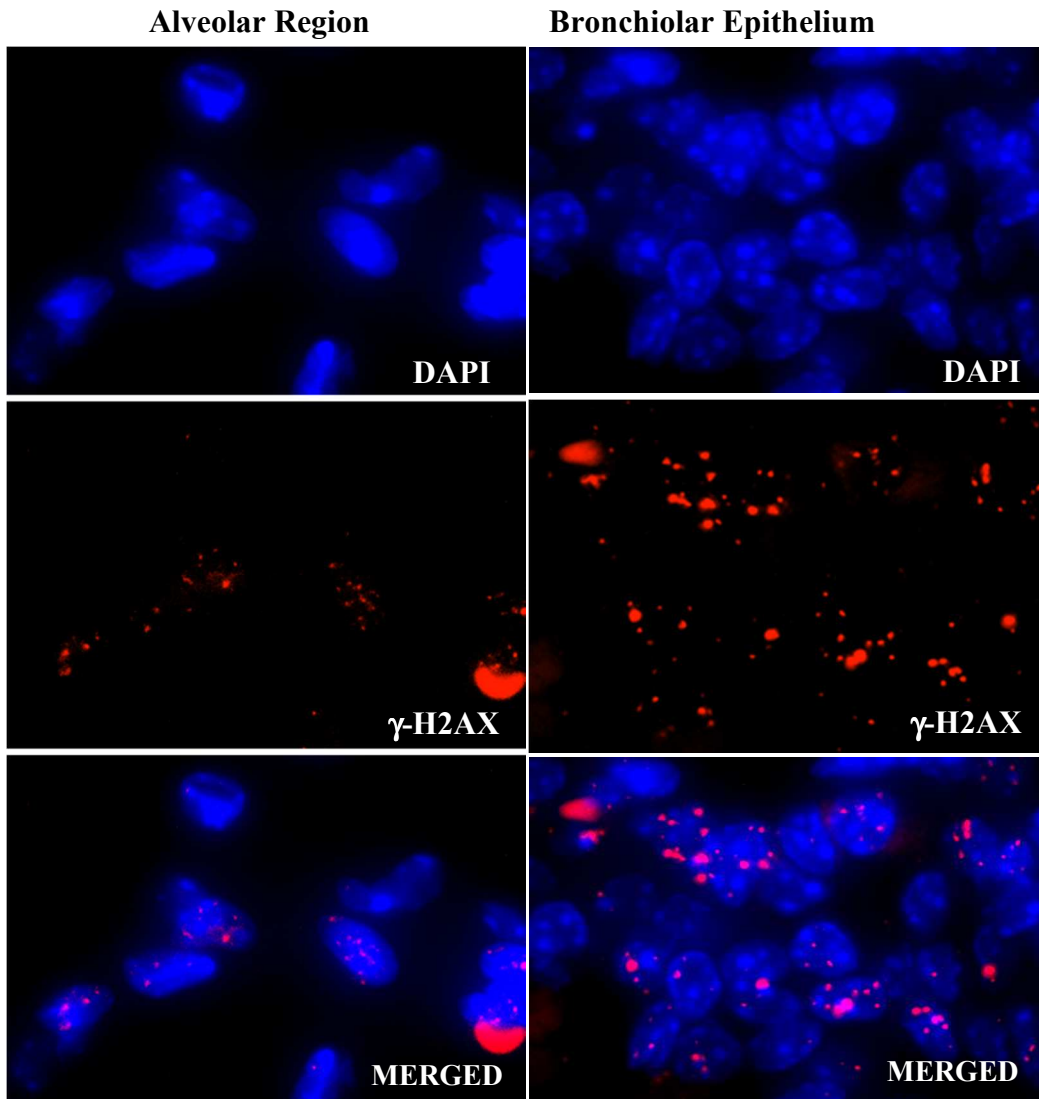
Figure 3.4: The epithelial cells have a more foci which are also larger in size than those formed in the parenchyma (alveolar cells) of the lungs. The mice were irradiated at a low dose rate of 10 cGy/h for 24 h (2.4 Gy cumulative) and euthanized immediately. Lungs were processed and subjected immunofluorescence staining for γ-H2AX. This outcome is an indication of the higher sensitivity of the epithelial cells to ionizing radiation.
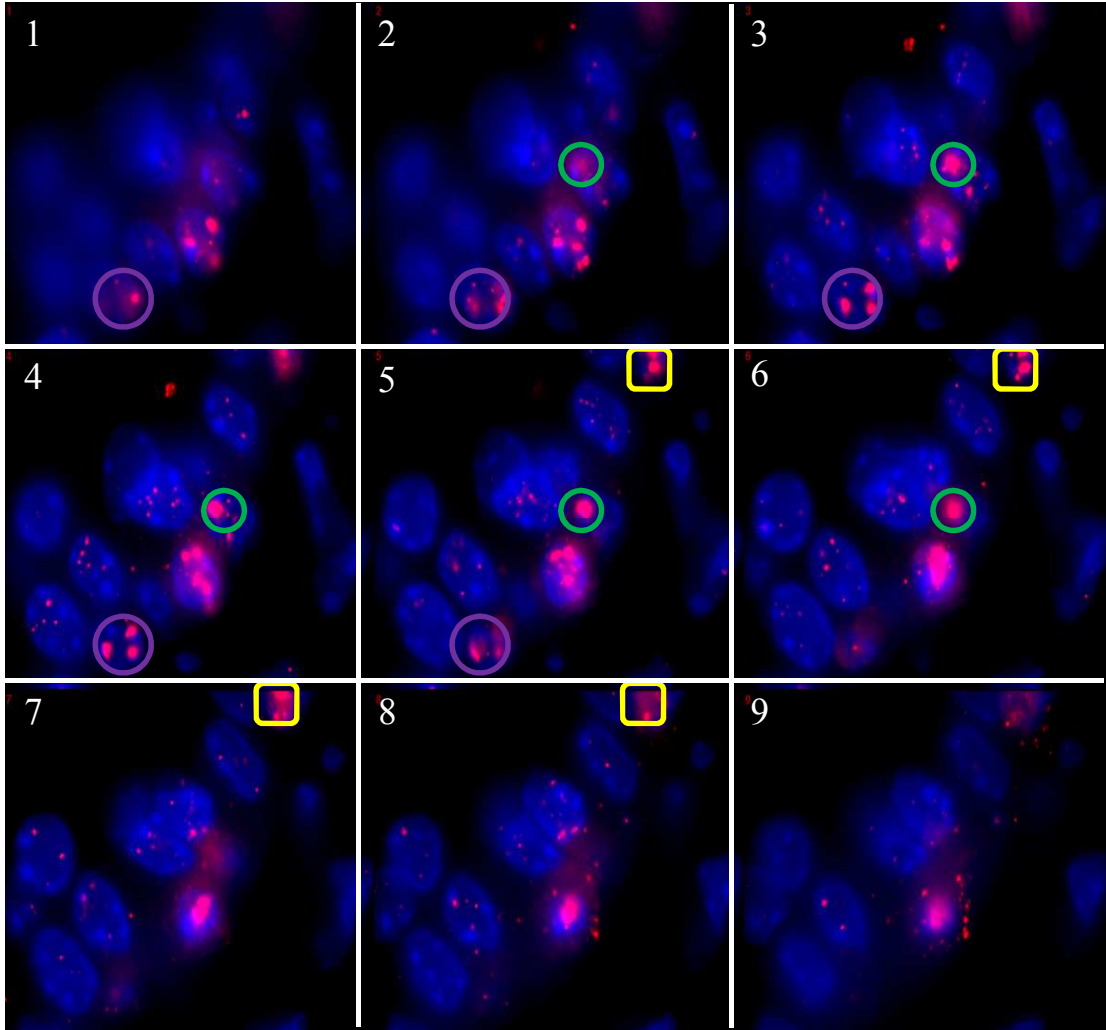
Figure 3.5: A montage of image stack showing evidence of coalescence of the DNA DSB repair centers. Some of the foci traverse up to 4 (yellow outlines) or 5 (green and purple outlines) slices, meaning the sizes of repair-induced foci can be ≥ 2 μm in diameter in some cases. Each slice represented by each panel is 0.5 μm in thickness.

Although some foci may have been the result of the formation of 'repair centers', that resulted in the impossibility to resolve them into different entities, they were treated as a single focus when they consistently appeared as a unit. It was obvious that fairly large foci were formed in some of the nuclei as stated above and some of the foci spanned 4 or even 5 planes of the stacks, each plane being 0.5 μm. The foci were therefore treated as one large focus.

Table 3.1: Summary of the largest foci sizes for the CcS/Dem strains that range from ~0.5 -1.75 μm in diameter. A total of 104 foci were sampled for each mouse with the measurements performed in triplicate, and the mean was computed from results.

Strain	Min	Max	Mean	Std.Dev	Std.Err	95% Conf	99% Conf
Ccs-1	0.53	1.29	**0.98**	**0.16**	0.016	0.033	0.043
Ccs-2	0.71	1.45	**0.96**	**0.17**	0.017	0.033	0.043
Ccs-3	0.65	1.74	**0.94**	**0.21**	0.021	0.041	0.055
Ccs-4	0.59	1.61	**0.87**	**0.20**	0.021	0.041	0.054
Ccs-5	0.65	1.48	**0.87**	**0.15**	0.016	0.032	0.042
Ccs-7	0.52	1.36	**0.86**	**0.16**	0.016	0.032	0.043
Ccs-8	0.59	1.25	**0.86**	**0.17**	0.018	0.035	0.047
Ccs-9	0.60	1.25	**0.85**	**0.14**	0.016	0.032	0.042
Ccs-10	0.65	1.45	**0.89**	**0.15**	0.016	0.032	0.043
Ccs-11	0.58	1.26	**0.88**	**0.16**	0.016	0.032	0.043
Ccs-12	0.65	1.32	**0.87**	**0.16**	0.013	0.026	0.034
CcS-13	0.71	1.35	**0.91**	**0.15**	0.017	0.033	0.044
CcS-14	0.65	1.51	**0.87**	**0.18**	0.018	0.035	0.046
CcS-15	0.65	1.46	**0.89**	**0.14**	0.014	0.032	0.038
CcS-18	0.65	1.47	**0.88**	**0.18**	0.018	0.035	0.047
CcS-19	0.71	1.48	**0.91**	**0.15**	0.015	0.032	0.041
CcS-20	0.65	1.77	**0.92**	**0.27**	0.026	0.043	0.058
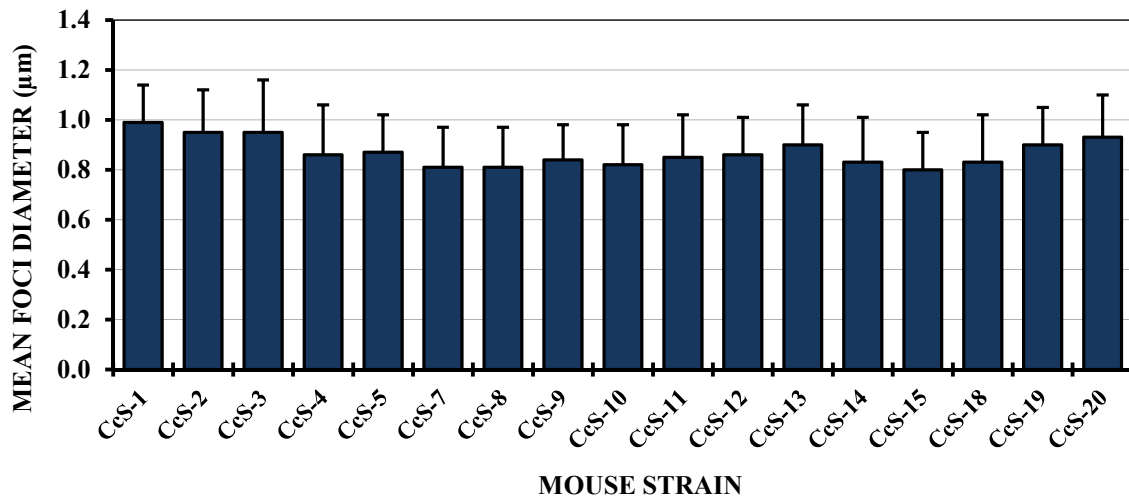
Figure 3.6: There were no significant differences in the average diameter of the largest γ-H2AX foci among all the CcS/Dem strains. The mice were irradiated using low dose rate γ-rays from a ^{137}Cs source delivered at the rate of 10 cGy/h for 24 h. The mice were euthanized immediately post-irradiation and lung samples processed for immunofluorescence. Immunofluorescence staining for γ-H2AX foci was followed by microscopic imaging. Measurement of the diameter of the five foci per image was performed after calibration where 1 pixel was equivalent to 64.5 nm. (Each bar, Mean ± STD).

From the calibrated images, the diameters of 5-8 of the largest foci were sampled for each image frame until at least 100 foci were measured. The average foci diameter ranged from ~0.85 ± 0.17 to 0.98 ± 0.15 (Table 3.1) and a graphical plot is represented in (Fig 3.6). The data obtained were tested for variation using different statistical tests. One way repeated measures analysis of variance was used to determine consistency of the differences or similarities within a stain or between the strains When subjected to statistical evaluation there were no statistical differencs among the different strains (P= 0.06). Similarly, using the Tukey test, there was no significant differences (p>0.05).

Most foci are formed outside or peripheral to heterochromatin region:

While analyzing the positions of the foci within each nucleus, it became apparent that wherever there is a dense DAPI staining area within the nucleus, which is composed of locations within the nucleus where the chromatin network is tightly compacted to form heterochromatin, there are either no foci formed or where they are present, they are mainly confined along the margin of the DAPI dense areas (Fig. 3.7). Relatively few are formed directly within the DAPI bright areas. When a count of the foci was carried out to categorize them into intra-heterochromatic or extra-heterochromatic, about 10-15% of the foci were observed to be located within or on the borders of heterochromatin regions in all the strain, including the STS and BALB/c founders. The foci formed within the heterochromatin are generally small in size even for nuclei in the basal layers of the bronchiolar epithelium, which usually have characteristic large sized IRIF that mainly within the euchromatin (Fig. 3.7A).
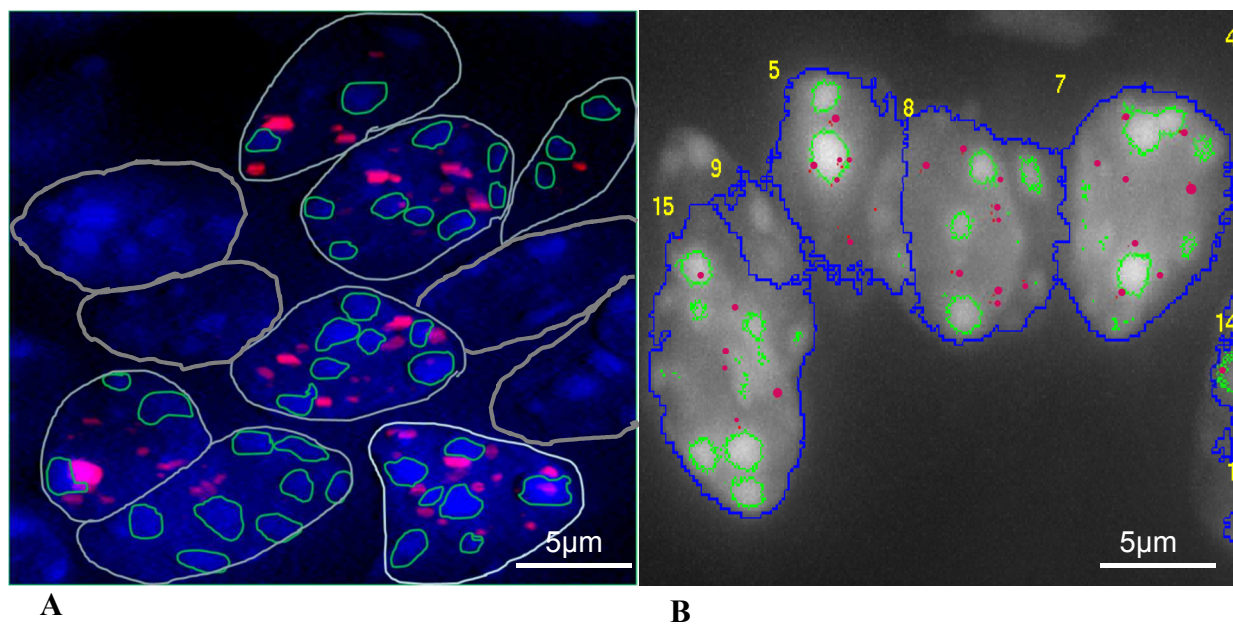
Figure 3.7: Most γH2AX foci are located in the euchromatic regions of the nuclei and are outside or peripheral to boundaries of the DAPI bright areas which are made up of dense heterochromatin (the bright blue areas with green outline in panel A; the green outlined light regions in panel B). In both panels, the γ-H2AX foci are the red dots. Less than 10-15% of the γ-H2AX foci are located directly within the DAPI bright heterochromatin areas.

It was observed here that the majority of the γH2AX foci are located in the euchromatic regions of the nuclei and the few that are close to the heterochromatin are usually peripheral to their boundaries (Fig. 3.7, the bright blue areas in panel A; the green outlined regions in panel B). In both panels, the γ-H2AX foci are the red dots. It was also estimated that less than 10-15% of the γH2AX foci are located directly within the DAPI bright areas. This observation is consistent with previous studies that reported the tendency of foci to be excluded from the heterochromatin regions (Jeggo, 1998). Directly related with our observation, Neumaier *et al*. (2012) also observed the tendency of IRIF to aggregate in defined spots within the nucleus to form what they referred to as repair centers within which repair factors appear to bring together the broken DNA ends into the 'repair factory" probably for the purpose of increased efficiency. This would not be

surprising as some of the foci we have observed in our study appear to be too big for a single broken DNA strand being rejoined. From our results some of the foci are more than 2 μm in diameter as demonstrated in Fig. 3.7.

The structure of the lung epithelium is distinctly different from that of the intestinal epithelium, both anatomically and functionally. In the intestines, there is always a rapid turnover of the lining requiring the continued proliferation of the epithelium and therefore stem cell and progenitor cell populations are reported to be abundant within the crypts. In the lungs there is a slow rate of turnover and therefore it is reported that the stem cell population is not very obvious (Stripp and Reynolds, 2007). The BASC are therefore not easily defined and it is a matter of contention that still needs further debate and research' (Reynolds *et al*., 2000b).

The possibility of tumor arising from the illegitimate fusion of genes that are induced to undergo breaks following IR treatment was suggested by a study carried out by Nikiforova *et al.,* (2000), where they found that the *RET* and *H4* genes were frequently found in close proximity within the interphase cells of the thyroid gland papillary region (at least 1 close proximity in 36 % the thyroid cells) and in 21% of peripheral blood leukocytes but only in 6 % of mammary epithelial cells. Certain tissues are therefore more prone to radiation induced tumor formation because of the ability of the radiation tracks to cause such illegitimate fusing to result in tumor formation. These hot spot mutations are reported to simply alter the topology of the protein rendering it incapable of folding in the right manner. But whether this is a pertinent issue in the cause of frequent tumor incidence in the lungs is not clear.

Post-irradiation foci number varied widely between the CcS/Dem strains

To compare the relative efficiency between the CcS/Dem recombinant congenic strains of mice and to determine any correlation between residual foci and the reported lung tumor incidence, immunofluorescence staining of slides was performed, and from this the images were captured to generate image stacks (10-12 slices per stack, each slice distance is 0.5 µm thick, 12 bit,) acquired as described in the Methods section. Because of the random nature of the DSB formed by Low –LET ionizing radiation compared to High-LET radiation generated by heavy ions/particles, the distribution of the of the foci was also random. It was therefore not possible to select any specific region of interest (ROI) for analysis of the outcome. Instead the ROI were also randomly selected purely based on the areas within the image frame where the nuclei had visibly the highest number of foci. One hundred nuclei were sampled for each slide and the experiments were repeated until a triplicate sample was analyzed.

As can be seen in Fig. 3.8A and B, there are no obvious patterns of the ionizing radiation-induced foci (IRIF) formation, an observation that has been made by others in previous experiments. The distribution is quite random and is characteristic of the pattern of DNA damage produced by low-LET radiation such as γ-rays. For quantitative considerations, foci that are well separated and clearly distinguishable from neighboring ones give the best opportunity to compare the strains. In this case there were rare instances where the foci were too close to demarcate, making it difficult to decide whether it was one large focus or if there were more than one. Where such nuclei were encountered, they were merely used for descriptive statistics and qualitative characterization of the foci and nuclei. An example can be seen in Fig. 3.8B where the foci within the nucleus (circled) are too close and impossible to demarcate from one another.

A   **B**
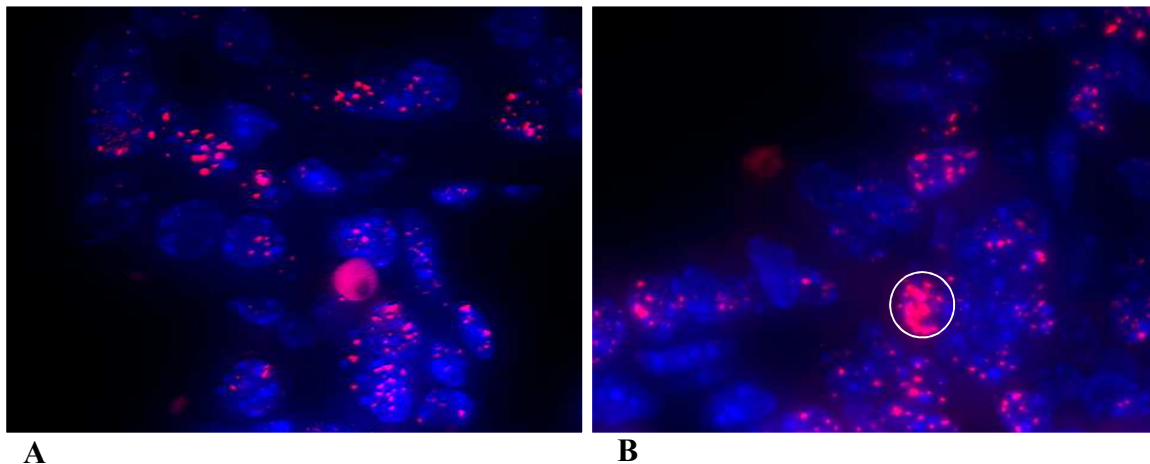
Figure 3.8: The distribution of IRIF is random and characteristic of low-LET radiation typical of DNA damage produced by γ-rays. The cells with more diffused γ-H2AX staining (outlined) is likely to be in S, G2 or M phase of the cell cycle since such cells are usually more sensitive to IR-induced DNA damage than the more terminally differentiated ones in G0 or G1 phase. The foci in the nucleus outlined are too close to one another to be used for quantitative comparison of DSB repair.

Such nuclei are excluded from the manual click-and-log counting. The resolution of the boundaries in such a case as this one is limited by the axial resolution of the microscope, even when the object was magnified 1000X (10X eye piece lens and 100X objective lens). However, when measurements are performed based on the foci intensity where the entire nucleus is outline and then the fluorescence intensity is automatically computed by the software, the nuclei can be included for quantitative estimation. The disadvantage in the first case is that it is assumed there is indeed likely more than one focus that have become aggregated into what others have referred to as "repair factory" or "repair center" (Neumaier *et al.,* 2012) during the repair process and it becomes practically impossible to discriminate the original individual foci. On the other hand it may indeed be possible that just one DSB resulted in one large aggregation of repair factors that may alter the pattern of binding of anti-γ-H2AX antibodies, or that H2AX is phosporylated on

more than the stated 2 Mb pairs of the DNA. This may also apply to some of the large foci mentioned under the qualitative characteristics, specifically the foci diameter being larger than the majority, some as large as $\geq$ 2 μm. In this case the actual number of DSB will be underestimated. Conversely, the disadvantage of estimating foci formation using total intensity within each nucleus is that even some background red fluorescence that is invariably present as a result of the immunofluorescence staining will be included in the estimation (Fig. 3.9).

DAPI   γH2AX   MERGED

DAPI INTENSITY   γH2AX INTENSITY
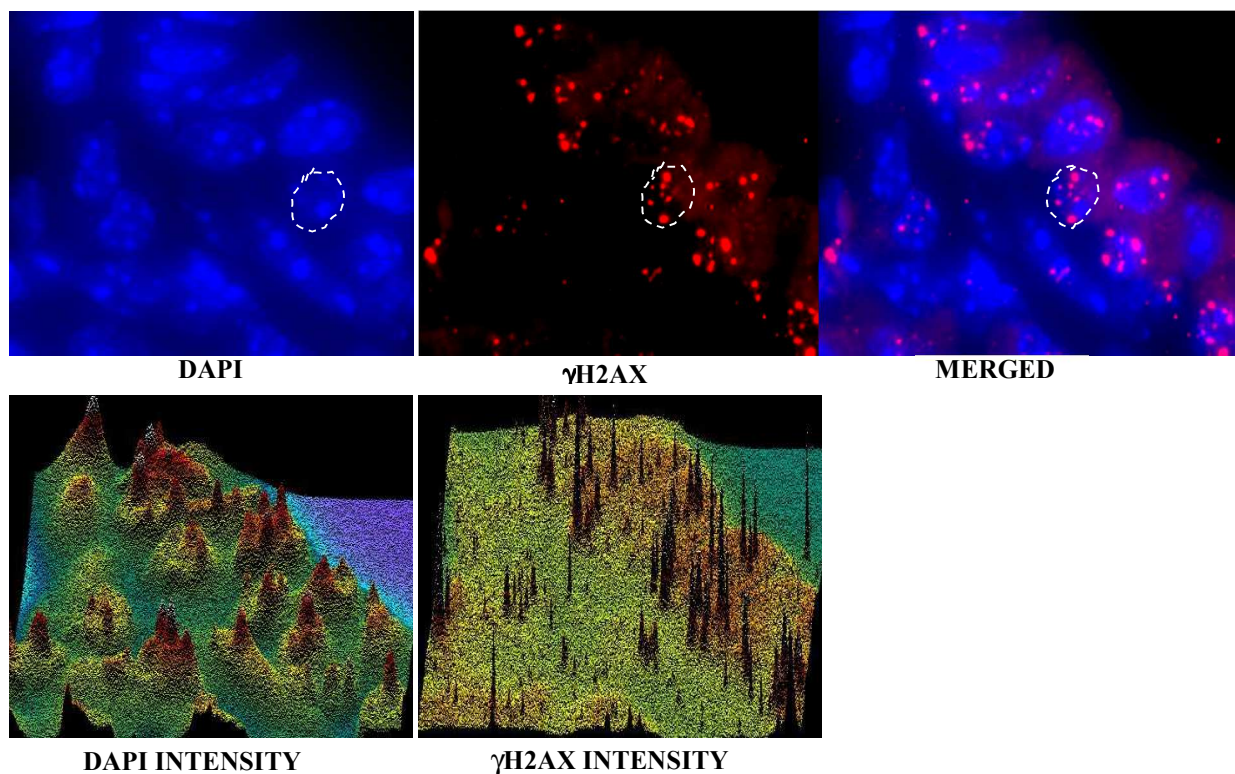
Figure 3.9: Images captured to generate z-stacks of 10 slices, each 0.5 μm in thickness, were then processed using Maximum Image Projection of the stack into 2D images for the DAPI and TexasRed channels. The images of the two channels were then merged. Below each, profiles of the DAPI and γH2AX staining intensities are presented to show how it can be used as alternative means of residual γH2AX foci quantification. An outline is drawn around the nucleus of interest as shown on the merged image and the integrated intensity of all the foci within the nucleus is measured and logged into the MS Excel spreadsheet. The results obtained are similar overall but there were significant between-experiment variations.

In this way relative DNA damage may be overestimated for some experiments than others as there is never a perfectly uniform background reduction during staining under all conditions. This therefore calls for developing and optimizing additional techniques to estimate the size of a single DSB. It may need to involve DSBs generated by enzyme or other techniques where the DSB are well isolated from other breaks and used to establish a baseline. Such a technique was attempted by Jakob *et al.* (2003) with some limited success. However, the limited success notwithstanding such a technique will be complicated by the complexity of the *in vivo* microenvironment of solid tissues, but if cell cultures are established as a monolayer, chances of success will be higher. Recently the FociPicker3D algorithm was developed to improve the discrimination of overlapping objects in an image (Du *et al.*, 2011) and hopefully it should help to sort out the complexity of the solid tissues.

Cognizant of and taking these factors into consideration, the manual click-and-log method was used to compare efficiency of DSB repair that is indirectly measured by the number of residual γH2AX foci at a given time point post-irradiation, although there is still some disagreement as to whether there is a direct correspondence between IRIF and DSBs, which Neumaier *et al*. (2012) attempted to address.

Having decided on the method to use, the images obtained were first examined visually to see whether one could tell at first glance the different groups to which the strains fall with respect to the number of residual foci. Representative images are given in Fig. 3.10 to show that indeed the differences in DSB repair efficiency of the different CcS/Dem RCS mice can be predicted from observing the pattern of distribution of IR-induced γH2AX foci after a low dose rate irradiation.
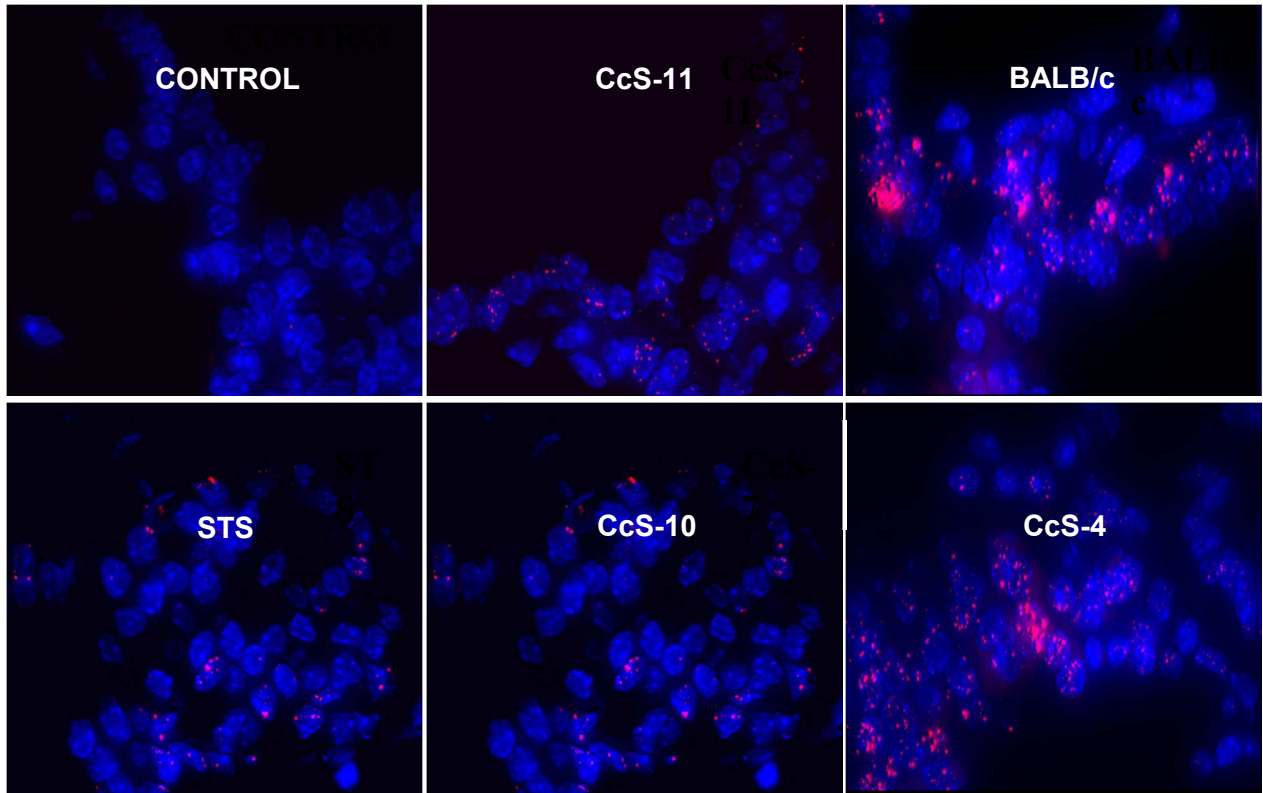
Figure 3.10: Comparison of representative images to illustrate strain-dependence of the formation of IR-induced γH2AX foci in the different CcS/Dem RCS of mice. The panels are color-combined images of different strains of mice treated with γ-rays delivered from a ^{137}Cs source at a low dose rate of 10 cGy/h for 24 h to give a cumulative dose of 2.4 Gy. The STS and BALB/c founders and sham irradiated control are included for comparison. There are visibly more foci in the CcS-4 strain than CcS-11 which in turn has more foci than CcS-10.

Laid side by side are color-combined images of different strains of mice treated with rays delivered from a ^{137}Cs source at a low dose rate of 10 cGy/h for 24 h to give a cumulative dose of 2.4 Gy and each strain used represents the main sub-group with respect to DSB repair efficiency. The STS and BALB/c founders and sham irradiated control are included for comparison. As can be seen from Fig. 3.10, there are visibly more foci in the CcS-4 strain than CcS-11 which in turn has more foci than CcS-10. These images clearly illustrate the strain-dependence of γ-H2AX foci formation and eventual resolution which in turn can be used to predict the susceptibility of these strains to developing IR- induced tumors.

The combined images were then used to count the number of residual foci at the end of the irradiation period. Manual counting by click-and-log into a MS Excel spreadsheet was performed in MetaMorph platform as described above. From the spreadsheets, the distribution of the foci in the different strains were assessed and presented in Fig. 3.11 which shows the distribution of foci among the different strains. Additionally, other useful data and illustrations can be derived from the counts to provide evidence to show that foci formation and resolution is strain-dependent. The results are summarized in Table 3.2. The table also includes the results of the previous study that formed the basis for the present study where the tumor incidences for the different strains were reported. The table was then used to generate other informative data sets that help to confirm that efficiency of DSB repair is strain-dependent.

In Fig. 3.12, the mean foci per nucleus for the different strains were plotted for the irradiated and non-irradiated control CcS RCS and their founder parental strains. Except for BALB/c which had 3 ± 1.3 background foci, all the other strains had $\sim1.5\pm1.2$ foci, likely the results of replication associated DSB. There are wide differences among the irradiated strains that ranged from 6.7 ± 2.4 to 23 ± 5.2.
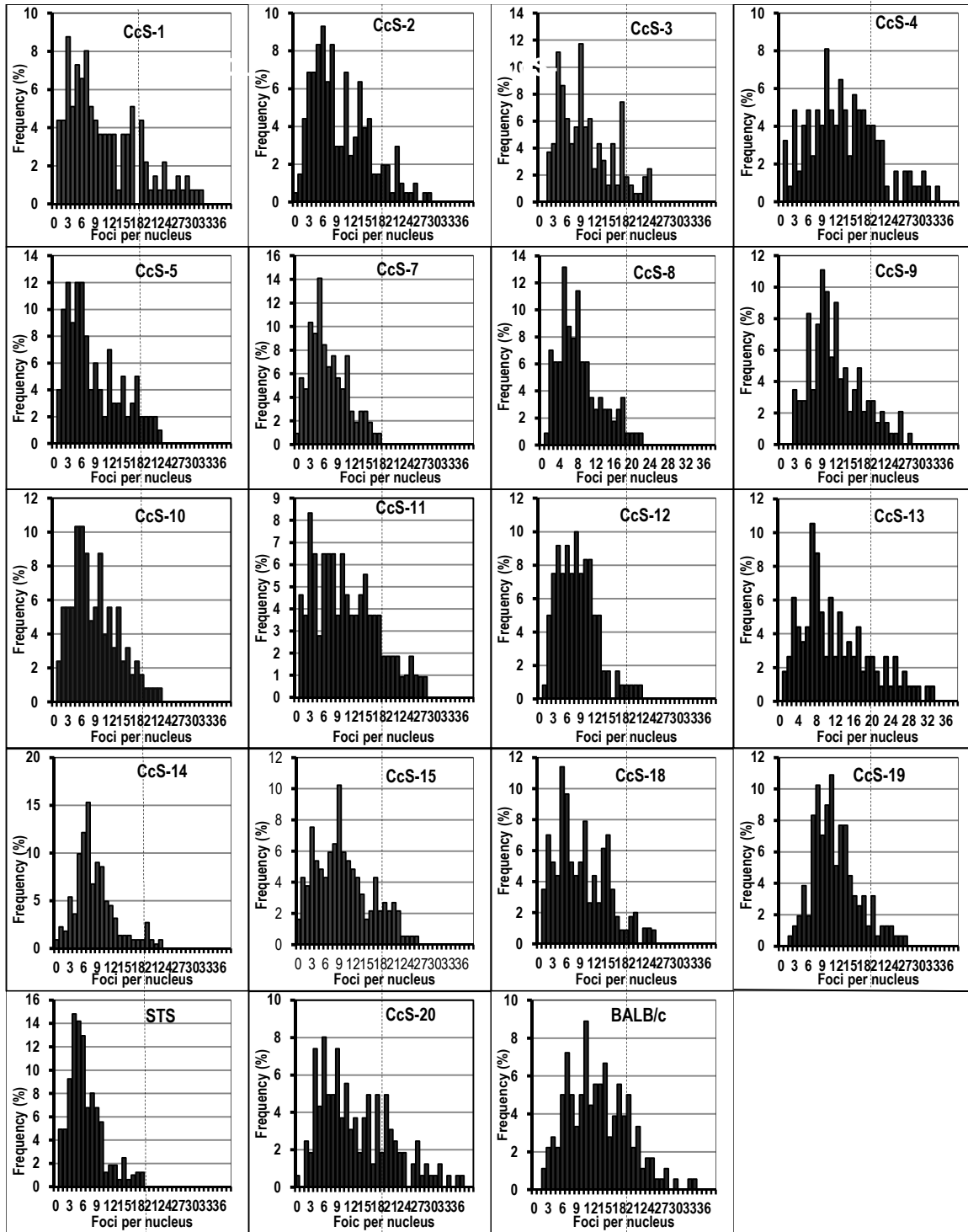
Figure 3.11: The distribution of IR-induced γH2AX foci in CcS/Dem mice is strain-dependent. The less radiosensitive strains have their distributions skewed to the left and the most sensitive ones extend far towards the right. The more efficient the strain in DSB repair the more skewed to the left the hiostogram. The vertical dotted lines show the wide difference between the strains compared to the STS strain with the lowest foci/nucleus.
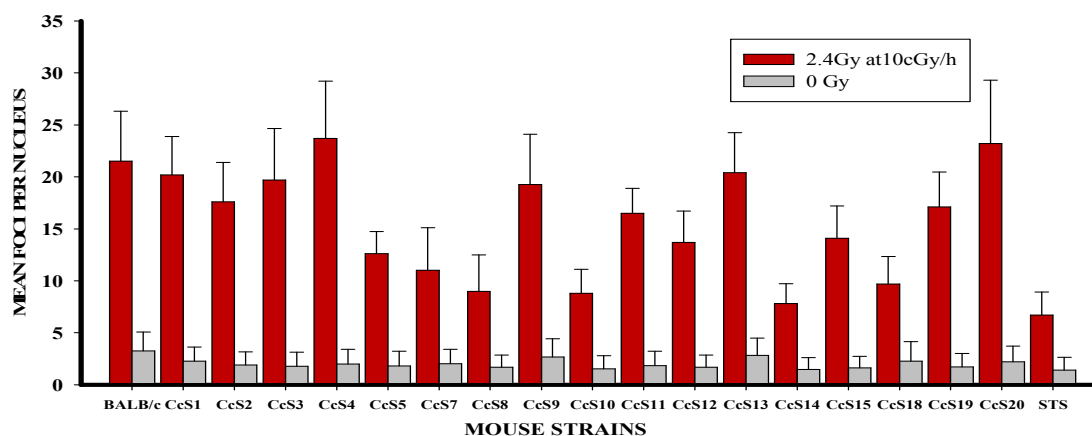
Figure 3.12: The mean foci per nucleus for the CcS/Dem RCS mice showing the wide variations in their capacities to repair DNA DSB.

To directly compare the foci data to the lung tumor incidence data, the plots in Fig 3 13 were generated. From these plots, the close similarity between the radiogenic lung tumor incidence and efficiency of radiation induced DNA damage repair response in the CcS/Dem RCS mice are very evident. In Fig. 3.13A, the mean % tumor incidence and mean residual foci per nucleus are plotted on the same scale. Although the values are quite different in magnitude, the two plots mirror one another showing that there is a close correlation between the two variables in these strains. Using these values as they are, the statistic shows they have high correlation (Spearman Rank correlation coefficient, R = 0.946, *P*< 0.001).

Table 3.2: There are about three categories of RCS mice with respect to DSB repair efficiency. Colum 2 of the table represents the % tumor incidence from the previous study and column 4 is the mean foci per nucleus from the present study. The Columns 3 and 5 are the fraction of the means for each parameter measured. The fraction of the mean is computer by getting the average of the figures in columns 2 and 4 respectively, and using the computed average as the denominator to calculate the value for each strain as a fraction of the average for all the strains. Here again the values for CcS-6, CcS-16 and CcS-17 are excluded as they were not used in the present study.

Strain	Mean % tumor incidence	Fraction of mean tumor incidence	Mean foci per nucleus	Fraction of mean foci #/nucleus
STS	*NA	*NA	6.7	0.44
CcS-10	10.2	0.39	8.7	0.57
CcS-14	11.9	0.46	8.2	0.54
CcS-7	12.5	0.48	11.2	0.73
CcS-8	15.1	0.58	11.1	0.73
CcS-18	15.5	0.59	10.0	0.66
CcS-15	21.5	0.82	14.5	0.95
CcS-12	24.1	0.92	13.7	0.90
CcS-5	24.1	0.92	12.6	0.83
CcS-11	26.8	1.03	16.5	1.08
CcS-1	32.2	1.23	17.8	1.17
CcS-2	32.1	1.23	18.1	1.19
CcS-19	32.5	1.24	17.1	1.12
CcS-9	35.4	1.35	19.3	1.27
CcS-13	35.6	1.36	20.0	1.31
CcS-3	37.8	1.45	18.3	1.20
BALB/c	39.2	1.50	19.8	1.30
CcS-4	42.7	1.63	23.1	1.52
CcS-20	43	1.65	22.9	1.50
MEAN	**27.34**		**15.24**	

- *NA- no data available for STS

For a better comparison, it was decided to compute the fractions of the means for the two variables and use them to compare radiation-induced lung tumor incidence and the residual DSB repair foci following the low-dose rate irradiation delivered at 10 cGy/h for 24 h. In this way, the magnitudes of the two variables are then similar and therefore give a better comparison. As can be seen in Fig. 3.13B, the very close similarity of the values for the two variables are remarkable,

clear indication that the efficiency with which radiation-induced DSB is repaired can be a suitable predictor of the susceptibility to tumor development in the lungs of these strains of mice (R=0.946, *P< 0.01).
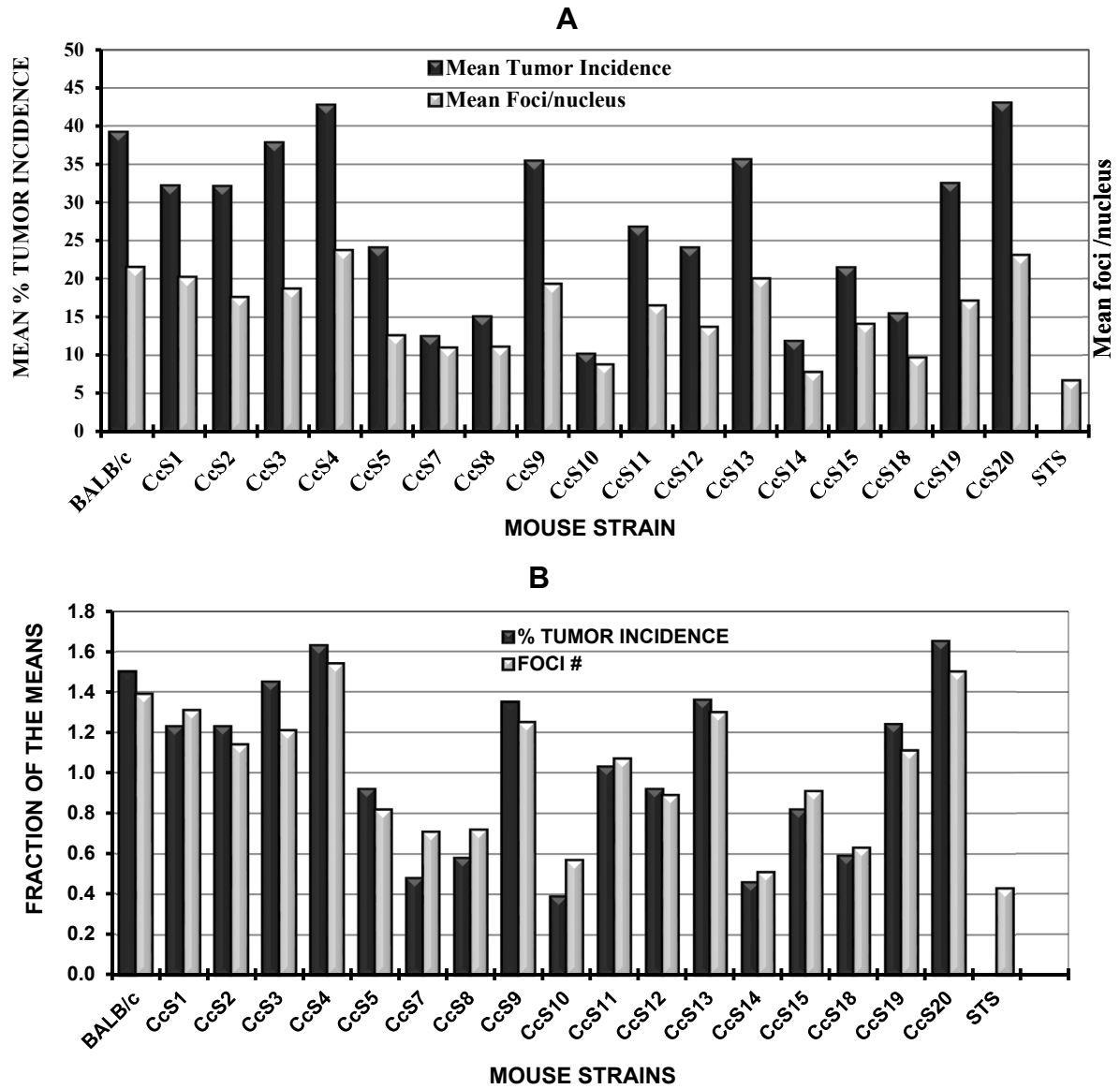
Figure 3.13: Plots to show the close similarity between the radiogenic lung tumor incidence and efficiency of radiation induced DNA damage repair response in the CcS/Dem RCS mice. In A, the mean % tumor incidence and mean residual foci per nucleus are plotted on the same scale. Though the values are quite different in magnitude the two plots mirror one another. In B, the fractions of the means were computed and used to compare lung tumor incidence and

foci/nucleus. In this way, the magnitudes of the two variables are similar and therefore give a better comparison.

For a better comparison, it was decided to compute the fractions of the means for the two variables and use them to compare radiation-induced lung tumor incidence and the residual DSB repair foci following the low-dose rate irradiation delivered at 10 cGy/h for 24 h. In this way, the magnitudes of the two variables are then similar and therefore give a better comparison. As can be seen in Fig. 3.13B, the very close similarity of the values for the two variables are remarkable, a clear indication that the efficiency with which radiation-induced DSB is repaired can be a suitable predictor of the susceptibility to tumor development in the lungs of these strains of mice (R = 0.946, P< 0.01).

For a better comparison, it was decided to compute the fractions of the means for the two variables and use them to compare radiation-induced lung tumor incidence and the residual DSB repair foci following the low-dose rate irradiation delivered at 10 cGy/h for 24 h. In this way, the magnitudes of the two variables are then similar and therefore give a better comparison. As can be seen in Fig. 3.13B, the very close similarity of the values for the two variables are remarkable, a clear indication that the efficiency with which radiation-induced DSB is repaired can be a suitable predictor of the susceptibility to tumor development in the lungs of these strains of mice (R = 0.965, P< 0.001).

A

B
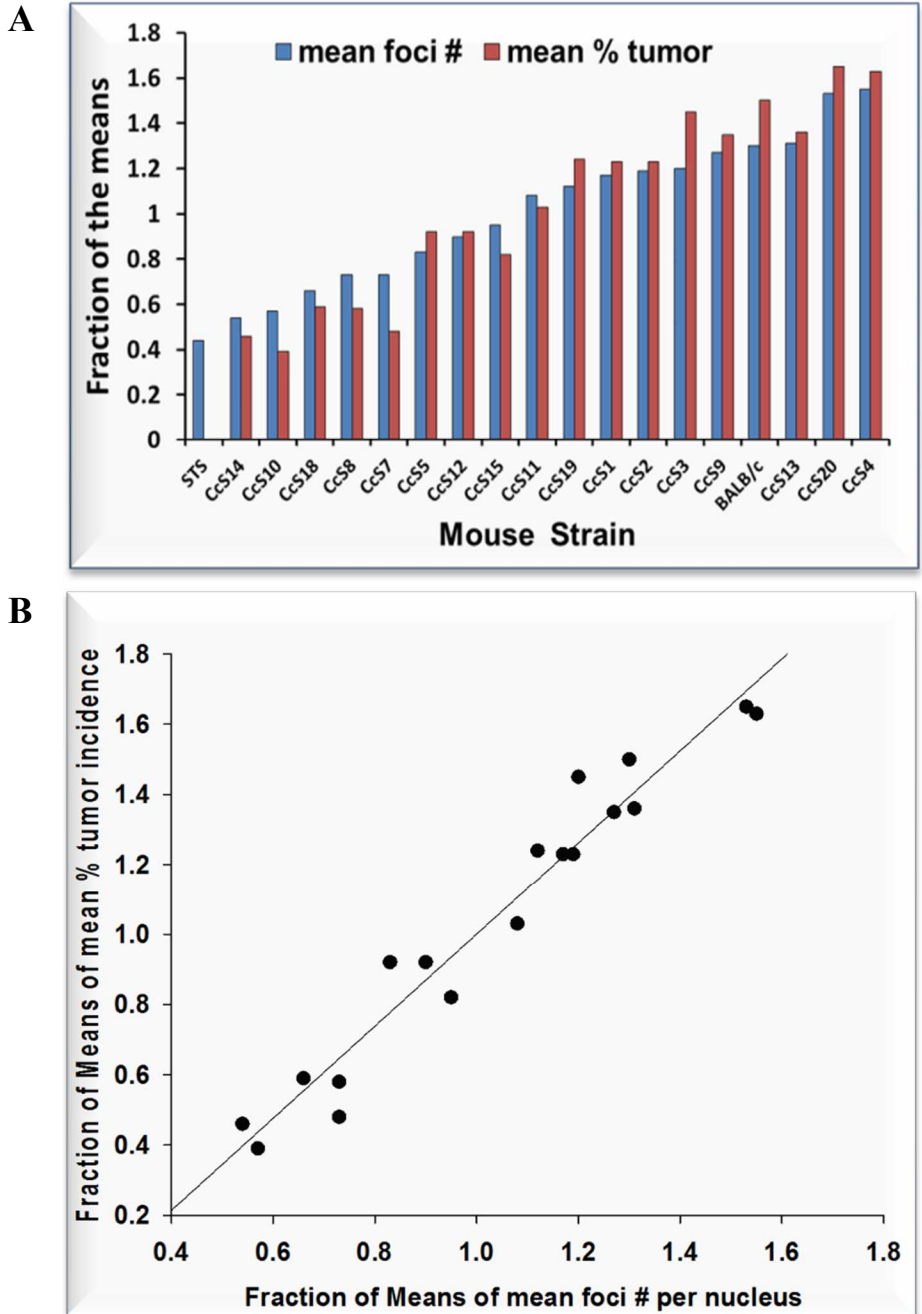
Figure 3.14: Comparing the γ-H2AX foci number and the percent tumor incidence in RCS mice: (A) Plot of the fraction of the means for foci number and tumor incidence for each of the mouse strain arranged with reference to increasing foci numbers. Strains with low tumor incidence tend to have low foci per nucleus. (B)Correlation plot of fractions of the means for mean % tumor incidence and mean number of foci per nucleus. Spearman Rank Correlation Coefficient, R=0.965, $P<0.001$.

Table 3.3: A summary of the major groupings based on the outcome of the number of residual foci per nucleus and the results of the test of significance from Pairwise comparisons ANOVA indicating no significant differences in foci numbers for the strains placed within the same group.

LOW	MED.	INT.	HIGH
CcS-7	CcS-5	CcS-1	BALB/c
CcS-8	CcS-11	CcS-2	CcS-4
CcS-10	CcS-12	CcS-3	CcS-20
CcS-14	CcS-15	CcS-9	
CcS-18		CcS-13	
STS		CcS-19	

This consistent observation of the images having most of the IRIF foci mainly excluded from the DAPI bright areas which represent regions of heterochromatin, or are peripheral to them and instead the foci mainly located in the non-DAPI bright areas where the euchromatin is predominant may be an intrinsic strategy employed by the cells to avoid the risk of chromosomal rearrangement in the closely compacted heterochromatic chromatin. Since highly repetitive sequences are reported to be enriched in heterochromatin domains, the presence of DSBs can easily lead to the risk of rearrangements between these repetitive sequences and this can easily lead to loss of genome integrity.

There are also reports to the effect that when a DSB forms in the heterochromatin, a series of activation process and relocation of the chromatin away from the center to the periphery of the heterochromatin that may partly explain the appearance of most foci in euchromatin (Zarebsk *et al*., 2009; Jakob *et al*., 2011)]. According to this theory, following the damage, a number of processes occur in several steps among which are the usual DSB detection, checkpoint

activation, and resection of portions of DNA where appropriate several steps that occur. In addition to these normal repair processes, studies involving MEFs and HeLa cells revealed that these steps are followed by a "dramatic increase in the movement of DSBs in heterochromatic regions toward euchromatic regions" (Jakob *et al.,* 2011). Perhaps due to the fact that there is extensive coiling of the nucleosome within the heterochromatin, re-localization may be a strategy to prevent rearrangements in repetitive DNA sequences present in heterochromatin as stated above. In another study with *Drosophila*, Rad51 foci were reported to form only after the heterochromatic DSBs move to the periphery of the heterochromatic region and the heterochromatin protein 1 (HP1) is reported to play a significant role in the re-localization (Jakob *et al.,* 2011). A working model to explain this kind of mechanistic strategy and the behavior of heterochromatic complex as presented in a review by Thompson (2012) which was suggested based on the fact that IR- induced DSB initiates the release of HP1β that promotes the complex of the histone acetyltransferase Tip60 and ATM (Tip60-ATM) to bind to tri-methylated H3^{K9-Me3} and it is this process that leads to activation of Tip60 and ATM to achieve relocation of heterochromatic DSBs (Jacob *et al.,* 2011).

From the evidence provided in the stated working model, it is apparent that the other histones are not mere passive bystanders in the DSB repair process but have vested interest in the welfare of the cell, and it must be for the sake of their own existence. There is apparently a closely knit interplay between the many factors that enable DSB repair including the reported relocation of the damaged DNA out of the heterochromatin. For instance, MRN complex is required for ATM activation at the site of a DSB and the recruitment of Tip60 into DSB as well as for efficient acetylation and phosphorylation of ATM. It is therefore evident that as H3^{K9-Me3} and HP1 are

found in euchromatin too (see review Thompson 2012; Vakoc *et al.,* 2006; Kwon *et al.,* 2008] and through their role in ATM$^{S1981-P}$ formation, these factors also participate in DSBs repair outside of the heterochromatin as well.

Foci numbers in normal tissue context vis. those reported for 2D cultures

The number of IRIF seen in tissues is slightly difficult to estimate compared to 2D culture cells. The latter category of cells is more spread out and the DNA is more widely spaced such that the individual foci can be teased apart. In their normal context and natural environments, the cells tend to have more compacted nuclei and the DNA is more crowded together. As a result there is a high apparent tendency for the foci to overlap, leading to underrepresentation of their true number. The other factor that cannot be overlooked in this regard is the likely influence of the neighboring cells in a tissue environment as opposed to a 2D monolayer culture. In the latter system, the cells are more isolated, and it is more likely that signaling networks for intercellular communication and information flow between cells will be different than in a tissue context. Additionally, the cell matrices interact through specialized cellular junctions between their borders, and this can alter cellular responses, among which is check point monitoring, halting proliferation in response to DNA damage, and even basic molecular processing involved in DNA DSB is expected to be different between the two systems. More neighbors means more external influence in the manner the cell responds to DNA damage, may be for the better, compared to cells in a 2D monolayer culture. The outcomes may mirror those *in vivo* but the absolute values are likely to be different than in culture. Comparing these results to those conducted by Kato *et al*, (2006) using MEF under similar irradiation regimen, the foci number appear higher in the 2D system than in our in our normal tissues. The tissues in question here though are entirely

different, and the responses may be cell type -dependent. However, results of experiments by Withers research group (Withers *et al.*, 1974; Masuda *et al.,* 1976) contend that there are no significant differences in the dose-response results and characteristics of the measured parameters in normal tissues and in 2D cultures. More recently, the Bedford group reported similar observations from experiments conducted using acinar or ductal structures in 3D Matrigel cultures and 2D monolayer cultures (Lin *et al.*, 2009) where they believe the outcomes were not different between the two systems.

Conclusion

From the foregoing it is very reasonable to say that since there is a very high correlation between the number of radiation-induced γH2AX foci and the incidence of lung tumor in these CcS/Dem RCS mice the efficiency with which IRIF are resolved, or the persistence of γH2AX foci can therefore be used as a reliable predictor of susceptibility to radiogenic lung tumor development or the likelihood that an individual will develop lung tumor with time. The results highlight the possible role of DNA DSB repair in protection against radiation-induced lung cancer. Additionally, low dose rate radiation exposure followed by immediate quantification of repair foci in exposed cells provides a sensitive assay for DNA DSB repair efficiency that can be employed for measurements after low dose rate exposures to ionizing radiation.

Chapter 4 :

USE OF γH2AX FOCI IN PERIPHERAL BLOOD LEUKOCYTES AS SURROGATES FOR DNA DAMAGE RESPONSE IN THE LUNGS OF CcS/Dem RCS MICE

Summary

In recent years, there has been growing interest in the use of the γH2AX assay as a potential tool for biodosimetry in cases of radiation disasters, especially where there are mass casualties that require large scale screening. While there are still problems associated with automation, one area this technique could find immediate use is in clinical applications for patient pre-screening to assess their suitability as candidates for radiotherapy, especially in fairly young ones who still have many years of potential lifespan ahead of them. Relapses following radiation therapy are not uncommon, which may result from unsuccessful irradiation of some stem cell-like tumor cells or could be the result of normal cells in the penumbra around the target tumor being irradiated that survived with improperly repaired DNA damage following irradiation. These can then acquire transforming mutations that later become overt tumors. However, it may not be a major concern to patients who think they lose nothing by undergoing radiotherapy even if the consequences are dire, since desperate times may require desperate measures. Our results have shown a strong correlation between inefficient DSB repair in cells of the bronchial epithelium and at the bronchio-alveolar junction and susceptibility to radiation-induced lung cancer. This part of the study is aimed at using peripheral blood leukocytes as a surrogate to assess DNA repair efficiency in the lungs. If the leukocyte results correlate with those of the lung study, it would allow the use of leukocytes, which, unlike lung tissues, are readily available to predict

susceptibility to radiogenic lung cancer development. Mice of the CcS/Dem recombinant congenic strains were subjected to whole body irradiation using γ-rays at a low dose rate of 10 cGy/h for 24 h. After euthanasia, heparinized blood was drawn directly from the heart and samples were then processed by the lyse/separate/fix method. The slides were stained for immunofluorescence microscopy and used for quantification of γ-H2AX foci in the peripheral blood leukocytes. Although the absolute mean values of foci in PBLs and bronchioalveolar cells were different, the inter-strain differences in DNA repair efficiencies correlated very closely to those in the lungs for all the six strains that were compared (Spearman rank correlation coefficient, R=0.948). From the comparison of the foci numbers in the PBLs and in the lungs it can be concluded that PBLs are good surrogates for DNA DSB repair efficiency in the lungs of CcS/Dem RCS mice.

Background

When cells are exposed to ionizing radiation or other genotoxic agents, there is large scale activation of specific DNA damage signaling and repair mechanisms involving the nucleosomal core histone variant H2AX that forms part of the cellular DNA damage response where it becomes phosphorylated in the vicinity of the DSBs (Rogaku *et al.*, 1998; Rodrigue *et al.*, 2006) to form γH2AX that extend ~2 Mb pairs upstream and downstream of the breakpoint (Rogakou *et al.*, 1999).

The responses to DNA damage appear to differ in actively proliferating cells and terminally differentiated cells. There is emerging evidence to show that cells that are terminally differentiated have some unique characteristic H2AX distribution that make them respond less

efficiently to DNA DSBs compared to actively proliferating cells. It was earlier reported by Chepelev *et al*. (2009) and later demonstrated by Jungmin *et al.* (2012) that for the same cell type, actively proliferating Jurkat T-cells, which is a model for acute T-cell leukemia, were found to have >8-fold H2AX expression compared to normal resting T cells which the authors think may reflect the cellular demand for DNA repair in Jurkat cells than in the resting T-cells. Differential distribution of H2AX was noted after comparing proliferating Jutkat T-cells that were reported to deposit most of the H2AX in the sub-telomeric and actively transcribed gene regions that are highly enriched in H2AX, while the H2AX protein in resting T-cells tended to have a slight preferential deposition in the non-transcribed region of the genome (Jungmin *et al.* (2012). The other observation was that sub-telomeric regions were less sensitive to exogenous sources of DSB than endogenous DSBs, particularly replication stress (Tsantoulis *et al.*, 2008). In terminally differentiated cells there also appears to be a global attenuation of DNA repair (Nouspikel and Hanawalt, 2002). This is reported to arise from repression of the H2AX miRNA by a species of microRNA in terminally differentiated cells (Lal *et al*., 2009) compared to actively proliferating cells. The implication for these observations is that, compared to cells that are actively proliferating where DSBs can occur during each round of replication, especially the S and G2 phases, cells that are in stationary phase are expected to have low background DSB levels since they have less replicative activity. This should be true of most circulating leucocytes, except the immature ones that are not yet fully differentiated and still within the bone marrow or the thymus.

As in other tissues of the body, the same molecular players modulate DNA damage response (DDR) and DSB repair in leukocytes through their involvement in γ-H2AX formation, namely:

the PIKK family proteins which may act in a redundant manner (Stiff *et al.,* 2004; Wang *et al.,* 2005). An important attribute of radiation induced DSB during the formation and loss of γ-H2AX foci measured following exposure to radiation is that foci yields have been shown to increase linearly with dose for radiation doses as low as 1 mGy (Rothkamm and Löbrich, 2003). Since there is a close correlation between the number of DSB and the observed γ-H2AX foci number, though an indirect relationship, the disappearance of γ-H2AX has been used as a reliable marker for DSB repair. Any factor(s) that compromise DSB repair will be reflected in the persistence of residual foci number (Rogakou *et al*., 1999; Rothkamm and Löbrich, 2003; Rothkamm *et al*., 2003; Kuhne *et al*., 2004).

At times of radiation emergencies when there is acute need for biodosimetry parameters to allow for effective triage, a readily accessible and immediately available source of samples for cells that is also minimally invasive will become essential. Scrapings from the buccal cavity do not offer any better advantage over blood samples that are easy to obtain and that people are acquainted with since phlebotomy has become a routine in clinics.

An important factor that is of practical significance is the issue of relapse following radiotherapy that may arise from any of three processes. First, relapse may result from unsuccessful treatment of some tumor cells with stem cell-like characteristics that make them resistant to radiotherapy. Secondly, it is possible that normal cells in the penumbra of the targeted tumor being irradiated may incur some damage but survive to acquire transforming mutations that later become overt tumor cells. The third possibility is that the actual tumor cells that are otherwise radiosensitive, survive the irradiation to continue proliferating. Whichever of these events may be the cause of

any relapse, it may be essential for pre-irradiation evaluation of the radiotherapy subjects for efficiency of RI-DNA DSB repair.

The manner in which patients respond to RT schedules is usually revealed by the differences in the degrees of normal tissue toxicity they exhibit and this is one reason that may limit the efficacy of treatment (Johansson *et al*., 2000). Normal tissue tolerance to RT has been the reason for the narrow limits of dose range that can be employed in clinical practice (Buchholz, 1999). Because of such concerns, a lot of research has gone into attempts to develop methods that could adequately predict radiation-induced toxicity (Hoeller *et al*., 2003; Ozsahin *et al*., 2005; Rübe *et al.,* 2010). Some of the research also simultaneously tried to address the ease with which samples can be obtained as well as the convenience to the individual patients Henríquez-Hernández *et al.*, 2012; Moquet *et al*., 2014). If a universal method could be developed and optimized, this would make it possible to have better individualized treatment schedules for patients. Developing individualized schedules of radiation treatment that are based on normal tissue prediction assays would improve the response to treatment and help to explore alternative therapy for cancer control or side effect amelioration.

From the results of comparative analyses of DSB repair and chromosomal radiosensitivity in *ex vivo* irradiated blood lymphocytes in women to compare those who displayed either marked or minimal late radiotherapy changes in their breasts, there were higher levels of residual DNA and chromosomal damage among the clinically radiosensitive patients (Chua *et al*., (2011a). Likewise, in an accompanying study with human skin (Chua *et al*., (2011b), wide inter-individual variation of DSB repair following a fixed test dose of ionizing radiation of skin samples from individuals with no overt radiosensitivity syndromes were also observed. The

results were consistent with findings of significant inter-individual variation of residual foci levels in the lymphocyte study (Chua *et al*., 2011a). Similar differences were also noted in DSB repair in lymphocytes after administering a fixed dose of radiation in patients with rare hyper-radiosensitivity syndromes, cancer patients with no overt reactions to radiation, and healthy controls (Rübe *et al*., 2010). From these various observations, the authors therefore concluded that differences in levels of residual foci between cases and controls are indicative of significant differences in DSB repair.

It is therefore reasonable to surmise that differences in radiosensitivity have close correlation with DSB repair in different individuals. That notwithstanding, wide inter-individual biological variation of radiation responses within a cohort of patients with no syndrome is seen as a major obstacle in the development of reliable assays for predicting clinical radiosensitivity (Bentzen, 1997).

The aim of this part of the study was therefore to use lymphocytes as surrogates to assess DNA damage response in the lungs or other tissues that are subjects of irradiation.This is based on the hypothesis that the repair efficiencies of radiation-induced DNA damage in leukocytes (or lymphocytes specifically) correlates directly with those in the lungs.of the CcS/Dem RCS mice

If the lymphocyte results correlate with those for the lung study, then the use of lymphocytes could be improved and optimized for use in clinical applications during patient pre-screening to assess their suitability as candidates for radiotherapy.

Materials and Methods

Animals: The animals used in the study are recombinant congenic strains derived from mating of BALB/cHeA mice which are susceptible to radiation induced lung cancers and STS/A mice that are resistant. The animals, generously provided by Dr. Peter Demant, were housed at the Laboratory Animal Resources (LAR) facility of Colorado State University where food and water were provided ad libitum. All animal work was approved by CSU's Institutional Animal Care and Use Committee (IACUC). The animals were allowed to acclimate for at least 7-10 days after shipment to CSU before being used.

Irradiations: The mice were transported from LAR vivarium to the irradiator facility at MRB building and were placed in 8 cm x 5 cm x 5 cm Plexiglas containers. Food and hydration gel were placed inside the container at the time of irradiation. The desired irradiation dose was delivered to the whole-body using γ-rays from 30Ci ^{137}Cs source J.L Shepherd Model Mark I-68 SS-070 irradiator in room MRB 006 at a low dose rate of 10 cGy/h for 24 h to give a cumulative dose of 2.4 Gy. For each strain 6 mice were; 4 mice were irradiated while 2 sham-irradiated mice served as controls.

Blood collection and processing: Within about 9-12 min after termination of irradiation, euthanasia by CO_2 asphyxiation was performed and about 0.2-0.5 mL of blood was collected using a 25G needle into a heparinized 1 mL syringe by direct cardiac puncture. The blood was transferred quickly into a 1.5 mL microfuge tube preloaded with 1 mL of ice-cold 1X PBS containing 2% normal goat serum and 20 units/mL heparin. The samples were then centrifuged at low speed (~1000g) for 5 min at 4 °C to pellet the RBCs and WBCs. After aspirating the

supernatant, the pellets were dispersed by gentle tapping of the tubes and then resuspended in 1 mL of ice-cold dH_2O followed by gentle inverting of the tubes to uniformly mix the cells in suspension. The cells were incubated on ice for 1 min to lyse the RBCs followed by addition of 100 µL of 10X PBS to terminate the RBC lysis. The WBCs were recovered by centrifugation at low speed and the supernatant containing the contents of the lysed RBCs was aspirated. Where there were residual RBCs that sedimented with the WBCs, the lysis and centrifugation process was repeated. The final pellet was resuspended in 100 µL of cold 1X PBS containing 2% normal goat serum and 20 units/mL of heparin. A small aliquot of the supernatant was mixed with an equal volume of 0.4% trypan blue to determine cell viability and concentration in a hemocytometer. The WBC suspension was diluted with the cold 1X PBS containing 2% normal goat serum and 20 units/mL of heparin to a final concentration of ~240 cells/µL. The WBCs were deposited directly onto poly-L-lysine-coated glass slides using a cytospin centrifuge at 800 rpm for 3 min. (Except for this stage of the process which was performed at 22-25 ℃, all the procedures from the time the blood was collected were performed at ~4 ℃).

Immunofluorescence staining for γ-H2AX: The cells were fixed using a 4% paraformaldehyde solution in PBS for 15 min at room temperature (RT) followed by washing in PBS 3 times for 5 min each. To permeabilize the cells, the slides were incubated in a solution of 0.5% Triton X-100 for 10 min followed by washing in PBS 3 times for 5 min each. Where it was necessary to reduce autofluorescence background due to excess residual RBC components, the slides were washed in freshly prepared sodium borohydride solution (1mg/mL) in PBS while shaking on a gentle rocking platform 3 times for 5 min each followed by washing in dH_2O and then in 1X PBS. Enough blocking solution (10% goat serum; Invitrogen) was added to the slides to cover the spot

containing the cells and incubated for 45 min at RT. The primary antibody solution, prepared as a 1:500 dilution of monoclonal rabbit anti-γH2AX antibody (Millipore, clone EP854(2)Y) in 10% goat serum was added and the slides incubated overnight at 4°C or for 2h at RT. After rinsing the slides twice and then washing 3 times for 5 min each in PBS, a 1:500 dilution of AlexaFluor 594-conjugated goat-anti-rabbit IgG secondary antibody solution (Invitrogen) in 10% goat serum (Invitrogen) was added to the slides and incubated at 37°C in the dark for 1 h. The slides were then washed 3 times for 5 min each in PBS and drained of any liquid. A small drop of Vectashield/Antifade-DAPI was added to each slide that was then mounted with a coverslip. The edges of the coverslips were sealed with nail polish (if necessary) and the slides were stored in the dark until use.

Immunofluorescence imaging and foci analysis: A fluorescent microscope (Nikon E600) equipped with CoolSNAP® CCD camera and controlled by a Prior *OptiScan* (Photometrics) coupled to a MetaMorph software-equipped computer was used to capture images as already described for lung tissue sections. The only difference here is that the slices in the image stacks were less than for the lung tissues sections since the cells were more flattened than the tissue sections. Both 2D and 3D images were generated for better focus localization and quantification. Occasionally, where there were 5 or less slices, the median slice was used for color combining without performing maximum image projection, which may result in fused foci with no distinct boundaries. To quantify the foci, visual counting using objective magnification of x100 was performed using the click-and-log method in MetaMorph where the data is logged directly into an MS Excel worksheet.

Data analysis: To compare the DSB repair capacity between the different CcS/Dem strains, statistical comparisons by ANOVA was performed using SigmaPlot software (Systat Software Inc, San Jose, CA). A value of $P < 0.05$ was taken as significant. To compute the correlation between the foci numbers in PBLs and the lungs, Spearman rank correlation was used. Other measures of variations were also performed using SigmaPlot to determine experimental sampling consistency.

Results and Discussion

The main goal of this part of the investigation was to determine if lymphocytes could be used as surrogates for predicting DNA repair capacity of lung tissues of CcS/Dem RCS mice that are exposed to ionizing radiation. Since it hypothesized that DNA DSB repair efficiency of lung tissue cells is inversely correlated with susceptibility to lung tumor development, correlating repair efficiency of irradiated lymphocytes with those of lung tissue cells would provide the most practical means of predicting an individual's susceptibility or likelihood to radiogenic lung tumor development. However, in situations of accidental radiation exposure requiring emergency triage, processing blood to obtain a high proportion of lymphocytes would be an expensive and time consuming undertaking. The use of total leukocytes may be a more practical thing to do. The lyse-deposit-and-fix approach was therefore used in this study. If found promising, peripheral blood leukocytes could be used as surrogates for lung tissue cells and achieve the stated goal.

High incidence of apoptosis occur in PBLs during protracted low dose rate irradiation

Various protocols are available to isolate either total leukocytes or lymphocytes from peripheral blood. Procedures that involve the lysis of red blood cells (RBCs) followed by sedimentation of the remaining PBLs are routinely used. The washing steps are usually followed by depositing the cells on the slides and then fixing them. Alternatively, Histopaque protocol, based on a method first described by Boyum in 1968, is a differential gradient centrifugation procedure that takes advantage of the differences in the sizes, shapes and densities of the different components of the blood cells and can be used to isolate nearly pure lymphocytes from whole blood. The RBCs and granulocytes are aggregated by the polysucrose and rapidly sedimented during centrifugation allowing them to be trapped in a column gradient, leaving the lymphocytes and other mononuclear cells in the interface. The platelets are mostly removed during the washing steps. In the present study, the lyse-deposit-and-fix procedure was used to prepare total PBLs. Either of the procedures requires time and during this delay period, the cells can resolve a lot of the repair foci, if they fail to repair, they undergo apoptosis. As can be seen in Fig. 4.1, there were likely some changes that could have occurred during this time. Some leukocytes (most likely lymphocytes) appear to have undergone or initiated apoptotic changes that are extensive in some cases, as indicated by diffuse γH2AX staining that are usually results of extensively fragmented genomic DNA by caspase-activated DNAse action (Wyllie, 1980; Wijsman *et al.,* 1993; Ohno et al., 1998; Samali *et al.,* 1999; review by Taatjes *et al.,* 2007). However, some of the non-irradiated cells also appear to have initiated the apoptotic process too (Fig. 4.1A). As is evident from the two images, the extent of the apoptosis-like changes in the irradiated sample (Fig. 4.1B) is comparatively more than in the non-irradiated (Fig. 4.1A). The results show some apparent differential apoptosis-like changes in the leukocytes but it is difficult to say at this point if such a

116

scenario is also true *in vivo* since the observed outcome could be radiation related or could have occurred during sample processing. It is therefore important to minimize any changes like those in the Fig. 4.1, which could cause extensive apoptosis-like appearance of the nuclei and therefore compromise the outcome
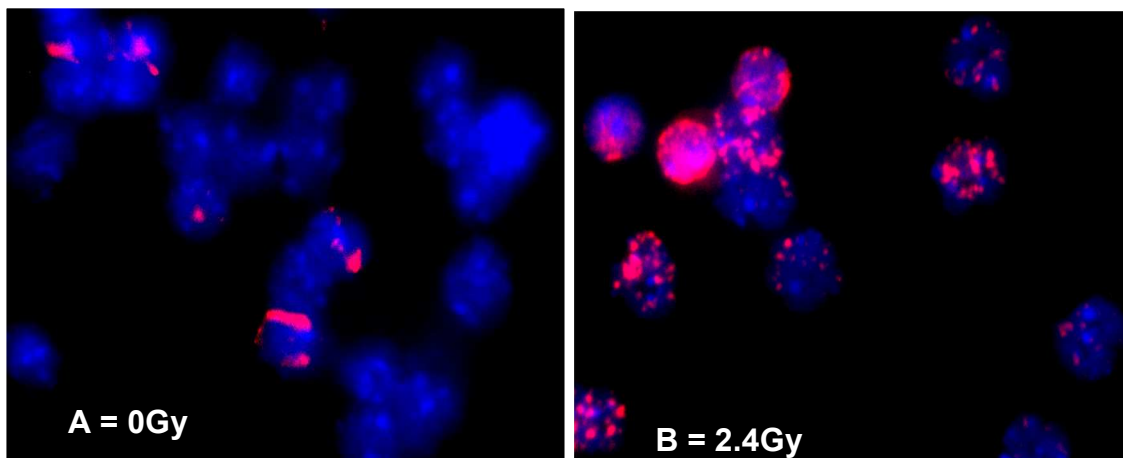
Figure 4.1: Images of peripheral blood leukocytes showing the likely apoptotic changes that could have occurred before or during the processing of the samples. Whole blood was obtained by right ventricular puncture into heparinized syringes, processed by the lyse-deposit-and-fix method and stained for γH2AX. Cells that appear to be lymphocytes have either initiated or have undergone apoptotic changes in both the non-irradiated sample (A) and the irradiated sample (B).

Some studies have suggested that certain cell types and some individuals have a tendency to initiate apoptosis following radiation-induced DNA damage (Endlich *et al*., 2000; reviews: Verheij and Bartelink, 2000; Shinomiya, 2001). Although apoptosis may appear to compromise tissue integrity, it may act as safeguard against malignant transformation of cells surviving radiation with genetic damage. It has been suggested that individuals who present with lower levels of initial DNA damage and higher levels of radiation-induced apoptosis (RIA) are at lower risk of suffering severe cutaneous late toxicity after clinical treatment at high radiation doses (Henriquez-Hernandez *et al*., 2011). If the observed differential changes in some of the leukocytes also occur *in vivo*, it could be a good mechanism to eliminate potential tumor-forming

117

cells from the body during irradiation. However, the strains of mice in which these changes were observed also had among the highest incidence of lung tumor. It does not mean such benefits arising from apoptotic elimination of such cell types will be enjoyed by the lung cells, but may still be applicable in the blood cell related tumors. Such a situation can be seen in the results of lymphoid cell tumors observed in a previous study that clearly indicated the wide differences between B-cell and myeloid tumors as compared to lung tumors (Szymanska *et al.,* 1999). The group did not see any apparent correlation between these types of tumors, even if the same mouse strains in question were subjected to similar radiation treatments. Those strains with high lung tumor incidences did not automatically have high B-cell or myeloid tumors. However some strains did have comparable T-cell and lung tumor incidences.

The other important observation is that there is no correlation between initial DNA damage and apoptosis, rather apoptosis is a cell type specific characteristic (Pinar *et al.,* 2010). In the present study no attempt was made to perform a time-course experiment to determine specific apoptosis kinetics.

The lyse-deposit-fix procedure resulted in low lymphocyte percentage on slides

The present work made use of the lyse-deposit-and-fix procedure that produces a cell suspension made up of lymphocytes and other white cell types as compared to the histopaque protocol for whole blood that produces a cell suspension enriched in lymphocytes. The one major drawback of the method used compared to the histopaque gradient enrichment is that the majority of cells in each microscopic field of view are other leukocytes than lymphocytes, making it very challenging to find enough lymphocytes for foci analysis (Fig. 4.2). Despite this apparent

disadvantage, it required relatively less blood and there was less sample loss during the less repeated washing steps. Additionally, the short time required to process the samples gave less opportunity for repair and resolution of the foci. On the other hand, in addition to being very demanding where a large number of mice are involved, the histopaque procedure required a larger blood volume from each mouse and it suffered progressive reduction of cells during the repeated washing steps. The lyse-deposit-and-fix protocol was adopted for use and it was decided to count the foci in all the leukocytes in the field of view. From cursory observation and later from the actual counts, there was no apparent difference between the foci numbers in the lymphocytes and the other types of leukocytes, some of which are obviously identifiable from the shapes/sizes of their nuclei as non-lymphocytes (Fig. 4.3). The other consideration for scoring all the leukocytes in the field of view is to avoid subjectivity since it was impossible to accurately distinguish lymphocytes from other small leukocytes in the lyse/deposit/fix procedure. To do so would require incorporating markers of leukocyte subpopulations into the assay. The MetaMorph software does not have any provision for positive discrimination of lymphocyte nuclei from those of other similarly shaped/sized leukocytes, which would have led to cells that may not be lymphocytes being included in foci scoring. Since there is always some background foci formation (Rogakou *et al.,* 1999; Rothkamm and Lobrich, 2003), enumeration of ionizing radiation-induced foci (IRIF) counts per nucleus must take into consideration nuclear foci in excess of the low background count.

While comparing the lyse/deposit/fix and the histopaque protocols, Moquet et al, (2014) noted that though the latter method has the advantage of producing cell suspensions highly enriched in lymphocytes, it is more demanding where there is large amount of whole blood sample to

process. In a situation where small numbers of samples are being processed it offers an advantage over the lyse-deposit-fix protocol.
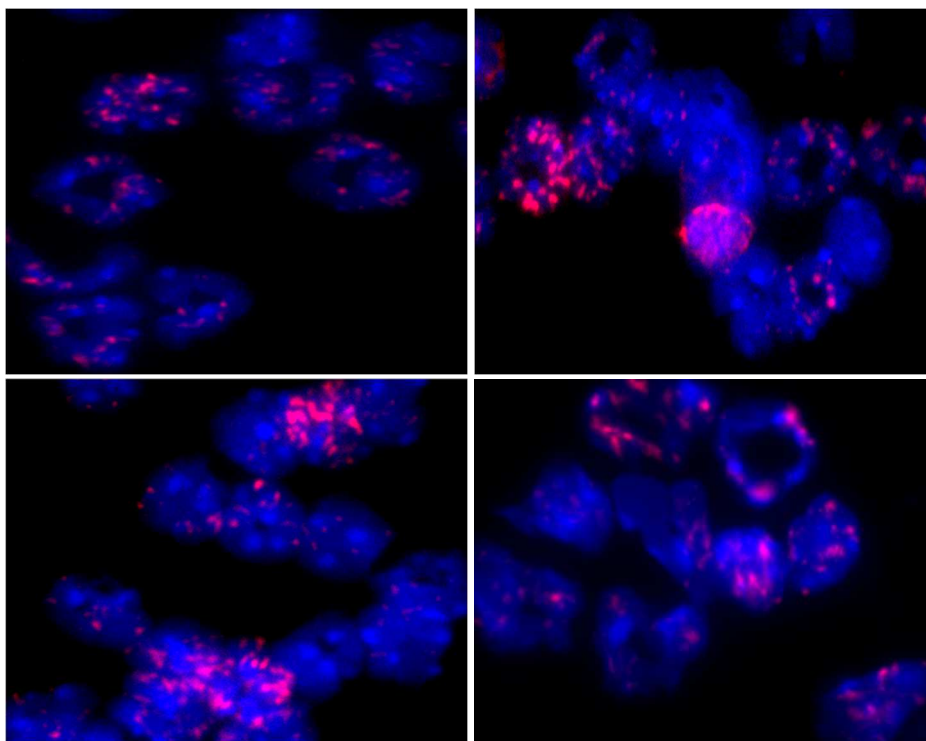
Figure 4.2: Fields from different slides prepared by the lyse-deposit-and-fix method show the low percentage of lymphocytes compared to the other leukocytes. After collecting blood by right ventricular perfusion into a heparinized tube, and transferring into a test tube on ice, hemolysis of RBCs was performed by adding cold dH_2O followed by mixing and incubating for 1 min on ice. Hemolysis was stopped by adding 10X PBS to the mix. The mix was centrifuged to pellet the leukocytes that were then deposited on slides and immunostained for γ-H2AX.

PBLs from protracted low-dose-rate irradiated mice show uniform γ-H2AX staining

From previous reports, there were instances where the authors reported observing foci counts that varied considerably between cells within the same microscopic field when they used partial body irradiation. This would be expected if the blood samples were collected immediately after an acute partial body exposure. In such a situation, since blood in the capillaries require a certain period of time to circulate and reach the site of exposure, insufficient time to mix completely may result in such differences in the foci scores. In the current study this was not of any concern

because the blood was collected after 24 h of low dose rate total body exposure, in which case all the blood cells would be exposed while circulating in the body. However, even in the present study some leukocytes did not have visible foci within the same microscopic field. It is not clear why such leukocytes did not have visible foci compared to their counterparts. It could not have been due to insufficient permeabilization since the slides were uniformly covered by the Triton-X-100 solution used to permeabilize the cells. It could only imply that probably they were more efficient in repairing the radiation-induced DNA damage than the other cells types, or they never attempted to repair the damage. Being terminally differentiated cells, such leukocytes may fall in the category of those cells that have a global attenuation of DNA repair (Nouspikel and Hanawalt, 2002) Since such cells are reported to have most of their H2AX preferentially deposited in the sub-telomeric regions that are less sensitive to exogenous sources of DSB and in non-transcribed regions (Tsantoulis *et al.*, 2008) they may just leave the damage unrepaired or have very poor repair due to low content of H2AX in the affected parts of the genome. However, the identity of those apparently more 'resistant cells' was not determined.

Residual foci/nucleus in PBLs and in the lung aredirectly correlated.

The main goal of this part of the study was to determine the correlation between foci numbers in leukocytes and the bronchioalveolar cells, and evaluate the general suitability of PBLs as surrogates for DSB repair efficiency in other tissues. Since the results of the lung foci study placed the strains into fairly 3 broad groups based on average residual foci, it was decided to assess the repair proficiency in selected strains that fall within these groups. As stated in background section above, all the PBLs showed fairly uniform foci distribution and it was decided to determine residual foci in all the nuclei within the microscopic field. Additionally, only 54 nuclei were sampled per mouse instead of the 100 that were sampled in the lung foci

study. The counts for the 4 mice per strain were computed and the results were expressed as the

Mean ± SEM (95% confidence). The results are presented in Table 4.1 and in Fig. 4.4.
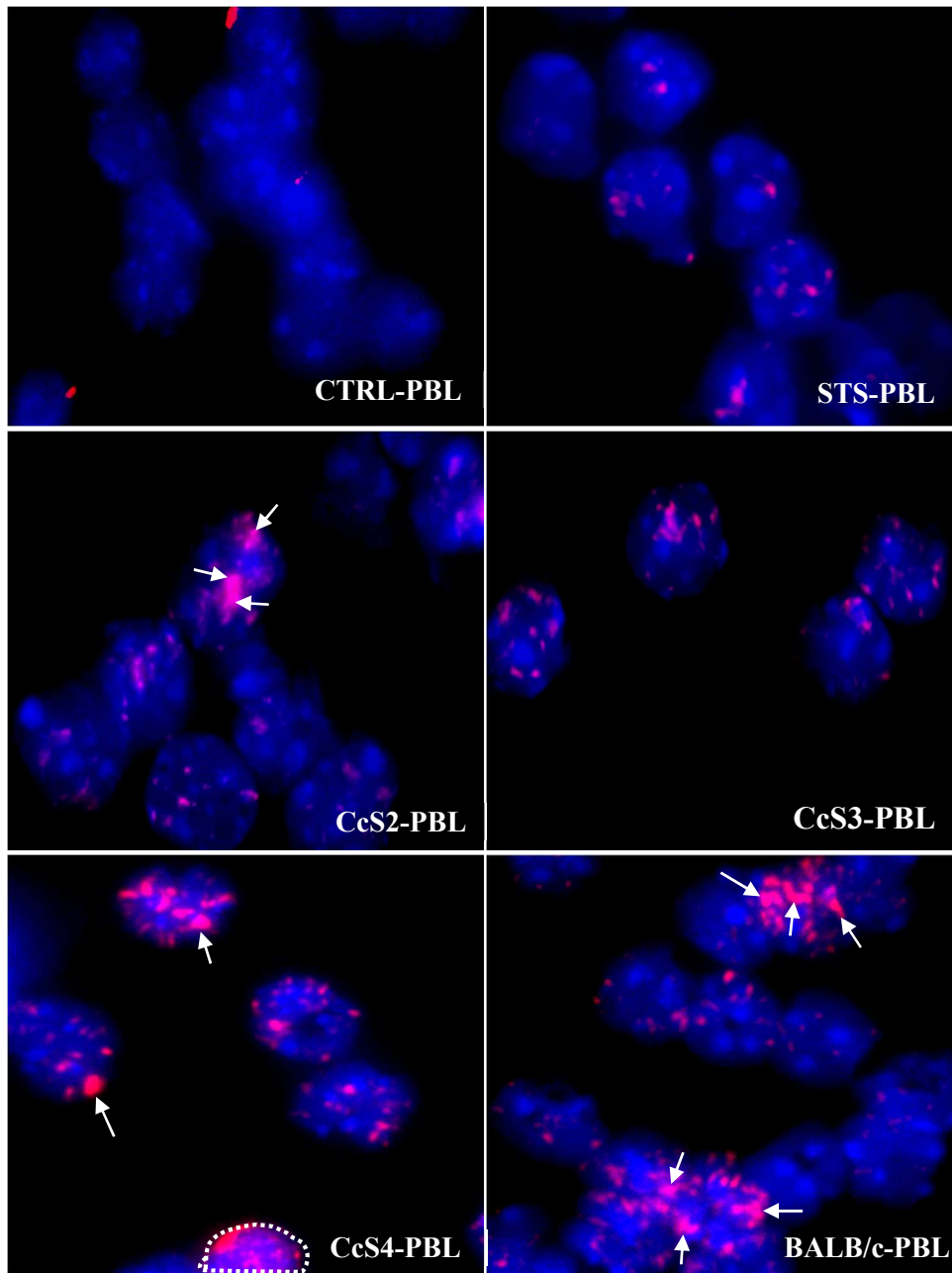
Figure 4.3: Immunofluorescence staining of peripheral blood leucocytes from CcS/Dem RCS mice irradiated to the whole body with γ-rays delivered using a JL Shepherd irradiator at a dose rate of 10 cGy/h for 24 h. Note the nucleus with dotted outline (CcS4-PBL) which appears to have started undergoing apoptotic changes, while other cells appear to have foci that have coalesced (arrows). Significant inter-strain differences in foci numbers and distribution are obvious by observation.

Table 4.1: The means, standard deviations and standard error of the means (light green- shaded) and the median, the 25% and 75% confidence levels (gray-shaded) of the γ-H2AX foci numbers for the PBLs in 5 representative strains used to compute the statistical significance and the graph in Fig. 4.4 and the fractions of the means used for the graph in Fig. 4.5.

Group	Mean	St Dev	SEM	Group	Median	25%	75%
BALB/c	16.7	4.0	0.54	BALB/c	17.0	13.0	20.0
STS	6.7	3.1	0.42	STS	6.5	4.0	9.0
CcS2	13.3	3.8	0.52	CcS2	12.0	10.0	14.0
CcS3	12.4	4.3	0.59	CcS3	11.0	9.0	15.0
CcS4	19.7	6.2	0.84	CcS4	20.0	15.0	23.0
CcS10	8.1	2.3	0.31	CcS10	7.5	6.0	10.0

Like in the lung foci study, the strains can be arranged into three broad groups with respect to residual foci numbers. Significant differences were noted between the strains in the different groups. STS and CcS-10 fall in the same group as they had no significant difference in the residual foci numbers in a Pairwise Multiple Comparison Procedures ANOVA (**Tukey Test**): CcS-10 vs. STS ($P= 0.483$). Similarly, foci numbers do not differ between CcS-2 and CcS-3 ($P= 0.853$). As was the case in the lung study, CcS-4 was significantly different than all the other strains with respect to foci number per nucleus, except CcS-20. In the PBL analysis it also had significantly more foci per nucleus that than all the other strains tested. For instance, in the Pairwise Multiple Comparison Procedures ANOVA (**Tukey Test**), CcS-4 was significantly different from BALB/c (P=0.003), while for the rest of the strains tested for foci in PBLs by pairwise comparisons, the differences were even more than for BALB/c (P<0.001). However, based on the Kruskal-Wallis one way ANOVA on Ranks which computes the median and the values at the 25% and 75% confidence level, there was no significant difference between CcS-4 and BALB/c using the Tukey test (P>0.05).

The plot in Fig. 4.4 compares the mean foci per nucleus in lung bronchio-alveolar cells in representative strains. The PBL results can be used to similarly group the strains into the low (CcS-10), medium (CcS-2 and CcS-3) and high (CcS-4) residual foci groups, just as was observed for residual foci in the lung. Compared to the foci counts in the lung, the absolute values for the PBLs appear to be lower but the plots have very similar patterns. To directly compare the results of the foci counts in the PLBs and those in the lungs, the fractions of the means were computed for the representative strains. The results are presented in Fig. 4.5. In Fig. 4.5A, the fractions of the means of mean foci per nucleus were computed for PBLs of six representative strains and plotted on the same scale with those for fractions of means of mean foci in the lungs of the same strains for comparison. In Fig. 4.5B, a correlation plot was made to compare the fractions of the means for the two tissue types. Both plots show high correlation between DNA DSB repair in the PBLs and in the lung, either using linear regression ($R^2=0.949$), or using Spearman Rank correlation plot (R = 0.948).
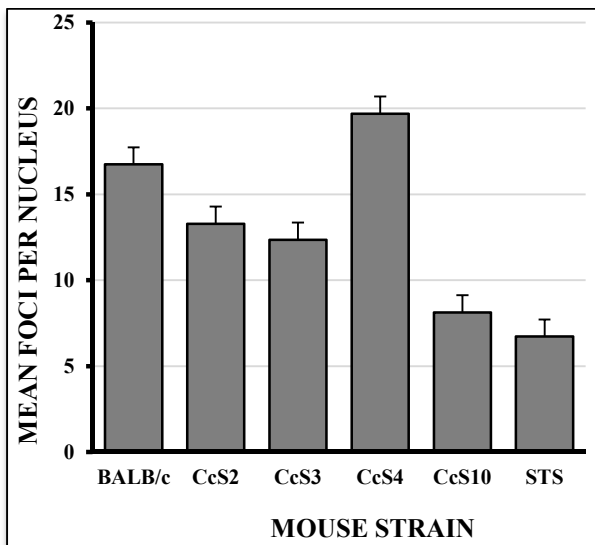
Figure 4.4: Comparison of mean foci per nucleus in PBLs of representative strains. Based on the lung foci results, selected strains in the low, medium and high residual foci lung foci groups were sampled for PBL foci counts. The histograms are Mean ± SEM of foci per nucleus in PBLs.
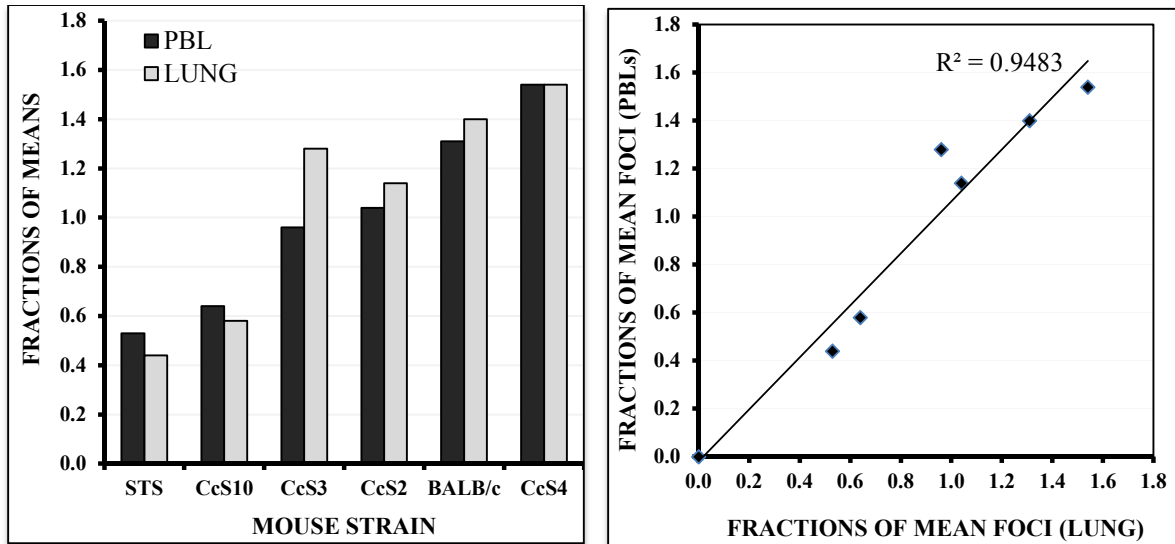
Figure 4.5: There is a direct correlation between radiation induced foci formation in the lung and peripheral blood leukocytes of CcS/Dem RCS mice. In (A), the fractions of the mean foci per nucleus were computed for the PBLs of six representative strains and plotted with those for foci in the lungs of the same strains, and arranged in ascending order for comparison. In (B), a correlation plot was made to compare the fractions for the two tissue types. The plot shows the very high correlation between for DNA DSB repair in the PBLs and lung either using linear regression (R^2=0.949) or using Spearman rank correlation plot (R = 0.948), (not included here).

Conclusion

From these results it is apparent that PBLs can be used as good surrogates to determine DSB repair capacities of these strains of mice. The results suggest the LDR γH2AX assay using PBLs can detect individuals susceptible to radiogenic cancer. The potential use of this assay would be for counseling individuals that have high occupational exposures to radiation (e.g. astronauts, interventional radiologists) or identifying radiotherapy and diagnostic patients who should be monitored for lung cancer.

Chapter 5 :

Prkdc SNP DOES NOT PREDICT RADIATION-INDUCED DNA DSB REPAIR EFFICIENCY IN CcS/Dem RECOMBINANT CONGENIC STRAINS OF MICE

Summary

Since the product of the *Prkdc* gene is known to be an important player in the DDR, we tested whether the R2140C SNP, which is known to influence DSB repair, has a significant role in the observed differences in the foci counts between different strains of CcS/Dem mice following radiation exposure. We amplified the segment of the *Prkdc* gene that contains the c>t transition that results in amino acid substitution that abolishes a *BsmBI* restriction endonuclease site. After digestion, the restriction fragments were run on a 2% agarose gel and the fragment migration was used to genotype the strains. There were three apparent genotypes among the CcS/Dem RCS mice with respect to the SNPs. They were either homozygous for the R2140 or C2140, or heterozygous R2140C. Unexpectedly, some of the strains homozygous for C2140, which is the BALB/c allele, had much fewer foci per nucleus than BALB/c, while others had similar foci number to BALB/c. Conversely, two of the R2140 SNP bearers that were expected to be more efficient in DNA repair and have had fewer foci per nucleus, had foci numbers similar to BALB/c. These results suggest that another gene (or other genes) polymorphic between BALB/c and STS/A determine(s) the strain differences in DNA DSB repair efficiency.

Background

Differences in radio-sensitivity and tumor susceptibility among various strains of mice were recognized and reported as early as the 1960s to the 1980s (Roderick, (1963); Storer *et al*. 1988). The BALB/c strain was found to be unusually susceptible to the lethal effects of radiation, and frequently developed defined and unique types of radiation-induced solid tumors. During the early times there was limited information on what is not commonly known about the relationship between non-homologous end joining (NHEJ) deficiency, radiosensitivity, and susceptibility to cancer development. With time, it was observed that of the two major mechanisms mammalian cells use to repair DNA DSBs, *i.e.* homologous recombination (HR) and NHEJ, the latter mechanism is reported to be the primary mode of DSB repair in mammalian cells, where DNA-PKcs is known to be a major player (Jeggo, 1998). However, much more still need to be unraveled to elucidate the exact mechanistic action of DNA-PKcs in non-homologous DNA end joining, among other functions. For instance, it is now known that this complex protein is such a large molecule that it can undergo modification at various sites, about 40 of which are phosphorylation sites alone (Davis *et al*., 2014).

From the previous demonstration that both lung and mammary adenocarcinomas could be induced in female BALB/c mice after exposure to ^{137}Cs radiation (Ullrich, 1983), it was later confirmed that the BALB/c strain is susceptible to spontaneous and radiation-induced lung and mammary adenocarcinomas (Ullrich, 1983; 1991) A study carried out to determine if BALB/c carries a defect in DNA DSB rejoining, it was demonstrated that though quantitatively different from that of SCID mice, the defect in BALB/c stood way above the other strains of mice and is possibly responsible for the observed radiation effects. The result showed that BALB/c mice

have a significant deficiency in radiation-induced DNA repair activity and repair time compared to other strains (Okayasu *et al*., 2000). Yu and colleagues identified two *Prkd*c sequence polymorphisms in BALB/c mice and linked the BALB/c variants to diminished DNA repair efficiency, decreased kinase activity and genomic instability (Yu *et al.,* 2001). Fabre and colleagues extended the study of *Prkdc* polymorphism effects by comparing the number of radiation-induced γ-H2AX foci at 15 min and 4 h post-irradiation, among other types of experiments. They observed that up to 82% of DSBs were repaired in C57BL/6 mice, only 48% in BALB/c mice, and only 29% in SCID mice over this period (Fabre *et al*., 2011). To further dissect this observation, they generated two congenic mouse strains, from the BALB/c and C57BL/6, where they introduced a BALB/c *Prkdc* allele (donor) on a <u>C</u>57BL/6 background as the recipient (to give a B6.C), and the other where the C57BL/6 *Prkdc* allele was introduced on a <u>B</u>ALB/c background as the recipient (to give a C.B6), a genetic process referred to as introgression (the incorporation of genes from one species into the gene pool of another as a result of hybridization). Note here that the donor strain is written first, followed by a period and then by the first letter for the recipient (underlined). The genomes of the two strains are fundamentally different depending on which one is the background strain. This approach eliminates most of the potential problems arising from the various mouse genetic backgrounds, which can complicate interpretation and evaluation of a role for the *Prkdc* allele.

In addition to the congenc strains, they used the LEWES strain LEWES/EiJ, which was derived from wild mice trapped in Lewes, Delaware, and is reported to have a pure *M. m. domesticus* genome (http://jaxmice.jax.org/strain/002798.html). Wild-derived mice are genetically distinct from the common laboratory mice for a number of complex phenotypic characteristics and have

128

become widely and routinely used for genetic mapping, evolution and systematics research (information available at www.jaxmice.jax.org/list/cat481389.html). The LEWES strain derived from wild trapped mice was found to have only one BALB/c-like SNP in the kinase domain. Additionally LEWES was found to be intermediate between BALB/c and C57BL/6 with respect to DNA-PKcs protein expression but there is no difference in the level of the transcript in all the three. Fabre and group then used the series to examine DNA-PKcs expression, DSB repair, and telomere function as measures of radiosensitivity in the two congenic mouse strains. The introgression resulted in significant changes. For instance, 79% DSB repair occurred in C.B6 mice, 58% in B6.C, and 56% in LEWES mice. Their conclusion was that the introgression of the common allele of *Prkdc* (into C.B6 congenic mouse) restored the DNA repair capacity to that observed in the C57BL/6 mice. Conversely, they reasoned, introgression of the BALB/c variant onto the C57BL/6 background (in the B6.C congenic) reduced DSB repair capacity to a level near that of BALB/c mice. These observations, derived from the use of congenic and LEWES mouse strains characterized with respect to DNA DSB repair kinetics, *Prkdc* mRNA expression, DNA-PKcs protein levels, and telomere function helps to provide further evidence that *Prkdc* indeed has significant impact on radiosensitivity phenotypes *in vivo* (Fabre *et al.,* 2011) Their result strengthened the previous observation that suggested a link between the BALB/c variant of *Prkdc* and DNA repair, kinase activity and genomic instability (Yu *et al.*, 2001).

With regards to lung cancer development, the genes that have been most extensively studied as potential risk modifiers are those involved in carcinogen activation and detoxification (Jeggo, 1998). The rapidly emerging class of genes involved in the recognition and repair of DNA damage may prove to have critical roles in determining inherent susceptibility to lung cancer.

Although the exact role of most of these genes cannot be stated with 100% certainty, ample evidence is available to provide useful clues about the possible contributions of these gene products in DNA damage response. For instance, there are about nine substitution variants that were identified by Lunn *et al*. (Lunn *et al*., 1999) in the exons of three nucleotide excision repair genes ERCC1, XPD and XPF and in the XRCC3 gene involved in double strand break repair/recombination, all of which lead to impaired functions of the pathways in which they are involved (Lunn *et al*., 1999).

Many studies have shown that different types of overt mutations that are highly penetrant, leading to defects in DNA damage response proteins including those of ATM, p53or BRCA1/2, among others, strongly correlate with increased risk for developing a number of different cancer types. However, it is becoming more apparent from a number of studies that subtle mutations or polymorphisms are associated with and play significant roles in carcinogenesis and cancer risks. Among the many studies that investigated and reported the roles of SNPs and other innocuous mutations in the increased risk of cancer, are those by (Mandal *et al*., (2010) regarding the roles of SNPs in the XRCC1 and XPD genes in the cause of prostate cancer in Northern India, the study by Matsuo *et al*., (2006) on the role of SNP that lead to amino acid substitution resulting in increased risks of colorectal cancer in Japan and those of Bhatti *et al.,* (2008) that showed direct association between three different SNPs in the *Prkdc* gene and elevated breast cancer incidences in the US (Matsuo *et al*., 2006; Bhatti *et al.,* 2008; Mandal *et al.,* 2010). In their report, Fabre *et al.,* (2011) examined a direct impact of SNPs in *Prkdc* on the function of the NHEJ protein DNA-PKcs and confirmed that the two SNP polymorphisms R2140C and M3844V are mechanistically responsible, necessary and sufficient for the reduced DSB repair capacity

observed in BALB/c mice.(Fabre *et al*., 2011). In addition to these subtle covert mutations (SNPs), general genetic background may play some minor but not insignificant roles in modifying the effects of these polymorphisms on the DNA-PKcs function associated with either DSB repair or telomere end capping functions of this protein. These observations appear to be related to and dependent on the location of M3844V in the kinase domain of DNA-PKcs with regards to DNA repair. In a pull-down assay both the expression and kinase activities of DNA-PKcs are lowered as a result of these two SNPs. Their results suggest that the R2140C SNP is related with telomere end capping function of DNA-PKcs, which requires the leucine zipper DNA binding domain of the protein. However, these authors could not state with any certainty if the R2140C SNP affects the specific activity of the DNA-PKcs protein or if the outcome was simply due to reduced expression of the protein, which is attributable to the M3488V SNP.

Because of these observations, it was decided to explore and the link between the SNP and radiation-induced DNA damage based on the hypothesis that residual oci numbers correlate directly with the presence of the R2140C SNPs in the different CcS/Dem recombinant congenic strains of mice and it could help as to determine whether DNA-PKcs is playing a predominant role in the DNA damage response that were observed in our study.

Materials and Methods

Mice: Female CcS/Dem recombinant congenic strains of mice used in the study were derived from founder parental BALB/cHeA strains which are susceptible to radiation-induced lung tumor development, and STS/A strains that are resistant. They were housed and maintained in specific-pathogen-free conditions at the AAALAC-approved Laboratory Animal Resource facility at Colorado State University and used at about 15 weeks of age. From the time the

animals were procured, they were allowed to acclimatize for at least 7-14 days during which time feeding and watering were provided ad libitum. All animal work and protocols were approved by and done in accordance to the standard recommendations of Institutional Animal Care and Use Committee (IACUC) at Colorado State University. Before tail tips were obtained for DNA extraction, euthanasia was performed by CO_2 asphyxiation after which, tails were obtained and immediately stored in a -80°C freezer until use.

Tail DNA extraction and PCR/RFLP analyses: The mice were genotyped in the Department of Environmental and Radiological Sciences at Colorado State University, Fort Collins. A small piece of tail (~2 mm) harvested post-euthanasia from each mouse was placed in an Eppendorf tube. Fresh Alkaline Lysis Buffer (50% NaOH, 0.5 M EDTA, pH 8.0 in dH_2O) was prepared just before use and 75 µL of the fresh buffer was then added to each sample, making sure the tail was immersed in the buffer and no air bubble was trapped at the bottom of the tube. The tubes were capped and loaded in a thermocycler preheated to 95°C and incubated for 30 min after which the tubes were promptly removed and cooled for 15 min at 4° C. An equal volume (75 µL) of neutralization buffer (40 mM Tris-HCl without pH adjustment) was immediately added to the contents of each Eppendorf tube and mixed briefly using a separate filter tip for each tail, 2 µL of the mixture was taken from the top of the 150 µL tail preparation, avoiding the debris at the bottom of the tube, and used for a 20 µL PCR reaction. PCR amplifications were carried out using a QIAGEN kit (QIAGEN, Chatsworth, CA) in a Peltier Thermal Cycler PTC-200 (MJ Research, Watertown, MA). The primer sequences for R2140C were consisted of the following: (F), GCCATGATCCTTAGCAAGTG, and (R), GCCTAAGGTAAGGTGCTGTA. PCR cycling conditions were 94°C for 30 s, 49°C for 30 s, and 72°C for 30 s for 40 cycles, followed by a final

extension at 70°C for 10 min. The entire 20 µL of the PCR product was digested with *BsmBI* at 55°C for 3 h according to the manufacturer's instructions. The PCR products were then analyzed on 2% agarose gels.

Data Analysis

To determine if the R2140C SNPs in *Prkdc* has an effect on the repair efficiency in the CcS/Dem strains, MS Excel was used to perform a Student's *t*-Test to compare the strain with the R2140 to those with C2140 which were designated the "STS group" and the "BALB/c group" respectively, with respect to DSB repair efficiency.

Results and Discussion

Figure 5.1 illustrates the *Prkdc* genotyping assay and results. From the results of the digestion and restriction fragment migrations, the strains belong to three groups with respect to the R2140C SNP. All the RCS mice that were interrogated in the SNP analysis are either homozygous for R2140 or for C2140, except CcS-11 which is appear to be heterozygous for R2140C (Fig. 5.1C and Table 5.1). Those which underwent the *c>t* transition for the **c**gt codon for arginine (R2140) to become homozygous **t**gt codon for cysteine (C2140) include CcS-1, CcS-4, CcS-5, CcS-8, CcS-9, CcS-10, CcS-13, CcS-14, CcS-15, CcS-18, CcS-19 and CcS-20, just like the BALB/c founder.

Those that are homozygous for the R2140 include CcS-2, CcS-3, CcS-7 and CcS-12. The only strain that appear to be heterozygous for the R2140C is CcS-11. The result for CcS-11 was surprising. This is because the strains have undergone extensive inbreeding after the backcross to

BALB/c founder ended and it was expected that by this time all the strains would have become homozygous in their individual groups. The result could be attributed to two factors: first, there may be a likelihood of the presence of residual heterozygosity whereby even after many generations of inbreeding, some loci are still heterozygous. Some of the CcS/Dem strains have undergone more than 25 generations of inbreeding following the last backcross. Alternatively, but more unlikely, some rare spontaneous occurrence of a nucleotide transition in the individual that could have occurred during the inbreeding that became stable and led to heterozygosities that are heritable in subsequent generations.

The second and most likely reason for this observation could be the result of incomplete digestion that was responsible for the appearance of the second band that corresponds to the uncut product. That notwithstanding, there appears to be no direct correlation between the R2140C SNP and DSB repair efficiency based on the comparison of the mean foci/nucleus and the SNP analysis results. By extension, since there appears to be a correlation between DSB repair capacity (indicated by comparative mean foci/nucleus for each strain) and tumor incidence, there is likely to be no direct correlation between R2140C SNP and radiation-induced lung tumor development in the RCS mice, at least with regards to the present results. However, it must be stressed that further work involving the actual analysis of incidence versus genotype still needs to be done to unequivocally rule out the apparent lack of correlation and the speculation that there may be other mutations or SNPs outside of the *Prkdc* gene within chromosome 16, or in other genes in other chromosomes that drive the response of these CcS/Dem RCS mice to IR.

This result provides further insight into the multigenic nature of DDR as already outline in the general background information. On another level, the, M3844V SNP on Ch16 in BALB/c has been reported to influence the expression of *Prkdc* (Fabre et al., 2011) but since we never determined the nature of the M3844V SNP in the CcS/Dem RCS mice, there are reservations in making any comments on the expression levels of DNA-PKcs as a function of the DDR in the different strains investigated with respect to γH2AX formation. So, this dual function of DNA-PKcs in NHEJ repair of DSB and telomere end capping will still need to be investigated in the CcS/Dem strains. It is therefore clear that DSB repair and the general DDR may require more than any normal functional *Prkdc,* at least in the CcS/Dem mice.

A:

Arg (R)

NH2   Cys (C)   COOH

B:

5'**gccatgatccttagcaagtg**atttgaaaaatgattttgtaaagtgaaagctgtcgctaggcacacagattttcgttccacgcactcg
ccatcttgctccctcatgttcttataatagcaaaatataacattcttttgttccttttttcagagtaagtttgtgtttttatttcagggttcaatacca
aaagatcttccaccgtggatgaaatttcttcatgacaaactaggaaatgcatcagtatctttaaat**atccgtctct**tcttagccaagcttgt
tattaatacagaagaggtatctaactttttttcctttatatcttaactgttctgtgcagttctgaccgtctatgttagcatcaccaaagcaaatg
aagcttttaagaaatagaacgtggagttactgttcttgcaatacatcagcaaccacatttaaacacttcctccaaatccttttgtcaaacgt
tattttctggcattgggagtgaactttct**gtacagcaccttaccttaggc**-3'

C:

Figure 5.1: Analysis of DNA-PKcs *Prkdc* genotype of the CcS/Dem RCS mice: A, schematic of R2140C *Prkdc* polymorphism showing the change in the single nucleotide that abolishes the *BsmBI* restriction site and results in an amino acid substitution; B, sequence for the PCR product that was subjected to *BsmBI* digestion. The underlined sequences at the beginning and end represent forward and reverse primer sites, the restriction site for *BsmBI* the underlined sequence in the middle; C, PCR/RFLP genomic analysis of R2140C with *BsmBI* digests resolved by 2% agarose gel electrophoresis. Digestion results in two restriction fragments of similar lengths, 252 bp and 260 bp that migrate as a single band in the gel. The pattern for CcS11 could result from residual heterozygosity but is more likely due to incomplete digestion. Empty well did contain the reaction mix without the genomic DNA and the cut and uncut represent reference PCR product that were digested and undigested respectively.

136

Table 5.1: Summary of the SNP analysis in the *Prkdc* of the CcS/Dem recombinant congenic strains of mice. PCR products were digested with *BsmB1* and run on a 2% agarose gel. A **c**-to-**t** transition abolishes the restriction site* for the *BsmB1* resulting in uncut fragment.

Mouse Strain	SNP
CcS-1	C2140
CcS-2	R2140
CcS-3	R2140
CcS-4	C2140
CcS-5	C2140
CcS-7	R2140
CcS-8	C2140
CcS-9	C2140
CcS-10	C2140
CcS-11	R2140C
CcS-12	R2140
CcS-13	C2140
CcS-14	C2140
CcS-18	C2140
CcS-19	C2140
CcS-20	C2140
BALB/c	C2140

* Restriction sequence for *BsmBI* ➔ 5´... C G T C T C (N)₁ ... 3´
3´... G C A G A G (N)₅ ... 5´

Since it is now known that the fragment at ~ the 9.6 -13.5 cM position on chromosome 16 carries

the *Prkdc* gene reported to be a major player in NHEJ repair, an abridged map of Ch16 ranging

from ~8-17 cM where the sequences for these CcS/Dem have been partially determined

(courtesy of Peter Demant, Rosewell Park Cancer Institute, Buffalo, NY) was used in attempt to

correlate the results of the γ-H2AX foci/nucleus already reported elsewhere in the main study

and the possible origin of the *Prkdc* gene in these strains, whether from BALB/c or STS founder.

The map showed that the *Prkdc* in CcS-1, CcS-4, CcS-5, CcS-6, CcS-8 CcS-9, CcS-10, CcS-13,

CcS-14, CcS-15, CcS-16, CcS-17, CcS-18, CcS-19, and CcS-20 were very likely derived from

the BALB/c founder parental fragment while those with *Prkdc* derived from STS founder

parental strain include CcS-2, CcS-3, CcS-7, CcS-11 and CcS-12. This observation indeed corresponds very well with our SNP results, showing that in all likelihood the strains acquired their *Prkdc* genome from the respective founders. Therefore, based on that grouping, Fig. 5.2 was constructed for the mean γ-H2AX foci/nucleus in the "STS group" or "BALB/c group". When the foci values of the two groups were subjected to Student's *t*-Test, there was no significant difference between them ($p = 0.5$). Some of the strains were expected to fall in a specific 'group' but the results obtained in our γ-H2AX study show that this was not the case. For instance, CcS-2/Dem and CcS-3/Dem strains, each with ~18 foci/nucleus, appear to be more closely related to BALB/c (~20 foci/nucleus) in their ability to effectively repair DNA DSBs, than to STS with just ~7 foci/nucleus. Similarly, the strains CcS-8, CcS-10, CcS-14 and CcS-18 (each with ~8-13 foci/nucleus) appear significantly different and with lower average foci than BALB/c founder.

The results are in agreement with those of the Demant group tumor incidence study (Szymanska *et al.*, 1999). The mean γ-H2AX foci values for these strains are worth commenting on. The CcS-2/Dem strain for instance was predicted to have the STS-like sequence in the immediate vicinity of the *Prkdc* locus based on the abridged map of Ch16, suggesting it may be carrying the STS-derived *Prkdc* gene that would confer a better ability to repair DNA DSB. However, it is among the least efficient in DSB repair with a very high foci number very close to its BALB/c founder. Conversely, the values for CcS-8, CcS-10, CcS-14 and CcS-18 are among the lowest observed from the study. They are therefore expected to be among those with a good dose of the genetic materials from STS founder donor since they appear to be more efficient in DNA repair.
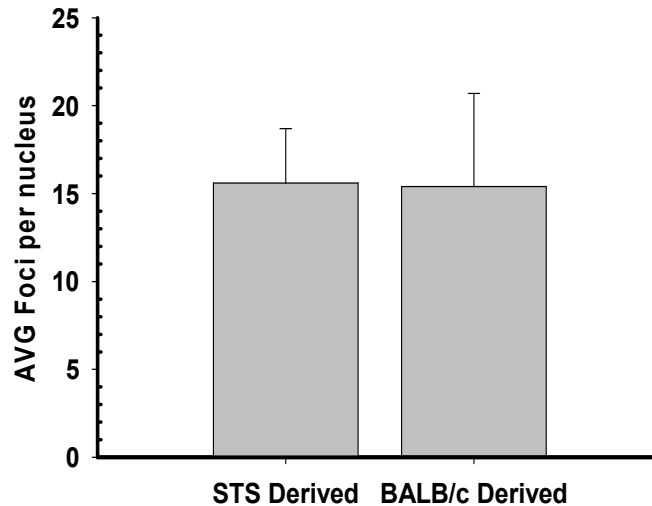
Figure 5.2: The expected cumulative average foci/nucleus in the CcS/Dem strains if the *Prkdc* gene on Ch16 were derived from the STS or BALB/c chromosome fragment at ~the 9.6-13.5 cM position. The STS values used are from CcS-2, CcS-3, CcS-7, CcS-11 and CcS-12 data while the BALB/c values are from CcS-1, CcS-4, CcS-5, CcS-8, CcS-9, CcS-10, CcS-13, CcS-14, CcS-15, CcS-18, CcS-19, and CcS-20. Three other CcS/Dem strains (CcS-6, CcS-16 and CcS-17) were not included in generating the graph since they were not used in the study. The values are means± STD for the listed strains in each category.

These results pose more questions that require looking for additional as yet unidentified mutations or SNPs other than those in the *Prkdc* gene in some of the strains theat cause significant alterations in the functions of the DNA-PKcs, which is the major player in NHEJ, or whether the role of DNA-PKcs in those strains are fully compensated for by other DSB repair genes that led to a higher efficiency in DSB repair in those strains. This therefore points to, or suggests the possibility of functional redundancies in this multigenic/multifactorial molecular process.

As mentioned above in the roles of SNP in expanding the horizons of cancer risks, the outcome of this brief analysis of the *Prkdc* SNP in the CcS/Dem mice throws the door wide open for

similarly expanding the search for causative factors that lead to individual differences in the efficiency of DNA damage response (DDR).

Conclusion

It is clear from the foregoing that linking a SNP mutation in one gene like *Prkdc* to the efficiency of DSB repair is not a straightforward matter. Other as yet unidentified mutations in other genes could be at play. In such a case those strains that have the C2140 but showed higher efficiency in DSB repair may be carrying other redundant DSB repair genes that compensated for the reduced function of *Prkdc* due to the observed mutation. More studies requiring an extensive genome-wide analysis, transcriptome, and proteomics of DDR may be necessary to resolve the outcome of these findings. It must be pointed out though, that available evidence suggest that sequence variants in the *Prkdc* gene are not responsible for differences between the CcS/Dem strains in DNA DSB repair efficiency. The variants may be important in other strain combinations.

References

American Cancer Society (ACS), Cancer Facts and Figures 2014. Atlanta, GA. USA.

American Cancer Society (ACS), Cancer facts and figures, 2012. Atlanta, GA. USA.

An, J., Huang, Y. C., Xu, Q. Z., Zhou, L. J., Shang, Z. F., Huang, B., . . . Zhou, P. K. (2010). DNA-PKcs plays a dominant role in the regulation of H2AX phosphorylation in response to DNA damage and cell cycle progression. *BMC Mol Biol,* **11**, 18.

Asselin-Labat M-L, Filby CE. (2012). Adult lung stem cells and their contribution to lung tumorigenesis. *Open Biol* **2:** 120094.

Bhatti P, Struewing JP, Alexander BH, Hauptmann M, Bowen L, Mateus-Pereira LH, Pineda MA,Simon SL, Weinstock RM, Sigurdson AJ. (2008). Polymorphisms in DNA repair genes, ionizing radiationexposure and risk of breast cancer in U.S. radiologic technologists. *Int. J. Cancer*. **122**:177–182.

Bahmed, K., Nitiss, K.C. and Nitiss, J.L. (2010).Yeast tdp1 regulates the fidelity of non-homologous end joining**.** *Proc Natl Acad Sci. USA*, **107:** 4057–4062.

Bahmed, K., Seth, A., Nitiss, K.C. et al. (2011).End-processing during non-homologous end-joining: A role for exonuclease 1.*Nucleic Acids Res*, **39:** 970–978.

Bailey**,** D. W. (1981) Recombinant inbred strains and bilineal congenie strains. In: The Mouse in Biomedical Research (Foster, H. L.,Small, J. D., and Gox, J. G.,eds) pp. 223-239, Academic, New York.

Bakkenist, C. J., and Kastan, M. B. (2003). DNA damage activates ATM through intermolecular autophosphorylation and dimer dissociation. *Nature***,** **421**(6922), 499-506.

Balajee A S, Geard C R. Replication protein A and gamma-H2AX foci assembly is triggered by cellular response to DNA double-strand breaks. *Exp Cell Res* 2004: **300**: 320–334.

Ball, H. L., Ehrhardt, M. R., Mordes, D. A., Glick, G. G., Chazin, W. J., & Cortez, D. (2007). Function of a conserved checkpoint recruitment domain in ATRIP proteins. *Mol Cell Biol,* **27**(9), 3367-3377.

Bannister, L. A., Waldman, B. C., & Waldman, A. S. (2004). Modulation of error-prone double-strand break repair in mammalian chromosomes by DNA mismatch repair protein Mlh1. *DNA Repair (Amst),* **3**(5), 465-474.

Banus, H. A, H. J. van Kranen, F. R. Mooi, B. Hoebee, N. J. Nagelkerke, P. Demant and T. G. Kimman. (2005) Genetic Control of *Bordetella pertussis* infection: identification of susceptibility loci using recombinant congenic strains of mice. *Infect. Immun.* **73:** 741-747.

Bekker-Jensen, S., and Mailand, N. (2010). Assembly and function of DNA double-strand break repair foci in mammalian cells. *DNA Repair (Amst),* **9**(12), 1219-1228.

Bennetzen, M.V., Larsen, D.H., Bunkenborg, J., et al. (2010). Site-specific phosphorylation dynamics of the nuclear proteome during the DNA damage response. *Mol Cell Proteomics*; **9:**1314-1323.

Bensimon A, Schmidt A, Ziv Y, et al. (2010). ATM-dependent and -independent dynamics of the nuclear phosphoproteome after DNA damage. *Sci Signal*; **3**:rs3.

Bertoncello, I. and McQualter, J.L. (2010). Endogenous lung stem cells: what is their potential for use in regenerative medicine? *Expert Rev. Respir. Med*. **4,** 349–362.

Bhattacharjee A et al. (2001). Classification of human lung carcinomas by mRNA expression profiling reveals distinct adenocarcinoma subclasses. *Proc.Natl Acad. Sci. USA* **98**, 13 790–13 795.

Bhogal, N., Jalali, F., & Bristow, R. G. (2009). Microscopic imaging of DNA repair foci in irradiated normal tissues. *Int J Radiat Biol,* **85**(9), 732-746.

Blanpain, C., Lowry, W.E., Geoghegan, A., Polak, L., and Fuchs, E. (2004). Self-renewal, multipotency, and the existence of two cell populations within an epithelial stem cell niche. *Cell* **118**, 635–648.

Bogliolo, M., Lyakhovich, A., Callen, E., Castella, M., Cappelli, E., Ramirez, M. J., . . . Surralles, J. (2007). Histone H2AX and Fanconi anemia FANCD2 function in the same pathway to maintain chromosome stability. *EMBO J,* **26**(5), 1340-1351.

Bonner, W. M., Redon, C. E., Dickey, J. S., Nakamura, A. J., Sedelnikova, O. A., Solier, S., & Pommier, Y. (2008). Gamma-H2AX and cancer. *Nat Rev Cancer, 8*(12), 957-967

Britton, S, Froment C, Frit P, et al. (2009). Cell non-homologous end joining capacity controls SAF-A phosphorylation by DNA-PK in response to DNA double-strand breaks inducers. *Cell Cycle,* **8**: 3717-3722.

Buchholz, T. A. (1999). Finding our sensitive patients. *Int J Radiat Oncol Biol Phys*, **45(**3), 547-548.

Burgio, G., M. Szatanik, Guénet J.L., Arnau M.R., Panthier, J.J and Montagutelli, X. (2007). Interspecific recombinant congenic strains between C57BL/6 and mice of the *Mus spretus* species: a powerful tool to dissect genetic control of complex traits. *Genetics* **177**: 2321-2333.

Burma, S., Chen, B.P., Murphy, M., Kurimasa, A. and Chen, DJ. (2001) ATM phosphorylates histone H2AX in response to DNA double-strand breaks. *J. Biol. Chem*., **276**. 42462-42467.

Calle'n E., Jankovic M, Wong N, et al. (2009). Essential role for DNA-PKcs in DNA double-strand break repair and apoptosis in atm-deficient lymphocytes. *Molecular Cell*; **34**: 285-297.

Calsou, P., Delteil, C., Frit, P., Drouet, J., & Salles, B. (2003). Coordinated assembly of Ku and p460 subunits of the DNA-dependent protein kinase on DNA ends is necessary for XRCC4-ligase IV recruitment. *J Mol Biol,* **326**(1), 93-103.

Cary, R. B., Peterson, S. R., Wang, J., Bear, D. G., Bradbury, E. M., & Chen, D. J. (1997). DNA looping by Ku and the DNA-dependent protein kinase. *Proc Natl Acad Sci U S A,* **94**(9), 4267-4272.

Cataldi, A., Di Giacomo, V.,Rapino, M., Zara, S. andRana, R.A. (2009).Ionizing radiation induces apoptotic signal through protein kinase c (delta) and survival signal through Akt and cyclic-nucleotide response element-binding protein (CREB) in Jurkat T-c ells. *Biol. Bull*. **217**: 202–212.

Celeste, A., Petersen, S., Romanienko, P. J., Fernandez-Capetillo, O., Chen, H. T., Sedelnikova, O. A., . . . Difilippantonio, M. J. (2002). Genomic instability in mice lacking histone H2AX. *Science,* **296**(5569), 922-927.

Celeste, A., Fernandez-Capetillo, O., Kruhlak, M. J., Pilch, D. R., Staudt, D. W., Lee, A., . . . Nussenzweig, A. (2003). Histone H2AX phosphorylation is dispensable for the initial recognition of DNA breaks. *Nat Cell Biol,* **5**(7), 675-679.

Chen, H. T., Bhandoola, A., Difilippantonio, M. J., Zhu, J., Brown, M. J., Tai, X., Rogakou, E. P., Brotz, T. M., Bonner, W. M. Ried, T , and Nussenzweig, A.(2000). Response to RAG-mediated VDJ cleavage by NBS1 and gamma-H2AX. *Science,* **290**(5498): 1962-1965.

Chen, S. L., Cai, L., Meng, Q. Y., Xu, S., Wan, H., & Liu, S. Z. (2000). Low-dose whole-body irradiation (LD-WBI) changes protein expression of mouse thymocytes: effect of a LD-WBI-enhanced protein RIP10 on cell proliferation and spontaneous or radiation-induced thymocyte apoptosis. *Toxicol Sci,* **55**(1), 97-106.

Cheok, C. F., Bachrati, C. Z., Chan, K. L., Ralf, C., Wu, L., & Hickson, I. D. (2005). Roles of the Bloom's syndrome helicase in the maintenance of genome stability. *Biochem Soc Trans,* **33**(Pt 6), 1456-1459.

Chepelev,L., Wei,G., Tang,Q. and Zhao,K. (2009) Detection of single nucleotide variations in expressed exons of the human genome using RNA-Seq. *Nucleic Acids Res*., **37**, e106.

Chiasson, B.J., Tropepe, V., Morshead, C.M., and van der Kooy, D. (1999). Adult mammalian forebrain ependymal and subependymal cells demonstrate proliferative potential, but only subependymal cells have neural stem cell characteristics. *J. Neurosci*.**19**, 4462-4471.

Chu, W. K., & Hickson, I. D. (2009). RecQ helicases: multifunctional genome caretakers. *Nat Rev Cancer, 9*(9), 644-654.

Chua M, Somaiah N, Bourne S, Daley F, A'Hern R, Nuta O, et al. (2011a). Inter-individual and inter-cell type variation in residual DNA damage after in vivo irradiation of human skin. *Radiother Oncol;* **99**: 225–230.

Chua, ML., Somaiah, N., A'Hern, R., Davies, S., Gothard, L., Yarnold, J. and Rothkamm, K.(2011b) Residual DNA and chromosomal damage in ex vivo irradiated blood lymphocytes correlated with late normal tissue response to breast radiotherapy**.** *Radiother Oncol,* **99:**.362-366.

Claesson, K., K. Magnander, H. Kahu, S. Lindegren, R. Hultborn, and K. Elmroth. (2011). RBE of alpha-particles from [211]At for complex DNA damage and cell survival in relation to cell cycle position. *Int. J. Radiat. Biol.*, **87**: 372–384.

Collins, F. S. (1992) Positional cloning: let's not call it reverse anymore. *Nature Genet.* **1**, 3-6.

Conde, J., Silva, S.N., Azevedo, A.P., Teixeira, V., Pina, J.E., Rueff, J. and Gaspar, J.F. (2009). Association of common variants in mismatch repair genes and breast cancer susceptibility: a multigene study. *BMC Cancer.* **9**, 344.

Cortez, D., Guntuku, S., Qin, J., Elledge, S.J. (2001). ATR and ATRIP: Partners in checkpoint signaling. *Science 294*:1713-1716.

Cowell, I.G., Sunter, N.J., Singh, P.B., Austin, C.A., Durkacz, B.W. and Tilby, J. (2007). Gamma H2AX foci form preferentially in euchromatin after ionising-radiation, *PLoS One* **2** e1057.

David S.S, O'Shea V.L, and Kundu S. (2007). Base-excision repair of oxidative DNA damage. *Nature*, **447**: 941-950.

Davis, A. S., Richter, A., Becker, S., Moyer, J. E., Sandouk, A., Skinner, J., & Taubenberger, J. K. (2014). Characterizing and Diminishing Autofluorescence in Formalin-fixed Paraffin-embedded Human Respiratory Tissue. *J Histochem Cytochem,* **62**(6), 405-423.

DeFazio, L.G., Stansel, R.M., Griffith, J.D. et al. (2002). Synapsis of DNA ends by DNA-dependent protein kinase**.** *Embo J.* **21:** 3192-3200.

deLara, C.M., T.J. Jenner, K.M. Townsend, S.J. Marsden, and P. O'Neill. (1995). The effect of dimethyl sulfoxide on the induction of DNA double-strand breaks in V79-4 mammalian cells by alpha particles. *Radiat. Res.*, **144**: 43-49.

Demant, P. (1992) Genetic resolution of susceptibility to cancer **-** new perspectives. *Semin. Cancer Bio* **L3,** 157-164.

Demant P (2003) Cancer susceptibility in the mouse: genetics, biology and implications for human cancer. *Nat Rev Genet* **4:** 721–734.

Demant, P., and Hart, A. A. M. (1986). Recombinant congenic strains: a new tool for analyzing genetic traits determined by more than one gene. *Immunogenetics* **24**, 416-422.

Demant, P., Oomen, L. C. J. M., and Oudshoorn-Snoek, M. (1989) Genetics of tumor susceptibility in the mouse: major histocompatibility complex and non-MHC genes. *Ado. Cancer Res.* **53**, 117-179.

DeVries-Seimon, T. A., Ohm, A. M., Humphries, M. J., & Reyland, M. E. (2007). Induction of apoptosis is driven by nuclear retention of protein kinase C delta. *J Biol Chem,* **282**(31), 22307-22314.

Di Virgilio, M., Ying, C. Y., & Gautier, J. (2009). PIKK-dependent phosphorylation of Mre11 induces MRN complex inactivation by disassembly from chromatin. *DNA Repair (Amst), 8*(11), 1311-1320.

Doetsch, F., Caille, I., Lim, D.A., Garcia-Verdugo, J.M., and Alvarez-Buylla, A. (1999). Sub-ventricular zone astrocytes are neural stem cells in the adult mammalian brain. *Cell* **97,** 703–716.

Endlich, B., Radford, I. R., Forrester, H. B., and Dewey, W. C. (2000). Computerized Video Time-Lapse Microscopy Studies of Ionizing Radiation-Induced Rapid-Interphase and Mitosis-Related Apoptosis in Lymphoid Cells. *Radiat Res,* **153**(1), 36-48.

Ewald, B., Sampath, D. and Plunkett, W. (2007). H2AX phosphorylation marks the gemcitabine-induced stalled replication forks and their collapse upon S-phase checkpoint abrogation. *Mol. Cancer Ther.* **6** (4): 1239-48.

Fabbro, M. Savage, K.I. Hobson, K., Deans A.J., et al. (2004). BRCA1/BARD1 complexes are required for p53Ser15 phosphorylation and a G1/S arrest following IR-induced DNA damage. *J. Biol. Chem.* **30:**31251–31258.

Fabre, K.M., Ramaiah, L., Dregalla, R.C., Desaintes, C., Weil, M.M., Bailey S.M. and Ullrich, R.L. (2011). Murine *Prkdc* polymorphisms impact DNA-PKcs function. *Radiat Res.* **175**, 493–495.

Falck, J., Coates, J., & Jackson, S. P. (2005). Conserved modes of recruitment of ATM, ATR and DNA-PKcs to sites of DNA damage. *Nature,* **434**(7033), 605-611.

Farago AF, Snyder EL, Jacks T. (2012). SnapShot: lung cancer models. *Cell.* **149:** 246–246 e241.

Fearon, E. R., and Vogelstein, B. (1990) A genetic model for colorectal tumorigenesis. *Cell* **61:** 759-767.

Fernandez-Capetillo, O., Chen, H. T., Celeste, A., Ward, I., Romanienko, P. J., Morales, J. C., . . . Nussenzweig, A. (2002). DNA damage-induced G2-M checkpoint activation by histone H2AX and 53BP1. *Nat Cell Biol*, **4**(12), 993-997.

Fernandez-Capetillo O, Lee A, Nussenzweig M, and Nussenzweig, A. (2004). H2AX: the histone guardian of the genome. *DNA Repair (Amst);* **3**: 959–967.

Fortin, A.,Diez, E.,Rochefort, D.,Laroche, L.,Malo, D., Rouleau,G.A., Gros, P.and Skamene, E. (2001). Recombinant congenic strains derived from A/J and C57BL/6J: a tool for genetic dissection of complex traits. *Genomics* **74**, 21-35.

Georgakilas, A.G., O'Neill, P. and Stewart, R.D. (2013). Induction and Repair of Clustered DNA Lesions: What Do We Know So Far? *Radiat. Res.,* **180**(1) 100-109.

Giangreco, A., Reynolds, S. D., & Stripp, B. R. (2002). Terminal bronchioles harbor a unique airway stem cell population that localizes to the bronchoalveolar duct junction. *American Journal of Pathology,* **161**(1), 173-182.

Giangreco A, Groot KR, Janes SM. (2007) Lung cancer and lung stem cells: strange bedfellows? *Am. J. Respir. Crit. Care Med.* **175**, 547–553.

Goodarzi, A. A., Jeggo, P., & Lobrich, M. (2010). The influence of heterochromatin on DNA double strand break repair: Getting the strong, silent type to relax. *DNA Repair (Amst),* **9(**12), 1273-1282.

Goodarzi, A.A. and P.A. Jeggo. (2012). The heterochromatic barrier to DNA double strand break repair: How to get the entry visa**.** *Int J Mol Sci*, **13** 11844–11860.

Gottlieb, T.M. and Jackson, S.P. (1993). The DNA-dependent protein kinase: Requirement for DNA ends and association with Ku antigen. **Cell 72**:131-142.

Gown AM, Willingham MC (2002). Improved detection of apoptotic cells in archival paraffin sections: immunohistochemistry using antibodies to cleaved caspase 3. *J Histochem Cytochem* **50**: 449–454.

Groot, P. C., C. J. A. Moen, W. Dietrich, J. P. Stoye. E. S. Lander, and P. Demant. (1992). The recombinant congenic strains for analysis of multigenic traits: genetic composition *FASEB J.* **6**: 2826-2835.

Gu, L., & Li, G. M. (2006). Analysis of DNA mismatch repair in cellular response to DNA damage. *Methods Enzymol,* **408,** 303-317.

Gunning, W.T., Stoner, G.D., and Goldblatt, P.J. (1991). Glyceraldehyde-3-phosphate dehydrogenase and other enzymatic activity in normal mouse lung and in lung tumors. *Exp. Lung Res*. **17,** 255-261.

Hammel, M., Yu, Y., Mahaney, B. L., Cai, B., Ye, R., Phipps, B. M., Tainer, J. A. (2010). Ku and DNA-dependent protein kinase dynamic conformations and assembly regulate DNA binding and the initial non-homologous end joining complex. *J Biol Chem,* **285**(2), 1414-1423.

Han, J., Handzel M.J., and Allalunis-Turner, J. (2006). Quantitative analysis reveals asynchronous and more that DFSB-associated histone H2AX phosphorylation after exposiure to ionizing radiation. Radiat Res. **165** (3): 283-292.

Hayes DN, Monti S, Parmigiani G, Gilks CB, Naoki K, Bhattacharjee A, Socinski MA, Perou C, Meyerson M. (2006). Gene expression profiling reveals reproducible human lung adenocarcinoma subtypes in multiple independent patient cohorts. *J. Clin. Oncol*. **24,** 5079–5090.

Henríquez-Hernández, L. A., Carmona-Vigo, R., Pinar, B., Bordón, E., Lloret, M., Núñez Mí, I., . . . Lara, P. C. (2011). Combined low initial DNA damage and high radiation-induced apoptosis confers clinical resistance to long-term toxicity in breast cancer patients treated with high-dose radiotherapy. *Radiat Oncol,* **6,** 60.

Heyer, W.D., K.T. Ehmsen, J. Liu, (2010). Regulation of homologous recombination in eukaryotes, *Annu. Rev. Genet.* **44**: 113–139.

Hoeijmakers J.H.J. (2001). Genome maintenance mechanisms for preventing cancer: A highly informative review of the links between DNA damage, DNA repair pathways and their defects contributing to tumorigenesis. *Nature,* **411**: 366-374.

Holt, S. M., Scemama, J. L., Panayiotidis, M. I., & Georgakilas, A. G. (2009). Compromised repair of clustered DNA damage in the human acute lymphoblastic leukemia MSH2-deficient NALM-6 cells. *Mutat Res,* **674**(1-2), 123-130.

Holt, I., Thanh Lam, L., Tome, S., Wansink, D. G., Te Riele, H., Gourdon, G., & Morris, G. E. (2011). The mouse mismatch repair protein, MSH3, is a nucleoplasmic protein that aggregates into denser nuclear bodies under conditions of stress. *J Cell Biochem,* **112**(6), 1612-1621.

Hong, K.U., Reynolds, S.D., Giangreco, A., Hurley, C.M., and Stripp, B.R. (2001). Clara cell secretory protein-expressing cells of the air- onic and adult stem cells. *Science* **298**, 597–600.

Hong, K.U., Reynolds, S.D., Watikins, S., Fuchs, E. and Stripp, B.R. (2004).Basal cells are a multipotent progenitor capable of renewing the bronchial epithelium. *Am J Pathol* **164**: 577-588.

Hong, Z., Jiang, J., Hashiguchi, K., Hoshi, M., Lan, L., and Yasui, A. (2008). Recruitment of mismatch repair proteins to the site of DNA damage in human cells. *J Cell Sci,* **121**(Pt 19), 3146-3154.

Horlings H, Demant P. (2005). Lung tumor location and lymphocyte infiltration in mice are genetically determined. *Exp Lung Res* **31**: 513–25.

Horn S, Barnard S, Rothkamm K. (2011). Gamma-H2AX-based dose estimation for whole and partial body radiation exposure. *PLoS One*; **6**:e25113.

Howlader N, Noone AM, Krapcho M, Neyman N, Aminou R, Altekruse SF, et al. SEER cancer statistics review. Bethesda, MD: U.S. National Institutes of Health, National Cancer Institute; 1973-2008.

Huang, S.N., Pommier, Y. and Marchand C. (2011). Tyrosyl-DNA phosphodiesterase 1 (tdp1) inhibitors. *Expert Opin Ther Pat*, **21:** 1285–1292.

Jackson, E.L, Willis, N, Mercer, K, et al., (2001).Analysis of lung tumor initiation and progression using conditional expression of oncogenic K-ras. *Genes Dev*. **15:** 3243-3248.

Jackson, S. P., and Bartek, J. (2009). The DNA-damage response in human biology and disease. *Nature,* **461**(7267), 1071-1078.

Jakob, B., Splinter, J., Conrad, S., Voss, K. O., Zink, D., Durante, M., . . . Taucher-Scholz, G. (2011). DNA double-strand breaks in heterochromatin elicit fast repair protein recruitment, histone H2AX phosphorylation and relocation to euchromatin. *Nucleic Acids Res,* **39**(15), 6489-6499.

Jeggo P. A. (1998). Identification of genes involved in repair of DNA double strand breaks in mammalian cells. *Radiat. Res.,* **150** (Suppl.):S80-S91.

Jeggo, P., & Löbrich, M. (2006). Radiation-induced DNA damage responses. *Radiat Prot Dosimetry,* **122**(1-4), 124-127.

Jeggo, P. A., & Löbrich, M. (2006). Contribution of DNA repair and cell cycle checkpoint arrest to the maintenance of genomic stability. *DNA Repair (Amst),* **5**(9), 1192-1198.
.
Jeggo, P. A., Geuting, V., & Löbrich, M. (2011). The role of homologous recombination in radiation-induced double-strand break repair. *Radiotherapy and Oncology,* **101(**1), 7-12.

Jemal A, Bray F, Center MM, Ferlay J, Ward E, Forman D. (2011). Global cancer statistics.CA *Cancer J. Clin*. **61**, 69-90.

Jiricny, J. (2006). MutL-alpha: at the cutting edge of mismatch repair. *Cell,* **126**(2), 239-241.

Jiricny, J. (2006). The multifaceted mismatch-repair system**.** *Nat Rev Mol Cell Biol*., **7:** 335-346.

Johansson, C.B., Momma, S., Clarke, D.L., Risling, M., Lendahl, U. and Frisen, J. (1999). Identification of a neural stem cell in the adult mammalian central nervous system. *Cell* **96:** 25-3

Johansson, S., Svensson, H., and Denekamp, J. (2000). Timescale of evolution of late radiation injury after postoperative radiotherapy of breast cancer patients. *Int J Radiat Oncol Biol Phys,* **48**(3), 745-750.

Kakarlapudi, N, Vernooy, JH, Quan, L, Fijneman, RJ, Demant, P. (2008). Control of lymphocyte infiltration of lung tumors in mice by host's genes: mapping of four Lynf (lymphocyte infiltration) loci. *Cancer Immunol Immunother* **57**: 217–25.

Kastan, M. B., and Bartek, J. (2004). Cell-cycle checkpoints and cancer. *Nature,* **432**(7015), 316-323.

Kato TA, Nagasawa H, Weil MM, Genik PC, Little JB, Bedford JS. (2006). γ −H2AX foci after low-doserate irradiation reveal Atm haploinsufficiency in mice. *Radiat. Res*.; **166**:47–54.

Kim, C.F, Jackson, E.L, Woolfenden, AE, Lawrence S, Babar I, Vogel S, Crowley D, Bronson ,RT, Jacks T. (2005). Identification of bronchioalveolar stem cells in normal lung and lung cancer. *Cell* **121**:823–35.

Kolas, N. K., Chapman, J. R., Nakada, S., Ylanko, J., Chahwan, R., Sweeney, F. D., . . Durocher, D. (2007). Orchestration of the DNA-damage response by the RNF8 ubiquitin ligase. *Science,* **318,** 1637-1640.

Kruger, G.M., Mosher, J.T., Bixby, S., Joseph, N., Iwashita, T., and E., Morrison, S.J. (2002). Neural crest stem cells persist in the adult gut but undergo changes in self-renewal, neuronal subtype potential, and factor responsiveness. *Neuron* **35**, 657-669.

Kurimasa, A., Ouyang, H., Dong, L. J., Wang, S., Li, X., Cordon-Cardo, C., . . . Li, G. C. (1999a). Catalytic subunit of DNA-dependent protein kinase: impact on lymphocyte development and tumorigenesis. *Proc Natl Acad Sci U S A,* **96**(4), 1403-1408.

Kurimasa, A., Kumano, S., Boubnov, N. V., Story, M. D., Tung, C. S., Peterson, S. R., & Chen, D. J. (1999b). Requirement for the kinase activity of human DNA-dependent protein kinase catalytic subunit in DNA strand break rejoining. *Mol Cell Biol,* **19**(5), 3877-3884.

Kusumoto, L. Dawut, C. Marchetti et al. (2008). Werner protein cooperates with the XRCC4-DNA ligase IV complex in end-processing. *Biochemistry* **47:** 7548-7556.

Kwon, J. M., & Goate, A. M. (2000). The candidate gene approach. *Alcohol Res Health, 24*(3), 164-168.

Kwon, S. H., Florens, L., Swanson, S. K., Washburn, M. P., Abmayr, S. M., & Workman, J. L. (2010). Heterochromatin protein 1 (HP1) connects the FACT histone chaperone complex to the phosphorylated CTD of RNA polymerase II. Genes Dev, 24(19), 2133-2145.

Lee, J.-H., & Paull, T. T. (2005). ATM activation by DNA double-strand breaks through the Mre11-Rad50-Nbs1 complex. *Science, 308*(5721), 551-554.

Lees-Miller, S., Sakaguchi, K., Ullrich, S., Apella, E. and Anderson, C. (1992). Human DNA-activated protein kinase phosphorylates serine 15 and 37 in the amino acid terminal transactivation domain of human p53. *Mol. Cell. Biol*. **12**, 5041-5049.

Li, X., and W.D. Heyer, (2008). Homologous recombination in DNA repair and DNA damage tolerance, *Cell Res*. **18** 99–113.

Lieber M.R. (2008). The mechanism of human non-homologous DNA end joining. *J Biol Chem*. **283:**1-5.

Lieber, M.R. (2010).The mechanism of double-strand DNA break repair by the nonhomologous DNA end-joining pathway. *Annu Rev Biochem*, **79** 181-211.

Lieber, M.R., Gu, J., H. Lu, Shimazaki, N. and Tsai, A.G. (2010). Nonhomologous DNA end joining (NHEJ) and chromosomal translocations in humans, *Subcell. Biochem*.**50:** 279–296.

Lisby, M. and Rothstein, R. (2004).DNA damage checkpoint and repair centers. *Curr Opin Cell Biol,* **16**: 328-334.

Loeb, L.A, and Monnat, R.J. Jr. (2008). DNA polymerases and human disease. *Nat Rev Genet*. **9:** 594-604.

Lunn, R.M., Langlois, R.G, Hsieh, L.L, Thompson, C.T and Bell, D.A. (1999). XRCC1 polymorphisms: effect on aflatoxin B1-DNA adducts and glycophorin A variant frequency. *Cancer Res*, **58**, 604-608.

Magnander, K., R. Hultborn, K. Claesson, K. Elmroth. (2010).Clustered DNA damage in irradiated human diploid fibroblasts: influence of chromatin organization**.** *Radiat. Res.,* **173:** 272–282.

Magnander, K., and Elmroth, K. (2012). Biological consequences of formation and repair of complex DNA damage. *Cancer letters,* **327**(1), 90-96.

Mahaney, B.L., K. Meek, S.P. Lees-Miller. (2009). Repair of ionizing radiation-induced DNA double-strand breaks by non-homologous end-joining. *Biochem J*.**417:** 639-650.

Mailand, N., Bekker-Jensen, S., Faustrup, H., Melander, F., Bartek, J., Lukas, C., & Lukas, J. (2007). RNF8 ubiquitylates histones at DNA double-strand breaks and promotes assembly of repair proteins. *Cell,* **131**(5), 887-900.

Malewicz, M, Kadkhodaei B, Kee N, et al. (2011). Essential role for DNA-PK-mediated phosphorylation of NR4A nuclear orphan receptors in DNA double-strand break repair. *Genes Dev* **25:** 2031-2040.

Mandal, R. K., R. Gangwar, A. Mandhani and R. D. Mittal, (2010).DNA repair gene x-ray repair cross-complementing group 1 and xeroderma pigmentosum group D polymorphisms and risk of prostate cancer: a study from north India. *DNA Cell Biol*. **29,** 183–190.

Mannironi, C., Bonner, W. M., and Hatch, C. L. (1989). H2AX histone isoprotein with a conserved C-terminal sequence, is encoded by a novel mRNA with both DNA replication type and poly A 3' processing signals. Nucleic Acids Res. **17:** 9113-9126.

Martin, L.M., Maples, M., Coffey, M., Lawler, M., Lynch, T.H., Hollywood, D. and Marignol, L. (2010). DNA mismatch repair and the DNA damage response to ionizing radiation: Making sense of apparently conflicting data

Mason RJ, Kalina M, Nielsen LD, Malkinson AM, Shannon JM. (2000). Surfactant protein C expression in urethane-induced murine pulmonary tumors. *Am J Pathol* **156:** 175-182.

Matsuo, K., Wakai, K., Hirose, K., Ito, H., Saito, T., Suzuki, T., Kato, T., Hirai, T., Kanemitsu, Y. and Tajima, K. (2006).A gene-gene interaction between ALDH2 Glu487Lys and ADH2 His47Arg polymorphisms regarding the risk of colorectal cancer in Japan. *Carcinogenesis* **27**, 1018–1023.

Matsuoka, S., Ballif, B.A., Smogorzewska, A, et al. (2007). ATM and ATR substrate analysis reveals extensive protein networks responsive to DNA damage. *Science* **316**:1160-1166.

McVey, M. and Lee, S.E. (2008). MMEJ repair of double-strand breaks (director's cut): deleted sequences and alternative endings. *Trends Genet*. **24:** 529-538.

Menon, V. and Povirk, L. (2014). Involvement of p53 in the repair of DNA double strand breaks: multifaceted Roles of p53 in homologous recombination repair (HRR) and non-homologous end joining (NHEJ). *Subcell Biochem,* **85**, 321-336.

Mimori, T., & Hardin, J. A. (1986). Mechanism of interaction between Ku protein and DNA. *J Biol Chem,* **261(**22), 10375-10379.

Mimori, T., Hardin, J. A., and Steitz, J. A. (1986). Characterization of the DNA-binding protein antigen Ku recognized by autoantibodies from patients with rheumatic disorders. *J Biol Chem,* **261**(5), 2274-2278.

Mladenov, E., & Iliakis, G. (2011). Induction and repair of DNA double strand breaks: the increasing spectrum of non-homologous end joining pathways. *Mutat Res,* **711**(1-2), 61-72.

Moen, C. J. A**.,** van der Valk, M. A., Snoek, M.,van Zutphen, L. F. M.,von Deimling, Hart, A. A. M., and Demant, P. (1991) The recombinant congenic strains **-** a novel genetic tool applied to the study of colon tumor development in the mouse. *Mammalian Genome* **1**, 217-227.

Moen, C.J. A., Snoek, M., Hart, A. A. M., and Demant, P. (1992). Scc-i, a novel colon cancer susceptibility gene in the mouse linkage to CD44 (Ly-24, Pgp-1) on chromosome 2. *Oncogene* **7,** 563-566.

Mohapatra, S., Yannone, S. M., Lee, S. H., Hromas, R. A., Akopiants, K., Menon, V., . . Povirk, L. F. (2013). Trimming of damaged 3' overhangs of DNA double-strand breaks by the Metnase and Artemis endonucleases. *DNA Repair (Amst),* **12**(6), 422-432.

Mohni, K. N., Livingston, C. M., Cortez, D., & Weller, S. K. (2010). ATR and ATRIP are recruited to herpes simplex virus type 1 replication compartments even though ATR signaling is disabled. *J Virol,* **84**(23), 12152-12164.

Morris, R.J., Liu, Y., Marles, L., Yang, Z., Trempus, C., Li, S., Lin, J.S., Sawicki, J.A., and Cotsarelis, G. (2004). Capturing and profiling adult hair follicle stem cells. *Nat. Biotechnol.* **22**, 411-417.

Mortusewicz, O., Rothbauer, U., Cardoso, M. C., & Leonhardt, H. (2006). Differential recruitment of DNA Ligase I and III to DNA repair sites. *Nucleic Acids Res,* **34**(12), 3523-3532.

Nadeau, J., Grant, P., and Kosowsky, M. (1990). Man on mouse homology map. *Mouse Genome* **87:** 55-60.

National Center for Health Statistics, Centers for Disease Control and Prevention, 2013.

Nielsen, F. C., Jager, A. C., Lutzen, A., Bundgaard, J. R., and Rasmussen, L. J. (2004). Characterization of human exonuclease 1 in complex with mismatch repair proteins, subcellular localization and association with PCNA. *Oncogene,* **23**(7), 1457-1468.

Noon, A. T., Shibata, A., Rief, N., Lobrich, M., Stewart, G. S., Jeggo, P. A., and Goodarzi, A. A. (2010). 53BP1-dependent robust localized KAP-1 phosphorylation is essential for heterochromatic DNA double-strand break repair. *Nat Cell Biol,* **12**(2), 177-184.

Ohashi, E., Takeishi, Y., Ueda, S., & Tsurimoto, T. (2014). Interaction between Rad9-Hus1-Rad1 and TopBP1 activates ATR-ATRIP and promotes TopBP1 recruitment to sites of UV-damage. *DNA Repair (Amst),* **21,** 1-11.

Ohno, M., Takemura, G., Ohno, A., Misao, J., Hayakawa, Y., Minatoguchi, S., . . . Fujiwara, H. (1998). "Apoptotic" myocytes in infarct area in rabbit hearts may be oncotic myocytes with DNA fragmentation: analysis by immunogold electron microscopy combined with In situ nick end-labeling. *Circulation,* **98**(14), 1422-1430.

Okayasu,R., Suetomi, K. Yu, Y., Silver, A., Bedford, J.S., Cox, R., and Ullrich, R.L. (2000). A Deficiency in DNA Repair and DNA-PKcs Expression in the Radiosensitive BALB/c Mouse. *Cancer Res, 60;* 4342.

Oleinick, N.L., and S.M. Chiu. (1994). Nuclear and chromatin structures and their influence on the radiosensitivity of DNA. *Radiat. Prot. Dosim.,* **52:** 353–358.

Ozsahin, M., Crompton, N. E., Gourgou, S., Kramar, A., Li, L., Shi, Y., . . . Azria, D. (2005). CD4 and CD8 T-lymphocyte apoptosis can predict radiation-induced late toxicity: a prospective study in 399 patients. *Clin Cancer Res,* **11**(20), 7426-7433.

Palmer KC. Clara cell adenomas of the mouse lung (1985). Interaction with alveolar type 2 cells. *Am J Pathol* **120**: 455-463.

Poulsen, M., Lukas, C., Lukas, J., Bekker-Jensen, S., & Mailand, N. (2012). Human RNF169 is a negative regulator of the ubiquitin-dependent response to DNA double-strand breaks. *J Cell Biol,* **197**(2), 189-199.

Povirk, L. F., Zhou, T., Zhou, R., Cowan, M. J., & Yannone, S. M. (2007). Processing of 3'-phosphoglycolate-terminated DNA double strand breaks by Artemis nuclease. *J Biol Chem,* **282**(6), 3547-3558.

Prise, K.M. G. Ahnström, M. Belli, J. Carlsson, D. Frankenberg, J. Kiefer, M. Löbrich, B.D. Michael, J. Nygren, G. Simone, B. Stenerlöw. (1998). A review of DSB induction data for varying quality radiations. *Int. J. Radiat. Biol.***74** 173–184.

Quan, L., Hutson A. and Demant, P. (2010). A locus on chromosome 8 controlling tumor regionality-a new type of tumor diversity in the mouse lung. *International Journal of Cancer* **126:** 2603–2613.

Ramsden, D.A. and K. Asagoshi. (2012). DNA polymerases in non-homologous end joining: Are there any benefits to standing out from the crowd? *Environ Mol Mutagen* **53:** 741-751.

Rass, U., Ahel, I. and West. S.C. (2008). Molecular mechanism of DNA deadenylation by the neurological disease protein aprataxin. *J Biol Chem* **283:** 33994–34001.

Rawlins, E.L and Hogan, B.L. (2006). Epithelial stem cells of the lung: privileged few or opportunities for many? *Development* **133:**2455-2465.

Rawlins, E.L and Hogan, B.L. (2008). Ciliated epithelial cell lifespan in the mouse trachea and lung. *Am. J. Physiol. Lung Cell Mol. Physiol*. **295,** L231-L234.

Rawlins, E.L., Ostrowski, L.E., Randell, S.H., and Hogan, B.L. (2007). Lung development and repair: contribution of the ciliated lineage. *Proc. Natl Acad. Sci. USA* **104**, 410-417.

Rehm S, Devor DE, Henneman JR, Ward JM. (1988). Origin of spontaneous and transplacentally induced mouse lung tumors from alveolar type II cells. *Exp Lung Res* **17**:181-95.

Rehm S, Ward JM, ten Have-Opbroek AA, Anderson LM, Singh G, Katyal SL, Rice JM. (1988). Mouse papillary lung tumors transplacentally induced by N-nitrosoethylurea: evidence for alveolar type II cell origin by comparative light microscopic, ultrastructural, and immunohistochemical studies. *Cancer Res* **48**:148-60.

Rehm S, Takahashi M, Ward JM, Singh G, Katyal SL, Henneman JR. (1989). Immunohistochemical demonstration of Clara cell antigen in lung tumors of bronchiolar origin induced by N-nitrosodiethylamine in Syrian golden hamsters. *Am J Pathol,* **134**(1), 79-87.

Reifsnyder P.C, and Leiter E.H. (2002). Deconstructing and reconstructing obesity-induced diabetes (diabesity) in mice *Diabetes* **51:** 825-832.

Reynolds, S. D., Giangreco, A., Power, J. H., & Stripp, B. R. (2000a). Neuroepithelial bodies of pulmonary airways serve as a reservoir of progenitor cells capable of epithelial regeneration. *Am J Pathol,* **156**(1), 269-278.

Reynolds, S. D., Hong, K. U., Giangreco, A., Mango, G. W., Guron, C., Morimoto, Y., & Stripp, B. R. (2000b). Conditional Clara cell ablation reveals a self-renewing progenitor function of pulmonary neuroendocrine cells. *Am J Physiol Lung Cell Mol Physiol, 278*(6), L1256-L1263.

Reynolds, M. F., Peterson-Roth, E. C., Bespalov, I. A., Johnston, T., Gurel, V. M., Menard, H. L., & Zhitkovich, A. (2009). Rapid DNA double-strand breaks resulting from processing of Cr-DNA cross-links by both MutS dimers. *Cancer Res,* **69**(3), 1071-1079.

Reynolds, P., Anderson, J.A., Harper, J.V. et al. (2012).The dynamics of ku70/80 and DNA-PKcs at DSBs induced by ionizing radiation is dependent on the complexity of damage. Nucleic Acids Res **40**:10821-10831.

Riballo, E., M. Kühne, N. Rief et al. (2004). A pathway of double-strand break rejoining dependent upon ATM, Artemis, and proteins locating to γ-H2AX foci**.** *Mol Cell* **16:** 715-724.

Risch, N. (1992) Genetic linkage: interpreting lod scores. *Science* **255**, 803-804.

Roderick T. H. (1963). The response of twenty seven inbred strains of mice to daily doses of whole body x-irradiation*. Radiat. Res.,* **20**:631-614.

Rogakou, E.P., Pilch, D.R., Orr, A.H., Ivanova, V.S. and Bonner, W.M. (1998). DNA double-stranded breaks induce histone H2AX phosphorylation on serine 139**.** *J. Biol. Chem*., **273** 5858-5868.

Rothkamm, K. and Löbrich. M. (2003). Evidence for a lack of DNA double-strand break repair in human cells exposed to very low X-ray doses. *Proc. Natl. Acad. Sci. USA*, **100:** 5057-5062.

Sakasai, R., & Tibbetts, R. (2008). RNF8-dependent and RNF8-independent regulation of 53BP1 in response to DNA damage. *J Biol Chem,* **283**(20), 13549-13555.

San Filippo J., Sung P, Klein H. (2008). Mechanism of Eukaryotic Homologous Recombination. Annu Rev Biochem. **77:**229-257.

Schipler, A., & Iliakis, G. (2013). DNA double-strand-break complexity levels and their possible contributions to the probability for error-prone processing and repair pathway choice. *Nucleic Acids Res, 41*(16), 7589-7605.

Sherr, C.J. and Roberts, J.M. (1999). CDK inhibitors: positive and negative regulators of G1-phase progression, *Genes Dev*. **13:** 1501–1512.

Shiloh, Y. (2003). ATM and related protein kinases: safeguarding genome integrity. *Nat Rev Cancer*. **3**(3):155-68.

Shiloh Y. The ATM-mediated DNA-damage response: taking shape. (2006). *Trends Biochem. Sci*. **31**: 402.

Smith, J., Tho, L. M., Xu, N., & Gillespie, D. A. (2010). The ATM-Chk2 and ATR-Chk1 pathways in DNA damage signaling and cancer. *Adv Cancer Res, 108*, 73-112.

Stassen, A.P.M., P.C. Groot, J.T. Eppig and P. Demant (1996). Genetic composition of the recombinant congenic strains. *Mammalian Genome* **7**, 55-58.

Stiff T, O'Driscoll M, rief N, et al. (2004). ATM and DNA-PK function redundantly to phosphorylate H2AX after exposure to ionizing radiation. *Cancer Res;* **64**: 2390-2396.

Stokes, MP, Rush J, Macneil J, et al. (2007). Profiling of UV-induced ATM/ATR signaling pathways. *Proc. Natl. Acad. Sci.USA*. **104**:19855-19860.

Storer, J. B., Mitchell T. J., Fry R. M. J. (1988). Extrapolation of the relative risk of radiogenic neoplasms across mouse strains and to man*. Radiat. Res*. **114:**331-353

Stucki, M., & Jackson, S. P. (2006). Gamma H2AX and MDC1: anchoring the DNA-damage-response machinery to broken chromosomes. *DNA Repair (Amst),* **5**(5), 534-543.

Sun, S., Schiller, J.H., and Gazdar, A.F. (2007). Lung cancer in never smokers: a different disease. *Nat Rev Cancer,* **7**:778-790.

Sun, F., Kanthasamy, A., Song, C., Yang, Y., Anantharam, V. and Kanthasamy, A.G. (2008). Proteasome inhibitor-induced apoptosis is mediated by positive feedback amplification of PKCδ proteolytic activation and mitochondrial translocation. *J. Cell Mol. Med.***12:**2467–2472.

Szymanska, H., Sitarz, M., Krysiak, E., Piskorowska, J., Czarnomska, A., Skurzak, H., . . . Demant, P. (1999). Genetics of susceptibility to radiation-induced lymphomas, leukemias and lung tumors studied in recombinant congenic strains. *Int J Cancer,* **83**(5), 674-678.

Thompson L H, Schild D. (1999The contribution of homologous recombination in preserving genome integrity in mammalian cells. *Biochimie*. **81**:87–105

Thompson, L.H. and Schild, D. (2001). Homologous recombinational repair of DNA ensures mammalian chromosome stability. *Mutat Res*. **477**(1-2):131-53.

Thompson, L.H. (2012). Recognition, signaling, and repair of DNA double-strand breaks produced by ionizing radiation in mammalian cells: the molecular choreography. *Mutat Res,* **751**(2), 158-246.

Travis, W.D. (2002). Pathology of lung cancer. *Clin. Chest Med.* **23**, 65-81.

Tripodis N, Demant P. (2001). Three-dimensional patterns of lung tumor growth: association with tumor heterogeneity. *Exp Lung Res* **27**: 521–531.

Tripodis N, Demant P. (2003). Genetic analysis of three-dimensional shape of mouse lung tumors reveals eight lung tumor shape-determining (Ltsd) loci that are associated with tumor heterogeneity and symmetry. *Cancer Res* **63:** 125–131.

Tropepe, V., Coles, B.L., Chiasson, B.J., Horsford, D.J., Elia, A.J., McInnes, R.R., and van der Kooy, D. (2000). Retinal stem cells in the adult mammalian eye. *Science* **287**, 2032-2036.

Uematsu, N., Weterings, E., Yano, K.-i., Morotomi-Yano, K., Jakob, B., Taucher-Scholz, G., . . . Chen, D. J. (2007). Autophosphorylation of DNA-PKCS regulates its dynamics at DNA double-strand breaks. *J Cell Biol,* **177**(2), 219-229.

Ullrich, R.L (1983).Tumor induction in BALB/c female mice after fission neutron or gamma irradiation. *Radiat. Res* **93**:506–515.

Ullrich, R.L. (1991). Cellular and molecular changes in mammary epithelial cells following irradiation. *Radiat. Res*. **128** (Suppl.), S136–S140.

Vakoc, C. R., Sachdeva, M. M., Wang, H., & Blobel, G. A. (2006). Profile of histone lysine methylation across transcribed mammalian chromatin. *Mol Cell Biol,* **26**(24), 9185-9195.

Van Der Schans, G.P. (1978). Gamma-ray induced double-strand breaks in DNA resulting from randomly-inflicted single-strand breaks: temporal local denaturation, a new radiation phenomenon? *Int. J. Radiat. Biol. Relat. Stud. Phys. Chem. Med*., **33**: 105-120.

Villemure, J. F., Abaji, C., Cousineau, I., & Belmaaza, A. (2003). MSH2-deficient human cells exhibit a defect in the accurate termination of homology-directed repair of DNA double-strand breaks. *Cancer Res,* **63**(12), 3334-3339.

Wang, B., & Elledge, S. J. (2007). Ubc13/Rnf8 ubiquitin ligases control foci formation of the Rap80/Abraxas/Brca1/Brcc36 complex in response to DNA damage. *Proc Natl Acad Sci U S A,* **104**(52), 20759-20763.

Wang, B., Matsuoka, S., Ballif, B. A., Zhang, D., Smogorzewska, A., Gygi, S. P., & Elledge, S. J. (2007). Abraxas and RAP80 form a BRCA1 protein complex required for the DNA damage response. *Science,* **316**(5828), 1194-1198.

Wang, C., & Lees-Miller, S. P. (2013). Detection and repair of ionizing radiation-induced DNA double strand breaks: new developments in nonhomologous end joining. *International Journal of Radiation Oncology* Biology* Physics,* **86**(3), 440-444.

Ward, I.M. and Chen, J. 2001. Histone H2AX is phosphorylated in an ATR-dependent manner in response to replicational stress *J. Biol. Chem*. **276**:47759-47762.
Watters D. (1999). Molecular mechanisms of ionizing radiation-induced apoptosis.Immunol Cell Biol. **7:** 263-271.

Weinfeld, M., Mani, R.S., Abdou, I.et al. (2011). Tidying up loose ends: The role of polynucleotide kinase/phosphatase in DNA strand break repair. *Trends Biochem Sci.* **36:** 262–271.

West, M.H.P and Bonner, W.M. (1980). Histone H2A: A heteromorphous family of eight protein species. *Biochemistry* **19**: 3238-3245.

Weterings, E., N.S. Verkaik, G. Keijzers et al. (2009). The ku80 carboxy terminus stimulates joining and artemis-mediated processing of DNA ends. *Mol Cell Biol.* **29:** 1134–1142.

Xie, A. A. Kwok, R. Scully. (2009). Role of mammalian MRE11 in classical and alternative non-homologous end joining. *Nat Struct Mol Biol,* **16:** 814–818

Yano, K.-i., Morotomi-Yano, K., Adachi, N., & Akiyama, H. (2009). Molecular mechanism of protein assembly on DNA double-strand breaks in the non-homologous end-joining pathway. *J Radiat Res,* **50**(2), 97-108.

Yu, Y., Okayasu, R., Weil, M. M., Silver, A., McCarthy, M., Zabriskie, R., Long, S., Cox, R. and Ullrich, R. L. (2001). Elevated breast cancer risk in irradiated BALB/c mice associates with unique functional polymorphism of the *Prkdc* (DNA-dependent protein kinase catalytic subunit) gene. *Cancer Res*. **61**, 1820–1824.

Zarebski, M., Wiernasz, E., & Dobrucki, J. W. (2009). Recruitment of heterochromatin protein 1 to DNA repair sites. *Cytometry A, 75*(7), 619-625.

Zhao, Y., Thomas, H.D., Batey, M.A. et al. (2006). Preclinical evaluation of a potent novel DNA-dependent protein kinase inhibitor nu744. *Cancer Res* **66:** 5354–5362.

Zhou, B. B. and S. J. Elledge (2000). "The DNA damage response: putting checkpoints in perspective." *Nature* **408**(6811): 433-439.

Zhou, T., Akopiants, K., Mohapatra, S., Lin, P. S., Valerie, K., Ramsden, D. A., . . . Povirk, L. F. (2009). Tyrosyl-DNA phosphodiesterase and the repair of 3'-phosphoglycolate-terminated DNA double-strand breaks. *DNA Repair (Amst), 8*(8), 901-911.

Ziv, Y., Bielopolski, D., Galanty, Y., Lukas, C., Taya, Y., Schultz, D. C., . . . Shiloh, Y. (2006). Chromatin relaxation in response to DNA double-strand breaks is modulated by a novel ATM- and KAP-1 dependent pathway. *Nat Cell Biol, 8*(8), 870-876.

Zou, L. and Elledge S.J. (2003**).** Sensing DNA damage through ATRIP recognition of RPA–ssDNA complexes. *Science*, **300:** 1542-1548.